NUREG/CR-6893

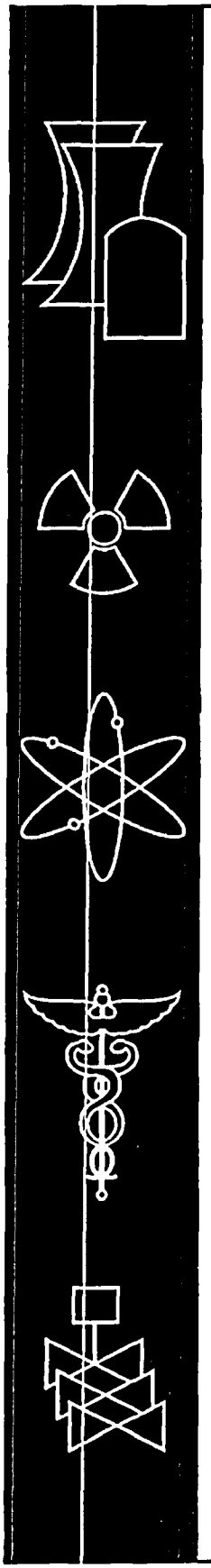

Modeling Adsorption Processes: Issues in Uncertainty, Scaling, and Prediction

U.S. Nuclear Regulatory Commission
Office of Nuclear Regulatory Research
Washington, DC 20555-0001

AVAILABILITY OF REFERENCE MATERIALS IN NRC PUBLICATIONS

NRC Reference Material

As of November 1999, you may electronically access NUREG-series publications and other NRC records at NRC's Public Electronic Reading Room at http://www.nrc.gov/reading-rm.html. Publicly released records include, to name a few, NUREG-series publications; *Federal Register* notices; applicant, licensee, and vendor documents and correspondence; NRC correspondence and internal memoranda; bulletins and information notices; inspection and investigative reports; licensee event reports; and Commission papers and their attachments.

NRC publications in the NUREG series, NRC regulations, and *Title 10, Energy*, in the Code of *Federal Regulations* may also be purchased from one of these two sources.

1. The Superintendent of Documents
   U.S. Government Printing Office
   Mail Stop SSOP
   Washington, DC 20402–0001
   Internet: bookstore.gpo.gov
   Telephone: 202-512-1800
   Fax: 202-512-2250
2. The National Technical Information Service
   Springfield, VA 22161–0002
   www.ntis.gov
   1–800–553–6847 or, locally, 703–605–6000

A single copy of each NRC draft report for comment is available free, to the extent of supply, upon written request as follows:

Address: Office of the Chief Information Officer,
Reproduction and Distribution
Services Section
U.S. Nuclear Regulatory Commission
Washington, DC 20555-0001
E-mail: DISTRIBUTION@nrc.gov
Facsimile: 301–415–2289

Some publications in the NUREG series that are posted at NRC's Web site address http://www.nrc.gov/reading-rm/doc-collections/nuregs are updated periodically and may differ from the last printed version. Although references to material found on a Web site bear the date the material was accessed, the material available on the date cited may subsequently be removed from the site.

Non-NRC Reference Material

Documents available from public and special technical libraries include all open literature items, such as books, journal articles, and transactions, *Federal Register* notices, Federal and State legislation, and congressional reports. Such documents as theses, dissertations, foreign reports and translations, and non-NRC conference proceedings may be purchased from their sponsoring organization.

Copies of industry codes and standards used in a substantive manner in the NRC regulatory process are maintained at—

The NRC Technical Library
Two White Flint North
11545 Rockville Pike
Rockville, MD 20852–2738

These standards are available in the library for reference use by the public. Codes and standards are usually copyrighted and may be purchased from the originating organization or, if they are American National Standards, from—

American National Standards Institute
11 West 42nd Street
New York, NY 10036–8002
www.ansi.org
212–642–4900

Legally binding regulatory requirements are stated only in laws; NRC regulations; licenses, including technical specifications; or orders, not in NUREG-series publications. The views expressed in contractor-prepared publications in this series are not necessarily those of the NRC.

The NUREG series comprises (1) technical and administrative reports and books prepared by the staff (NUREG–XXXX) or agency contractors (NUREG/CR–XXXX), (2) proceedings of conferences (NUREG/CP–XXXX), (3) reports resulting from international agreements (NUREG/IA–XXXX), (4) brochures (NUREG/BR–XXXX), and (5) compilations of legal decisions and orders of the Commission and Atomic and Safety Licensing Boards and of Directors' decisions under Section 2.206 of NRC's regulations (NUREG–0750).

NUREG/CR-6893

Modeling Adsorption Processes: Issues in Uncertainty, Scaling, and Prediction

Manuscript Completed: December 2005
Date Published: February 2006

Prepared by
L.J. Criscenti[1], M. Eliassi[1], R.T. Cygan[1], C.F. Jové Cólón

S. Goldberg[2]

[1] Sandia National Laboratories
Albuquerque, NM 87185

[2] USDA-ARS
George E. Brown Jr. Salinity Laboratory
Riverside, CA 92507

E.O'Donnell, NRC Project Manager

Prepared for
Division of Systems Analysis and Regulatory Effectiveness
Office of Nuclear Regulatory Research
U.S. Nuclear Regulatory Commission
Washington, DC 20555-0001
Job Code Y6464

ABSTRACT

Adsorption of contaminant species to mineral surfaces is largely responsible for the retardation of radionuclides in the subsurface environment. However, despite much research effort, the advancement of models that can be used to successfully calculate or predict adsorption is still somewhat limited. This report covers three different aspects of modeling adsorption of radionuclides with an emphasis on the use of surface complexation models (SCM). The methods provide a rigorous and thermodynamic-based alternative to the more conventional and empirical K_D approach often used inappropriately in the performance assessment of nuclear waste sites.

The first study provides an example of how adsorption constant uncertainty propagates through a one-dimensional reactive-transport code and can strongly influence the calculated aqueous metal (i.e., uranyl) concentrations as a function of distance and time from a contaminant source. In this study, the hydrology and mineralogy of the Naturita uranium mill tailings site in Colorado are used to establish initial conditions and processes to incorporate into a one-dimensional (1-D) reactive-transport model. An electrostatic surface complexation model is used to describe adsorption onto smectite, an abundant clay mineral at the Naturita site. A probabilistic investigation demonstrates that uncertainty in adsorption constants can dramatically change the calculated shape of contaminant concentration profiles. This study demonstrates the importance of selecting appropriate adsorption constants when using reactive-transport models in performance assessment to evaluate risk and pollution attenuation at contaminated sites.

Adsorption processes at the solid-water interface can be investigated at different levels of chemical detail: electronic, atomistic, and thermodynamic. The second study addresses this scaling issue by describing how electronic- and atomic-scale investigations provide useful insight for the development of accurate bulk thermodynamic models (for example, SCM). Molecular modeling can be used to investigate the stoichiometries and relative adsorption energies of possible surface complexes. Both quantum and molecular mechanics calculations that focus on the submicroscopic details of the adsorption process can provide us with new, more quantitative ways to bound the uncertainties associated with "averaging" surface site characteristics and for selecting only one or two surface reactions to describe the adsorption of a contaminant over a range of environmental conditions. These atomic-scale studies may provide us with a more definitive appreciation for how detailed an SCM is necessary for accurate reactive-transport simulations of contaminant migration.

The third study reviews recent progress in developing an internally-consistent database to describe adsorption over a wide range of solution and solid compositions. Substantial progress has been made to establish a database for a specific SCM (triple-layer model). Newly-defined standard states for surface species allow us to normalize and compare experimental adsorption data collected using different solid to liquid ratios. X-ray standing-wave measurements, X-ray absorption spectroscopy, molecular modeling, and ab initio modeling all contribute to a greater understanding of surface complexation, and in particular, to the nature of contaminant surface species that need to be incorporated into larger-scale thermodynamic models. Combining approaches ranging from bulk adsorption measurements to ab initio quantum calculations in our investigation of processes at the solid-water interface and synthesizing information for different interfacial systems, may lead to major breakthroughs in adsorption modeling in the next decade.

FOREWORD

The U.S. Nuclear Regulatory Commission (NRC) uses environmental models to evaluate the potential release of radionuclides from NRC-licensed sites. In doing so, the NRC recognizes that, at many sites, groundwater-related pathways could contribute significantly to the potential doses received by members of the public. Consequently, consistent with its mission to protect the health and safety of the public and the environment, the NRC and others have developed contaminant transport models to predict the locations and concentrations of radionuclides in soil as a function of time.

Because many radionuclides temporarily attach, or adsorb, to the surfaces of soil particles, their mobility is reduced compared to that of compounds that move with the groundwater without interacting with soil surfaces. As a result, most subsurface-transport models used by the NRC and its licensees estimate the effects of the anticipated interactions between radionuclides and solids in the ground. Toward that end, these subsurface-transport models use a "distribution coefficient" which is assumed to be constant and reflects the proportion of a radionuclide in groundwater compared to the radionuclide associated with the solids in the ground. These distribution coefficients are widely used by licensees and, consequently, the relevant literature documents ranges of their values for various soil types and radionuclides. However, the ranges can be very large because the chemical reactions that cause radionuclides to attach to solids are very sensitive to water chemistry and soil mineralogy. As a result, uncertainties in the parameters used to characterize the adsorption of radionuclides in soils have been identified as a major source of uncertainty in decommissioning, uranium recovery, and radioactive waste disposal cases evaluated by the NRC.

Surface-complexation and ion-exchange models offer a more realistic approach to considering soil-radionuclide interactions in performance assessment models. These models can also account for variable chemical environments that might affect such interactions.

The focus of this report is a probabilistic analysis of sorption parameter uncertainty and its influence on radionuclide migration. Toward that end, the report provides an example of how uncertainty in adsorption constants can influence estimates of contaminant plume migration, reviews how atomic-scale studies of the solid-water interface can improve the development of bulk adsorption models, and describes recent progress toward developing a systematic thermodynamic database for metal adsorption on soil minerals. This report will help the staff define realistic site-specific ranges of the distribution coefficient values used to evaluate NRC licensed sites.

The views and opinions presented in this report are those of the individual authors, and publication of this report does not necessarily constitute NRC approval or agreement with the information contained herein. As such, this report is not a substitute for NRC regulations. The approaches and/or methods described are provided for information only, and compliance is not required. Moreover, use of product or trade names herein is for identification purposes only and does not constitute endorsement by the NRC or Sandia National Laboratories.

Carl J. Paperiello

Carl J. Paperiello, Director
Office of Nuclear Regulatory Research
U.S. Nuclear Regulatory Commission

CONTENTS

Figures

Tables

1. INTRODUCTION

A major program objective of the U.S. Nuclear Regulatory Commission's "Radionuclide Transport in the Environment Research Program" is to provide a defensible, science-based understanding of radionuclide migration and retardation for assessing contaminant transport in the environment. Performance assessment (PA) calculations are used to estimate radionuclide concentrations in ground and surface water, treat the uncertainty in those estimates, and evaluate the consequent dose impact to the public from NRC licensed activities. The PA calculations are used in the licensing and decommissioning of nuclear facilities and clean-up of contaminated sites, including reclamation of uranium mill tailings disposal sites. Current PA models use simplified conceptual models for radionuclide retardation that are based on linear and reversible partition coefficients (K_D's) measured for a specific set of experimental conditions, which usually are laboratory measurements of soil samples. Unfortunately, experience shows that this approach often fails to correlate with field measurements of actual transport (e.g., Bethke and Brady, 2000). The reason is that the experimental K_D's represent localized properties and are sometimes not applicable over time and at other locations considering the range of nonlinear geochemical phenomena and chemical conditions that can significantly affect radionuclide transport (temperature, pH, fluid composition, ionic strength, mineral substrate, organic complexation, etc.). Therefore, it is critical to understand and model radionuclide retardation processes over a wide range of environmental conditions that are relevant to NRC licensing concerns. Since adsorption and desorption processes are important to radionuclide retardation in soils, they need to be addressed in PA models. Once radionuclide adsorption and desorption mechanisms are better understood, more appropriate retardation models such as surface complexation models can be incorporated into the PA to allow for improved treatment of uncertainty when making estimates of dose to the public.

Despite the effort of the last ten to fifteen years, the development of conceptual models that can be used to successfully calculate or predict adsorption onto minerals is still very much in its infancy. Various chemical surface complexation models have been developed to describe potentiometric titration and metal adsorption data at an idealized oxide-solution interface. In contrast to empirical K_D methods, surface complexation models provide descriptions of metal adsorption using an equilibrium approach that defines surface species, chemical reactions, mass balances, and charge balances. These models provide insight into the stoichiometry and reactivity of adsorbed species. Application of these models to reference oxide minerals has been extensive but their use in describing ion adsorption by clay minerals and mixed sediments that are typical of most NRC regulated waste sites is limited. Surface complexation models share at least four common assumptions: (1) oxide surfaces can be described as idealized and flat planes of surface hydroxyl sites and equations can be written to describe reactions at each of these specific surface sites; (2) reactions at surfaces are at local equilibrium and can be described using thermodynamic mass law equations; (3) variation in charge at the mineral surface is a direct result of chemical reactions at the surface; (4) the effect of surface charge on measured equilibrium constants can be calculated and the intrinsic equilibrium constants can be extracted from experimental measurements (see Section 4.1; Dzombak and Morel, 1990; Koretsky, 2000).

This report covers three different aspects of modeling adsorption with an emphasis on the use of surface complexation models (SCM). Chapter 2 represents the joint work of L. J. Criscenti, M. Eliassi, R. T. Cygan, and C. F. Jové Cólón during the first two years of the project. It provides an

example of how adsorption constant uncertainty propagates through a one-dimensional reactive-transport code and can strongly influence the calculated aqueous metal (i.e., uranyl) concentrations as a function of distance and time from a contaminant source. The simulations are made using the hydrology and mineralogy of the Naturita uranium mill tailings site in Colorado to establish initial conditions and processes. An electrostatic surface complexation model is used to describe adsorption onto smectite, an abundant clay mineral at the Naturita site. The simulations illustrate that uncertainty in adsorption constants can dramatically change the calculated shape of contaminant concentration profiles. This study demonstrates the importance of selecting appropriate adsorption constants when using reactive-transport models to evaluate risk and pollution attenuation at contaminated sites.

Chapter 3 was originally published as: L. J. Criscenti "Adsorption processes: At what spatial scale do we need to understand them?" in the Proceedings of the 11th International Symposium on Water-Rock Interaction, WRI-11, 27th June – 2 July 2004, Saratoga Springs, NY. Eds. R. B. Wanty and R. R. Seal, A. A. Balkema Publishers, New York, and is reprinted here with permission of the publisher. This conference paper summarizes an invited talk for L. J. Criscenti and highlights her investigations into adsorption processes using different modeling approaches. Examples used in this chapter are taken from research sponsored by the Sandia National Laboratories Laboratory Directed Research and Development program, the DOE ASC program, the U.S. Nuclear Regulatory Commission, and the U.S. Department of Energy, Basic Energy Sciences program. The chapter describes how small-scale investigations provide useful insight for the development of accurate bulk thermodynamic models (i.e., SCM). For example, molecular modeling can be used to investigate the stoichiometries and relative adsorption energies of viable surface complexes. Both quantum and molecular mechanics calculations that focus on the atomic-level details of adsorption processes can provide us with detailed information about the relative importance of different interfacial variables in determining the likelihood of contaminant adsorption. These atomic-scale methods allow us a more critical approach for discriminating what types of data should be included in an SCM database for accurate reactive-transport simulations of radionuclide migration.

Chapter 4 represents a subset of material written by L. J. Criscenti and S. Goldberg for the draft white paper on reactive processes prepared by the Interagency Memorandum of Understanding Working Group 3: Subsurface Reactive Transport Modeling as well as a draft chapter on adsorption modeling written by S. Goldberg (U.S. Department of Agriculture, Agricultural Research Service) and L. J. Criscenti (Sandia National Laboratories) for an International Union of Pure and Applied Chemistry (IUPAC) volume. The MOU working group is part of a collaborative effort of several government agencies to develop conceptual models for subsurface reactive transport modeling of inorganic contaminants, radionuclides, and nutrients. Details of this collaboration and summaries from a recent reactive transport workshop are published on the internet (www.iscmem.org). The material presented in this last chapter emphasizes the work of Sverjensky and his students to develop an internally-consistent database for the Triple-Layer Model. The results of spectroscopic and molecular modeling studies are gradually being incorporated into an adsorption model that will be useful for reactive-transport simulations of contaminant migration.

2. EFFECTS OF ADSORPTION CONSTANT UNCERTAINTY ON CONTAMINANT PLUME MIGRATION: ONE-DIMENSIONAL NUMERICAL STUDIES

2.1 Abstract

This chapter is an update of Criscenti *et al.* (2002; NUREG/CR-6780). In this study, the hydrology and mineralogy of the Naturita uranium mill tailings site in Colorado are used to establish initial conditions and processes to incorporate into a one-dimensional (1-D) reactive-transport model. This model describes adsorption using an electrostatic surface complexation approach. This study is the first to examine variations in reactive-transport model predictions due to uncertainties in the equilibrium constants associated with an electrostatic model for adsorption. This work demonstrates the importance of selecting appropriate adsorption constants when using reactive-transport models to evaluate risk and pollution attenuation at contaminated sites. In our simulations, uranium is removed from mill tailings leachate through adsorption onto smectite, an abundant clay mineral at the Naturita site. Uranium adsorbs to specific surface sites on both the basal planes and edges of the smectite. Because uranium adsorbs predominantly to the aluminum edge surface sites [$>(e)AlOH$], we chose to examine uncertainty only in the equilibrium constants associated with these sites. One-hundred pairs of equilibrium constant (log K) values for the surface species $>(e)AlO^-$ and $>(e)AlOUO_2^+$ were selected from normal distributions of each log K using the Latin Hypercube Sampling method. For the 1-D simulations, two distinct groups of uranium concentration versus distance profiles can be identified. In the first group, the concentration profiles exhibit a classical sigmoidal shape whereas in the second group the concentration profiles display higher uranium concentrations in solution over greater distances and times. These two groups are clearly separated by two different ranges of log K $>(e)AlO^-$ values or two different ranges for the smectite point of zero charge. Preliminary 2-D simulations also demonstrate that both transverse and longitudinal plume migration are influenced by the choice of adsorption constants.

2.2 Introduction

This study builds upon recent investigations of uranium mill tailings sites where uranium [U(VI)] has leached into the surrounding soil for many years (e.g., Morrison and Cahn, 1991; Landa and Gray, 1995; Zhu and Burden, 2001; Zhu *et al.*, 2001, 2002; Bain *et al.*, 2001). One site under investigation is Naturita, Colorado where the Nuclear Regulatory Commission is working cooperatively with the U. S. Geological Survey and Sandia National Laboratories to investigate both hydrological and geochemical conditions as a function of time, and to assess the ability of surface complexation models coupled with hydrologic models to predict radionuclide migration through the soil (Davis, 2001; Davis and Curtis, 2003; Davis *et al.*, 2004; Curtis *et al.*, 2004; Jové-Colón *et al.*, 2001; Jacobs Engineering Group Inc., 1994; Kohler *et al.*, 2004). Naturita is one of several UMTRA (Uranium Mill Tailings Remedial Action) Title 1 sites where the mine tailings have been removed by the U.S. Government to reduce contaminant levels. However, lingering uranium dissolved in groundwater and adsorbed in shallow alluvium still remains, creating some concerns regarding the extent of contaminant transport within the site. In this study, coupled reactive-transport models are used to better conceptualize and predict uranium migration at the contamination sites, with particular application to the hydrology and mineralogy

associated with Naturita. This work demonstrates the importance of selecting the appropriate adsorption constants when using reactive-transport models to evaluate pollutant attenuation and potential risk at contaminated sites.

The issue of uncertainty analysis and its importance when using various mathematical models to describe contaminant migration in the subsurface environment is not a new one. Several studies have investigated uncertainty in geochemical modeling (Criscenti *et al.*, 1996; Stipp, 1990; Schecher and Driscoll, 1987, 1988; Nordstrom and Ball, 1989; Anderson, 1976). While reactive-transport modeling has also been used in the past to investigate the migration of uranium in mill tailings, such studies have primarily focused on examining the development of reaction fronts due to mineral precipitation and dissolution (Zhu and Burden, 2001; Zhu *et al.*, 2001; Bain *et al.*, 2001; Erikson *et al.*, 1990). Several studies have also examined the sensitivity of reactive-transport simulations to uncertainty in hydrological parameters (e.g., Hamed *et al.*, 1996; Nitzsche *et al.*, 2000).

More recently, Tebes-Stevens and Valocchi (2000) and Tebes-Stevens *et al.* (2001) have studied the relative effects of transport and reaction parameters on the results of a solute transport model. Uranium(VI) hydrolysis species are transported through a two-dimensional domain with a spatially variable pattern of surface complexation sites (Tebes-Stevens *et al.*, 2001). Using a non-electrostatic surface complexation model, their calculations indicated that the model is most sensitive to the initial concentration of one of two types of surface sites, the formation constant for one of three uranyl (UO_2^{2+}) surface complexes, and the hydraulic conductivity within the reactive zone.

To the best of our knowledge, this is the first study to investigate the effects of uncertainty in two equilibrium adsorption constants in an electrostatic surface complexation model, on calculated contaminant plume migration using simple one- and two-dimensional (1-D and 2-D) reactive-transport models. Our investigation focused on examining uranium adsorption onto clay surfaces, one of several possible retardation mechanisms at the Naturita site, and the influence of the adsorption constants on calculated uranium concentration versus distance profiles and plume migration. Adsorption onto other solid phases such as ferrihydrite has also been suggested at the Naturita site (Davis *et al.*, 2004). In addition, ongoing analytical research suggests that uranium contamination at the Naturita site is strongly affiliated with iron-rich coatings (Jové Cólón *et al.*, 2005). Although in a real aquifer such as Naturita, adsorption of fulvic and humic acids, other inorganic cations and anions, and bacterial exopolymers will compete with uranyl adsorption onto smectite, for the uncertainty analysis presented here, our model only considers uranyl and proton adsorption to two active adsorption sites, one each on the basal and edge surfaces of smectite clay. This simple model for uranyl adsorption is sufficient to demonstrate that uncertainties in adsorption constants can lead to widely differing predictions of uranium migration in the subsurface environment; differences that are sufficiently large that they can pose a problem when assessing the risk associated with contaminant migration from mill tailings.

2.3 Governing Equations

We consider the advective-dispersive-reactive (ADR) transport model in a 2-D system to evaluate the flow conditions for our reactive-transport system. Under water-saturated conditions, the governing equation for ADR, described in 2-D tensor notation, can be stated as (Bethke,

1997a):

$$\phi \frac{\partial C_i}{\partial t} = \frac{\partial}{\partial x_l}\left(\phi D_{lm} \frac{\partial C_i}{\partial x_m}\right) - \frac{\partial}{\partial x_l}(q_l C_i) - \phi \sum_k \left(\frac{\partial C_i}{\partial t}\right)_k + \phi Q_i \qquad (2.1)$$

where ϕ is the porosity, C_i [M/L^3] is the concentration of the transport component, i, t [T] is time, $x_l=(x,y)$ [L] represents the cartesian coordinates, D_{lm} [L^2/T] is the dispersion tensor, q_l [L/T] is the specific discharge, subscripts m and l refer to the spatial directions, the term involving the summation over k refers to the mass transfer among the various transport species, and Q_i [M/TL^3] is the source/sink term which accounts for changes in solution composition due to geochemical reaction.

The stoichiometry of each species in a geochemical system is described in terms of chemical components. The components in the system examined in this study include (1) water, the solvent species, (2) a mineral (i.e., smectite in our case) that is in equilibrium with the aqueous solution, (3) two gas phase species set at known fugacity, (4) aqueous species in solution representing the major cations and anions present, and (5) two different types of surface sites. Each independent reaction that forms an aqueous species in the system, has an associated equilibrium constant K_j at the temperature of interest and therefore can be described by a mass action equation.

Mass action equations are also written for each surface species within the framework of the diffuse-layer model (DLM) of Dzombak and Morel (1990). The DLM describes the mineral surface in terms of metal-hydroxyl sites that can react with ions in solution. It accounts explicitly for the electrical state of the mineral surface as it varies with the pH, ionic strength, and solution composition. In order for an ion to adsorb to the surface from solution, it must first move through the electrical potential field created by the surface. Therefore, the mass action equations for the DLM surface complexes include an electrostatic term $10^{z_q F\Psi / 2.303RT}$, where z_q is the electrical charge on each complex q, F [96,485 C/mol] is the Faraday constant, Ψ[V] is the surface potential, R [8.3143 V·C/mol·K where 1 V·C = 1 Joule] is the gas constant, and T [K] is absolute temperature.

The mass action equations are incorporated into mass balance equations that express the conservation of mass in terms of mole number for water (M_w), each component (M_i), mineral (M_k), gas (M_m), and site type (M_p). The mass balance equations form a set of governing equations that describe multicomponent equilibrium in the presence of an adsorbing mineral surface.

The principle of electroneutrality requires that the ionic species in aqueous solution remain charge balanced on a macroscopic scale. This requirement is met by adjusting M_i for one component in a manner analogous to that used in other geochemical codes [e.g., EQ3NR (Wolery, 1992); GEOSURF (Sahai and Sverjensky, 1998)]. By default this component is chloride (Cl^-) because it is in abundant concentration and because most commercial laboratories report a chloride concentration calculated by a rough charge balance (Bethke, 1996). In this study either Cl^- or SO_4^{2-}, another major anion in uranium mill-tailings leachate, is used as the charge-balancing anion.

To numerically solve the system of transport and geochemical equations, we use the Xt software

codes [X1t and X2t software codes for 1-D and 2-D simulations, respectively (Bethke, 1997a, b]. In the Xt package, the spatial derivatives of transport equations are discretized based on the cell-centered finite difference method. Additionally, Xt uses the Strang operator splitting approach in the ADR to advance the time step, where the flow equation is first solved to arrive at the nodal hydraulic potential values, and thus compute the flux between two neighboring nodes. Next, the ADR equations are solved using explicit time stepping, where the spatial averaging across cell boundaries is performed by first-order upwind weighting. We should note that to ensure numerical stability, Xt also calculates the time-step size based on a combination of the Courant condition for the advective and von Neumann's criterion for the dispersive components of the transport equations.

The numerical methods used to solve the geochemical equations in X1t and X2t have been described by Bethke (1996, 1998) and are analogous to those used in the geochemical codes MINEQL (Westall *et al.*, 1976), HYDRAQL (Papelis *et al.*, 1988), and MINTEQA2 (Allison *et al.*, 1991). To summarize, at each time step, equilibrium speciation and partitioning between the solid matrix, mineral surfaces, and aqueous solution are calculated using a Newton-Raphson iteration method (Bethke, 1996). The Newton-Raphson iteration step is complicated by the need to account for the surface charge and potential when setting values for m_q. Westall (1980) was the first to develop an algorithm treating the surface potential as a basis species. An additional calculation is performed at each step in the Newton-Raphson iteration to locate the appropriate surface potential.

2.4 Geochemical Model

Because of our interest in the Naturita field site, we developed both 1-D and 2-D conceptual models that mainly focus on uranium migration in the subsurface environment. In our models, the initial system consists of an aqueous solution that is in equilibrium with a clay mineral comprised of basal and edge surfaces; we assume there is no interlayer exchange with uranium. This equilibrium system is buffered by CO_2 and O_2 reservoirs representative of an aquifer environment. A complete list of the chemical species considered in our conceptual models is provided in Table 2.1.

In the 1-D conceptual model, leachate from the uranium mill tailings is assumed to have already saturated the subsurface porous system with uranium. Therefore uranium is initially distributed homogeneously in the subsurface. The initial groundwater composition (see Table 2.2) reflects prior mixing with uranium mill tailings leachate; it contains much higher concentrations of SO_4^{2-} (1500 mg/kg), Cl^- (84 mg/kg), Na^+ (230 mg/kg), Ca^{2+} (209 mg/kg), and Mg^{2+} (61 mg/kg) than are typically present in natural groundwater. This composition is representative of water samples collected downstream from the Naturita site during 1999 by the U. S. Geological Survey (Kohler *et al.*, 2004, Davis *et al.*, 2004). The inlet rainwater composition is that reported by Berner and Berner (1996) for precipitation in the inland western United States. We examine the mixing of the rainwater with contaminated groundwater in the 1-D model, similar to what is occurring at Naturita today.

Table 2.1 List of chemical species considered in geochemical model

Components

H^+	Ca^{2+}	Cl^-	>(*b*) *AlOH*
Na^+	Fe^{2+}	NO_3^-	>(*e*) *AlOH*
K^+	Fe^{3+}	HCO_3^-	
Mg^{2+}	Al^{3+}	SO_4^{2-}	
SiO_2	UO_2^{2+}		

Aqueous Complexes

OH^-	$CaOH^+$	$FeOH^+$	$AlOH^{2+}$	$(UO_2)_2(OH)_2^{2+}$
	$CaCl^+$	$Fe(OH)_2$	$Al(OH)_2^+$	$(UO_2)_3(OH)_4^{2+}$
HCl	$CaHCO_3^+$	$Fe(OH)_3^-$	$Al(OH)_3$	$(UO_2)_3(OH)_5^+$
HSO_4^-	$CaCO_3$	$FeHCO_3^+$	$Al(OH)_4^-$	$(UO_2)_3(OH)_7^-$
	$CaSO_4$	$FeCO_3$	$Al_{13}O_4(OH)_{24}^{7+}$	$(UO_2)_4(OH)_7^+$
$NaOH$	$CaH_3SiO_4^+$	$FeCl^+$	$Al_2(OH)_2^{4+}$	UO_2SO_4
$NaCl$	CaH_2SiO_4	$FeCl_2$	$Al_3(OH)_4^{5+}$	$UO_2(SO_4)_2^{2-}$
$NaHCO_3$	$Ca(H_3SiO_4)_2$	$FeSO_4$	$AlSO_4^+$	$UO_2(NO_3)_2$
$NaSO_4^-$	$CaNO_3^+$		$Al(SO_4)_2^-$	$UO_2SiO(OH)_3^+$
$NaCO_3^-$				$(UO_2)^{2+}(CO_3)(OH)_3^-$
NaH_3SiO_4	$MgOH^+$	$FeOH^{2+}$	$H_3SiO_4^-$	UO_2CO_3
	Mg_2OH^{3+}	$Fe(OH)_2^+$	$H_2SiO_4^{2-}$	$UO_2(CO_3)_2^{2-}$
KOH	$Mg_4(OH)_4^{4+}$	$Fe(OH)_3$	$H_3SiO_4^-$	$UO_2(CO_3)_3^{3-}$
KCl	$MgCl^+$	$Fe(OH)_4^-$	$H_4(H_2SiO_4)_4^{4-}$	
KSO_4^-	$MgHCO_3^+$	$Fe_2(OH)_2^{4+}$	$H_6(H_2SiO_4)_4^{2-}$	
	$MgCO_3$	$Fe_3(OH)_4^{5+}$		
CO_3^{2-}	$Mg_2CO_3^{2+}$	$FeCO_3^+$		
$CO_2(aq)$	MgH_2SiO_4	$FeCl_2^+$		
	$MgH_3SiO_4^+$	$FeCl_4^-$		
	$Mg(H_3SiO_4)_2$	$FeCl_3$		
	$MgSO_4$	$FeH_3SiO_4^{2+}$		
		$FeSO_4^+$		
		$Fe(SO_4)_2^-$		
		$FeNO_3^{2+}$		

Solid Phase

Low-Fe-Mg Smectite

$Na_{.15}Ca_{.02}K_{.2}Mg_{.9}Fe_{.45}Al_{1.25}Si_{3.75}O_{10}(OH)_2$

Surface Complexes

>(*e*)*AlO*$^-$	>(*e*)*AlOH*$_2^+$	>(*e*)*AlOUO*$_2^+$
>(*b*)*AlO*$^-$	>(*b*)*AlOH*$_2^+$	>(*b*)*AlOUO*$_2^+$

Table 2.2 Initial Groundwater, rainwater, and leachate compositions used in 1-D and 2-D simulations

	1-D Simulations		2-D Simulations		
	Contaminated Groundwater	Rainwater	Initial Groundwater	Incoming Groundwater	Leachate
pH	7	5.8	7	7	7
f_{CO2} (*atm*)	$10^{-2.5}$	$10^{-3.5}$	$10^{-2.5}$	$10^{-2.5}$	$10^{-2.5}$
f_{O2} (*atm*)	0.2	0.2	0.2	0.2	0.2
Na^+ (*mg/kg*)	226	0.4	25	25	226
K^+ (*mg/kg*)	7.85	0.2	2	2	7.85
Mg^{2+} (*mg/kg*)	60.5	0.1	20	20	60.5
Ca^{2+} (*mg/kg*)	209	1.4	70	70	209
Fe^{2+} (*mg/kg*)	0.10	1×10^{-8}	0.10	0.10	0.10
Fe^{3+} (*mg/kg*)	0.01	1×10^{-8}	0.01	0.01	0.01
UO_2^{2+} (*mg/kg*)	3.14	1×10^{-32}	1×10^{-6}	1×10^{-6}	3
SiO_2 (aq) (*mg/kg*)	12	1×10^{-8}	10.7	10.7	12
Cl^- (*mg/kg*)	84 (810)[1]	0.41 (0.61)[1]	11	11	84 (68)
NO_3^- (*mg/kg*)	0.03	1.20	0.03	0.03	0.03
SO_4^{2-} (*mg/kg*)	1500	3.0	315 (1210)[1]	315 (260)[1]	1100
Al^{3+} (*mg/kg*)	0.013[2]	1×10^{-8}	0.013[2]	0.013	0.013

[1]() indicates concentration after charge balance. These new concentrations are well within the range reported at the Naturita site.
[2]Concentration of Al^{3+} that is in equilibrium with low-Fe-Mg smectite.

The 2-D conceptual model examines a somewhat different application, where contaminant is leached from a point source into the uncontaminated groundwater. This scenario is representative of the processes associated with the initial development of a uranium groundwater plume. For this second model, the initial groundwater composition is characteristic of those reported at wells upstream from the uranium mill-tailings at the Naturita site. This groundwater composition is assumed to be constantly flowing through the domain. An injection well in the model represents a point source of contamination from which leachate with the composition of the currently contaminated groundwater at the Naturita site is injected into the system.

In order to investigate the effects of adsorption constant uncertainty on uranium migration, the soil in both the 1-D and 2-D conceptual models is represented by a clay mineral, smectite (2.5% by volume), and an inert solid (97.5%). The precipitation and dissolution of other phases like hydrous ferric oxide and gypsum that might occur in this system are neglected. In addition, our model only considers uranium adsorption to one solid phase although uranium may adsorb to several solid phases at the Naturita site, such as ferrihydrite. The mineral selected as a representative clay substrate, is a low-Fe-Mg smectite, with a composition given by $Na_{0.15}Ca_{0.02}K_{.2}Mg_{0.9}Fe_{0.45}Al_{1.25}Si_{3.75}O_{10}(OH)_2$, that forms according to the following fundamental reaction:

$$0.29\ Fe^{2+} + 0.16\ Fe^{3+} + 0.02\ Ca^{2+} + 0.2\ K^+ + 0.15\ Na^+ + 0.9\ Mg^{2+} + 1.25\ Al^{3+} + 3.75\ SiO_2(aq) + 4.5\ H_2O \leftrightarrow 7\ H^+ + Na_{0.15}Ca_{0.02}K_{.2}Mg_{0.9}Fe_{0.45}Al_{1.25}Si_{3.75}O_{10}(OH)_2 \quad (2.2)$$

with an association constant of $10^{-11.5537}$ (log K = -11.5537) at 25°C that is reported in the thermodynamic database contained in Geochemist's Workbench 3.0 (Bethke, 1998). Smectite is a layered sheet aluminosilicate containing thin platelets of alumina octahedra and silica tetrahedra coordinated to interlayer cations (i.e., Na^+, K^+, Ca^{2+}, Fe^{2+}, Fe^{3+}, and Mg^{2+}).

Recent molecular modeling of cesium adsorption on kaolinite (Cygan *et al.*, 1998), a simpler clay mineral, suggests that cesium adsorbs directly to the Al octahedra on the (100), (010), and (110) surface edges of kaolinite and is coordinated to four aluminols to form a strong inner-sphere complex. Similar reactive surface sites are suggested for the smectite clays. Zachara and McKinley (1993) and McKinley *et al.* (1995) fit bulk data for uranyl adsorption onto smectite minerals using a computational model that includes fixed-charge sites and edge aluminum hydroxyls. A different surface complexation model, the triple-layer model (TLM, Davis and Leckie, 1978, Davis *et al.*, 1978), was applied to edge-site complexation. The uranyl adsorption data is consistent with a surface speciation scheme dominated by ion exchange and aluminol edge complexation ($>AlOUO_2^+$, where > indicates that the species is bound to the surface). More recent spectroscopic work (Hennig *et al.*, 2002) also suggests that uranyl adsorption occurs preferentially to aluminol groups on montmorillonite. Therefore, as a first approximation, we assume that the uranyl cation only binds to the Al surface sites of smectite.

These surface sites are divided into two groups with different characteristics based on whether they occur on the basal planes or edges of smectite (Fig. 2.1). Following Pabalan *et al.* (1998), who developed a model for the adsorption of uranyl onto montmorillonite derived from experimental data, we assume a total surface site density of 2.53 sites/nm^2, similar to the value of 2.3 sites/nm^2 recommended by Davis and Kent (1990) for all minerals and by Dzombak and Morel (1990) for ferrihydrite.

For ferrihydrite, Dzombak and Morel (1990) used two different types of surface sites – high affinity and low affinity -- to fit metal adsorption data with the DLM. For ferrihydrite, the high-affinity surface sites are much less abundant (0.06 sites/nm^2) than the low-affinity sites. For the mineral in our system, low-Fe-Mg smectite, the surface sites on the platelet edges have a higher affinity for cation adsorption (e.g., UO_2^{2+}) and a higher site density (see Fig. 2.1). Following Pabalan *et al.*'s (1998) approach for another clay mineral, montmorillonite, we assumed a total surface area (100 m^2/g) for smectite. The surface area for smectite edges (10 m^2/g) is much smaller than for the basal planes (90 m^2/g) (Brady *et al.*, 1998; Schlegel *et al.*, 1999); however, we did not take this difference in surface area into account in these calculations. Therefore, our hypothetical smectite exhibits a much larger capacity for uranyl adsorption than expected for the actual mineral.

The edge Al surface sites are amphoteric in nature and, depending on the pH of the solution, they can protonate and deprotonate to form charged surface sites. For example, a neutral Al edge surface site [$>(e)AlOH$] gains or loses a proton to create a positively-charged (z_q =1) or negatively-charged (z_q = -1) surface species, according to the following reactions within the context of the DLM:

$$>(e)AlOH + H^+ \leftrightarrow >(e)AlOH_2^+; \quad K = \frac{m_{>(e)AlOH_2^+}}{m_{>(e)AlOH} a_{H^+}} 10^{(+F\Psi/2.303RT)} \qquad (2.3a)$$

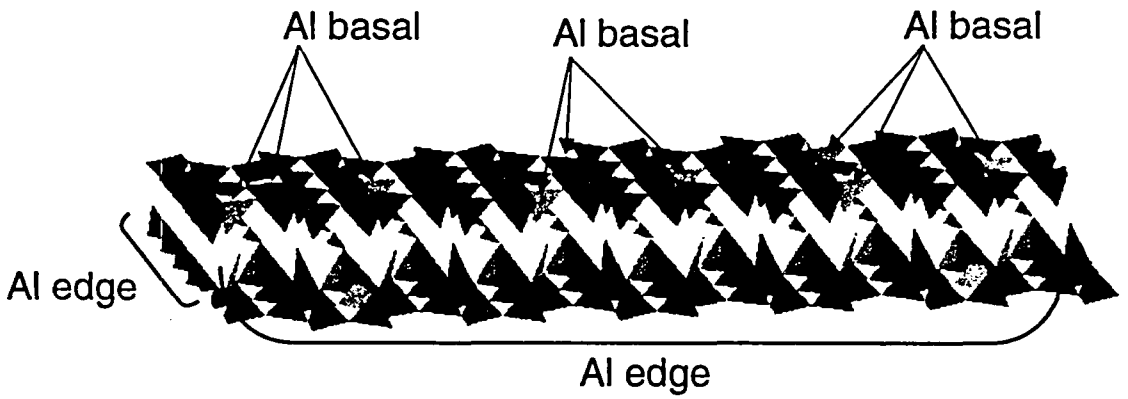

Surface Area		100 m^2/g
	Low Affinity Site	**High Affinity Site**
Site Density (sites/nm^2)	0.23	2.3
Surface Species	**Log *K* of Formation**	
$>AlOH_2^+$	-8.33*	-8.33*
$>AlO^-$	1.00	9.73*
$>AlOUO_2^+$	-4.00	-2.70*

*From Pabalan *et al.* (1998)

Figure 2.1 Aluminum surface sites found on a platelet of clay mineral. Two types of Al surface-sites, basal plane tetrahedral Al sites and edge octahedral Al sites are present. The site densities assumed for both the basal plane and edge of smectite, and the adsorption constants associated with each site-type are tabulated.

$$>(e)AlOH \leftrightarrow >(e)AlO^- + H^+; \quad K = \frac{m_{>(e)AlO^-} a_{H^+}}{m_{>(e)AlOH}} 10^{(-P\Psi/2.303RT)} \tag{2.3b}$$

where all variables have been previously defined. Analogous equations can be written for protonation and deprotonation of the basal Al surface sites [>(*b*)*AlOH*] but experimental evidence suggests that only deprotonated sites exist on this surface for most conditions (Zhang *et al.*, 2001). In our model, only two surface complexes with uranium are considered, $>(e)AlOUO_2^+$ and $>(b)AlOUO_2^+$, where uranium adsorbs to the edge (*e*) and basal (*b*) surface sites respectively. Each of these complexes forms according to the following type of reaction

$$>AlOH + UO_2^{2+} \leftrightarrow\!> AlOUO_2^+ + H^+; \quad K = \frac{m_{>AlOUO_2^+} a_{H^+}}{m_{>AlOH} a_{UO_2^{2+}}} 10^{(+P\Psi/2.303RT)} \tag{2.4}$$

Other types of uranyl surface complexes may be present on clay surfaces in the subsurface environment. In particular, uranyl carbonate and bicarbonate surface complexes are expected to play an important role in uranium attenuation in carbonated groundwater (e.g., Waite *et al.*, 1994; Thompson *et al.*, 1998). Recent spectroscopic studies suggest that uranyl adsorption

occurs as a bidentate inner-sphere complex (e.g., Sylwester *et al.*, 2000, Hennig *et al.*, 2002) on numerous mineral surfaces including montmorillonite at neutral pH values. Chisholme-Brause *et al.* (2001) found two uranyl surface complexes commensurate with an inner-sphere complex and exchange-site complex at pH values between 3 and 7 with low to moderate surface coverage, an outer-sphere complex at low pH (3.7 and 4.4), and a polymeric hydroxide-like sorption complex at moderate surface coverage. Uranium adsorption may occur by the formation of different uranyl complexes as a function of pH and surface loading. Uranyl adsorption may also occur in combination with different ligands (e.g., UO_2CO_3, $UO_2HCO_3^+$, $UO_2NO_3^+$, UO_2SO_4) depending on the solution composition. In this study, we want to investigate the sensitivity of calculated uranium migration to uncertainties in adsorption constant values. Therefore, we have limited our model to including only two simple uranyl surface complexes, $>(e)AlOUO_2^+$ and $>(b)AlOUO_2^+$ and examine the variability of the K given in equation (2.4) for the formation of $>(e)AlOUO_2^+$. This is undoubtedly a simplification of the retardation processes that occur at a uranium mill tailings site like Naturita; however, our model is more than sufficient to develop an appreciation of the importance of adsorption constant values in reactive/transport models.

Following Pabalan *et al.* (1998), the optimal (mean) acidity constants for surface protonation and deprotonation on the Al edge sites are assumed to be equivalent to those for corundum (Turner and Sassman, 1996). Also, the optimal uranyl adsorption constant for the Al edge sites is taken to be equivalent to that for Al edge sites on montmorillonite (Pabalan *et al.*, 1998). Adsorption on the basal surface of a clay mineral is independent of pH and is ascribed to the negative charge associated with the substitution of aluminum for silicon in the tetrahedral sheet (Brady *et al.*, 1996). Therefore, for the Al basal sites, the protonation constant was set equal to that for the edge sites and the deprotonation constant was assigned a low value to ensure that these sites remain deprotonated over the pH range (i.e., pH 5.8 to 8.0) considered in the simulations. The reactivity of the basal aluminol sites for a clay mineral is considerably less than that of the edge sites (e.g., Brady *et al.*, 1996). Therefore, for uranyl adsorption to the basal planes, an equilibrium constant was selected such that adsorption is less than onto on the smectite edges, but large enough to provide a non-zero baseline for uranium adsorption plots. This non-zero baseline is observed experimentally and attributed to ion-exchange in the clay interlayer (Chisholme-Brause *et al.*, 2001; Hyun *et al.*, 2001).

2.5 One-Dimensional Simulations

To examine the influence of adsorption constant values on the conceptual geochemical models, we now focus on a series of 1-D simulations. We first discuss the effect of grid spacing on the numerical solution. Next, we consider the uncertainty associated with adsorption constants and their influences on transport. The 1-D system considered here consists of a 500 m long domain. We introduce rainwater through the upstream boundary which was subject to a recharge rate of 20 m/yr, representative of the groundwater flux at Naturita. The annual precipitation at Naturita is approximately 33 cm (Kohler *et al.*, 2004). We exaggerate the influence of the rainwater in order to examine its potential to alter the subsurface environment. The downstream boundary is assumed to be open. The aquifer is initially contaminated (see the groundwater compositions in Table 2.2), where uniform aquifer porosity and permeability of 0.2 and 3.12×10^{-13} m^2 respectively were used throughout the domain. The coefficient of molecular diffusion used is the default value in Xt, 10^{-6} cm^2/sec and the longitudinal dispersivity was chosen to be 5 m. Simulations were performed for model times up to 20 years.

2.5.1 Effect of Grid Spacing on Numerical Solution

Figure 2.2 illustrates concentration versus distance profiles for uranium in fluid over a 5 year period, using grid spacings Δx of 5, 2.5, and 1.25 m, where the concentration has been normalized to C/C_0. Here, C is the uranium concentration in ppm and C_o is the initial concentration in the contaminated groundwater in ppm. The continuous influx of rainwater dilutes the contaminated groundwater such that, after approximately 4 years at a distance of about 380 m, the normalized concentration has been reduced by over 50%. More importantly, however, the profiles of uranium concentration versus distance are similar for all three Δx values. This suggests that for the system considered here, the numerical solution is relatively insensitive to the choice of grid spacing. Therefore, we allow the grid spacing to be 5 m in subsequent 1-D simulations in order to efficiently use our computational resources. We note that, for Δx=5 m, the grid Peclet number (i.e., $P_e=\Delta x/\Delta_L$) is equal to one, which is well within the customary constraint of $P_e \leq 2$ (e.g., see Frind and Germain, 1986).

2.5.2 Baseline Case for 1-D Simulations

The geochemical system that we are examining includes (1) the mixing of rainwater with contaminated groundwater, (2) a mineral, smectite, that is allowed to dissolve and precipitate in the simulations, and (3) surface site speciation including protonation, deprotonation, and the adsorption of uranium to two different types of surface sites. This system is sufficiently complicated to warrant discussion, prior to examining the effects of uncertainty in log K >(e)AlO^- and log K >(e)$AlOUO_2^+$.

The first point to note is that the scenario that we are examining is one in which the groundwater/soil system is pre-contaminated and the simulation exposes this pre-contaminated system to clean rainwater. From field data, we know that 3 ppm represents the upper limit of observed aqueous uranium concentrations at the Naturita site (Kohler *et al.*, 1994; Curtis *et al.*, 2004). Using the log Ks established from the literature (see Fig. 2.1), we calculated that in our initial equilibrated system, over 1150 mg/kg uranium must be adsorbed to smectite for 3 ppm uranium to be present in solution. The high concentration of uranium adsorbed is due to the high concentration of high-affinity or edge surface sites used in our calculations (2.3×10^{20} sites/gm smectite). Uranium desorption makes a significant contribution to uranium concentrations in solution over time. However, during the 20-year simulation, 99% of the uranium remains adsorbed throughout the simulation domain. The contaminated groundwater has much higher leachate-like uranyl concentrations than the rainwater. Therefore the concentration profiles illustrate initially high concentrations of uranium being replaced by lower ones (Fig. 2.2). This is the opposite of a typical simulation starting with a pristine groundwater and introducing a contaminated plume.

The second point is that smectite dissolution and precipitation occurs as a result of changes in solution composition. Our simulations are designed so that smectite is always present and in equilibrium with the solution, however there is enough smectite available to allow for small changes in smectite concentration, without becoming undersaturated with this solid phase. In

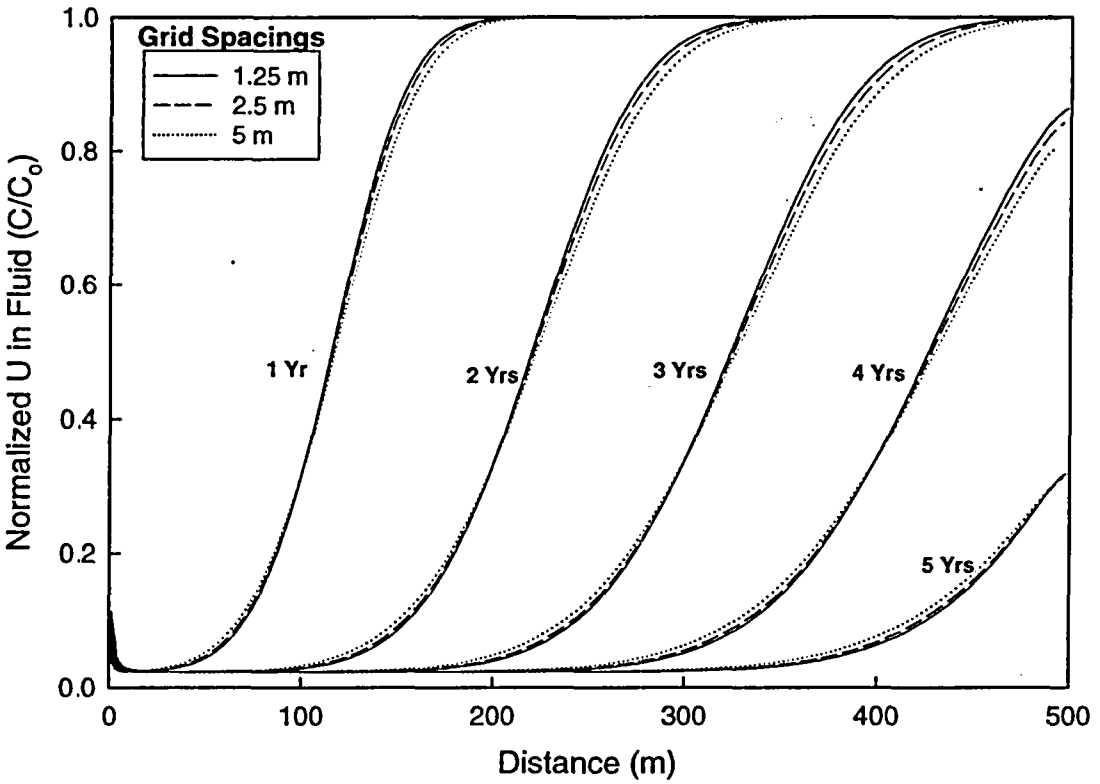

Figure 2.2 Effect of grid spacing on uranium in fluid profiles, as a function of time, using X1t. Solid, dashed, and dash-dot lines respectively refer to a grid spacing of 5, 2.5, and 1.25 m, where all simulations are performed using the mean log *K* values for >(e)AlO^- and >(e)$AlOUO_2^+$.

this simulation, smectite dissolution occurs as rainwater displaces groundwater. From equation (2.2), it can be seen that a decrease in the pH from 7 (that of the contaminated groundwater) to 5.8 (that of the rainwater) will favor smectite dissolution. Smectite dissolution will in turn increase the pH. In 20 years, the volume % of smectite changes from 2.5 to 2.4 at the inlet, and minor smectite dissolution is calculated to occur only in the first 50 m of the streamtube. Fig. 2.3a illustrates that the pH at the inlet of the streamtube is influenced by both of these processes, resulting in a minor increase in pH followed by a minor decrease in pH in the first few elements of the streamtube. The size of the elements influences the shape of this curve; the larger they are, the greater this pH variation is dampened by the dominance of the subsurface groundwater and smectite system. The pH variation and smectite dissolution would also be substantially reduced if the influx of rainwater was reduced to reflect a more typical annual precipitation rate.

Although only a small volume of smectite dissolves relative to the total smectite present, the dissolution of smectite releases uranium into solution affecting the calculated fluid concentration of uranium. This is illustrated in the concentration versus distance profiles (Fig. 2.2) by the small increase in uranium concentration in solution at the boundary between the groundwater/smectite system and the influent rainwater. The dissolution of smectite decreases the available surface area and number of surface sites available for uranyl adsorption; therefore uranium is released into solution along with the iron, calcium, potassium, sodium, magnesium, aluminum, and silica that make up the smectite mineral itself. This influx of uranium into solution from smectite

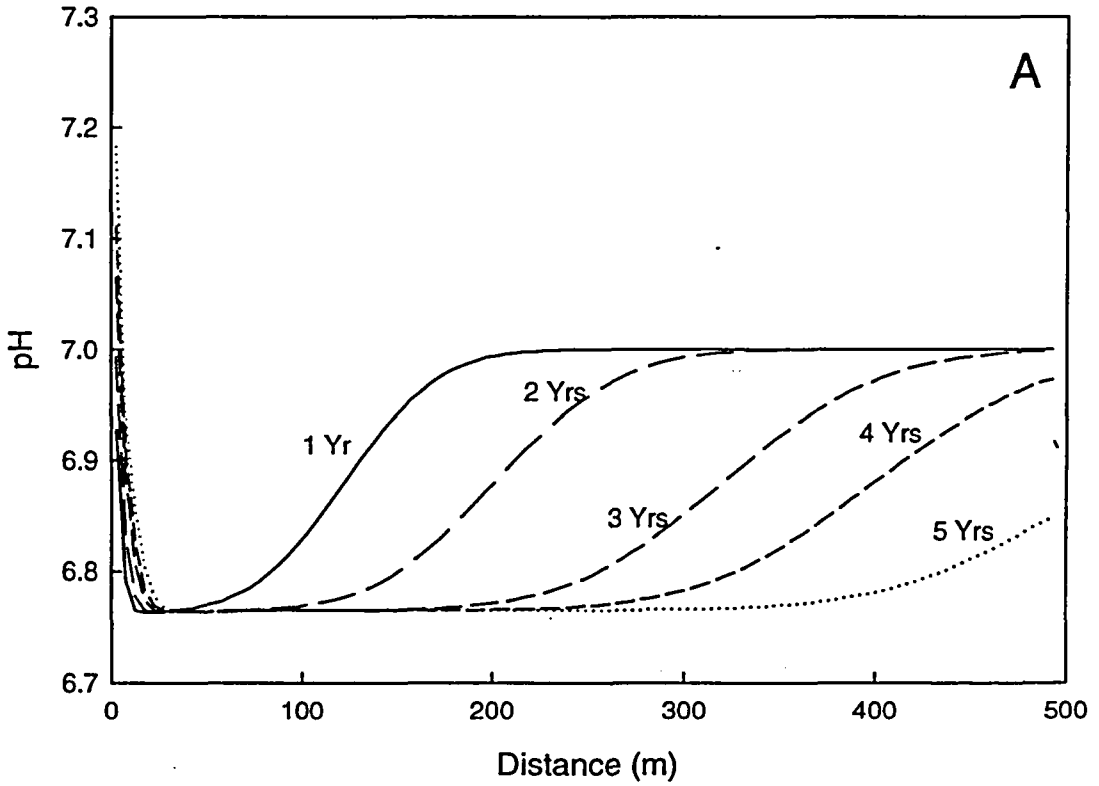
A
pH
7.3
7.2
7.1
7.0
6.9
6.8
6.7
0
100
200
300
400
500
Distance (m)
1 Yr
2 Yrs
3 Yrs
4 Yrs
5 Yrs

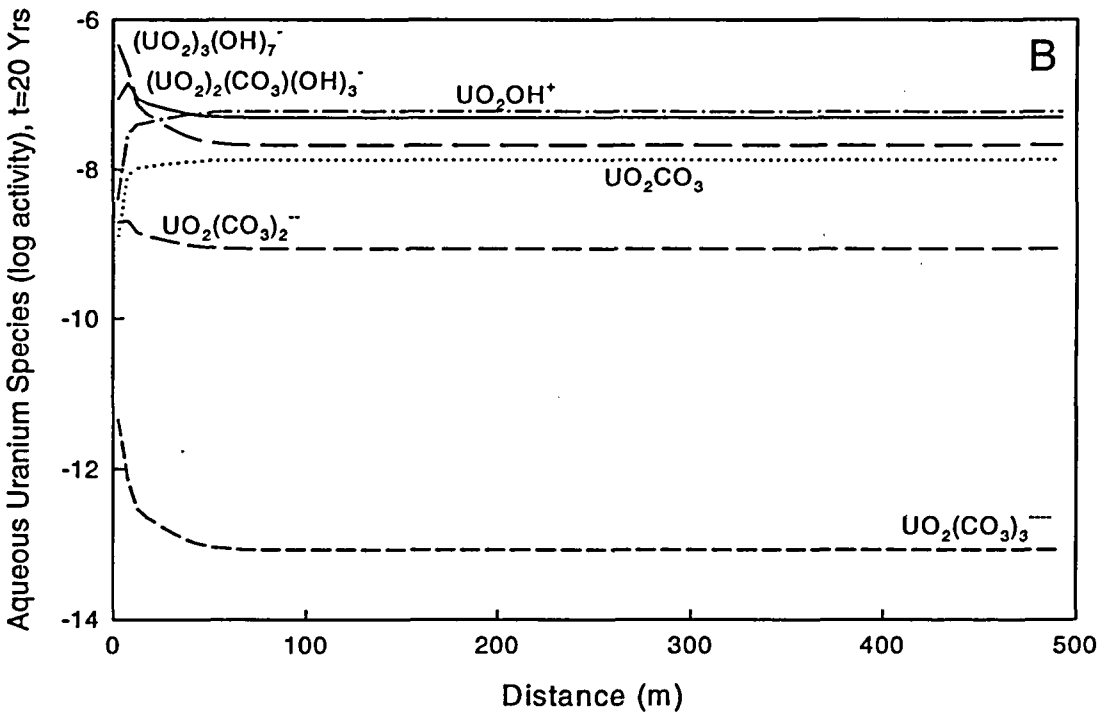
B
Aqueous Uranium Species (log activity), t=20 Yrs
-6
-8
-10
-12
-14
0
100
200
300
400
500
Distance (m)
$(UO_2)_3(OH)_7^-$
$(UO_2)_2(CO_3)(OH)_3^-$
UO_2OH^+
UO_2CO_3
$UO_2(CO_3)_2^{--}$
$UO_2(CO_3)_3^{---}$

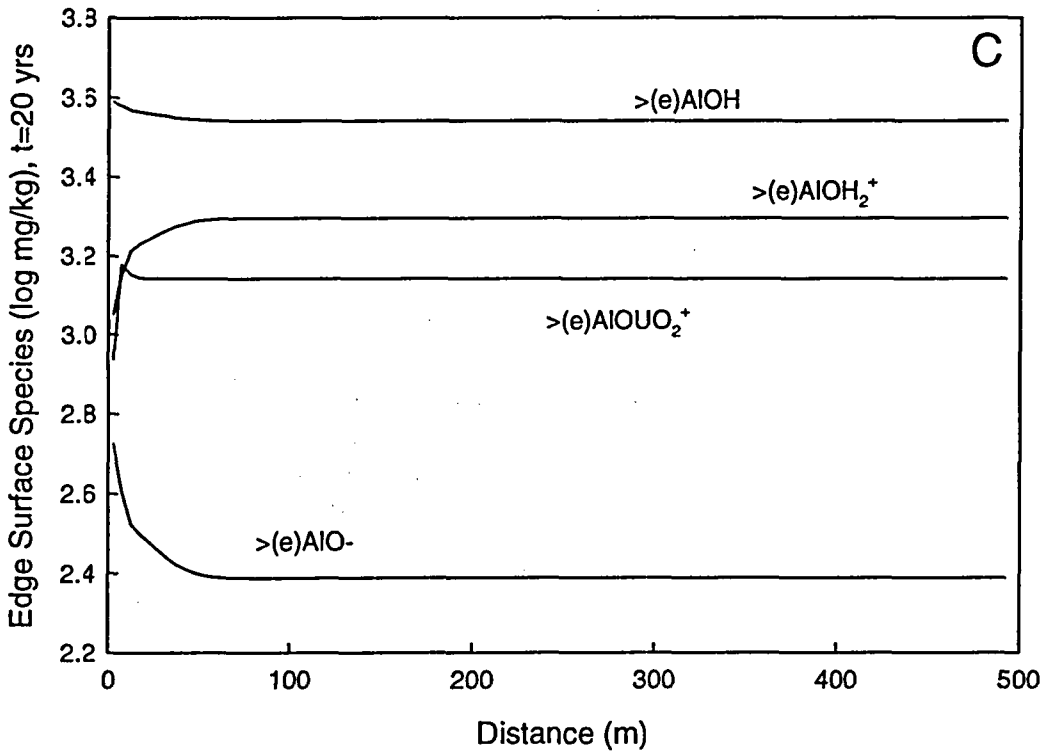

Figure 2.3 Baseline Case (a) pH versus distance, (b) dominant aqueous species of uranyl calculated to be present after 20 years of rainwater infiltration, (c) surface complexation of smectite edge sites after a 20-year simulation.

dissolution occurs at the same time as rainwater, with no dissolved uranium, displaces contarninated groundwater. For this baseline case, the two processes counteract each other, so that the concentration of uranium in solution is not dramatically affected at the boundary.

The displacement of one fluid by another (i.e., contaminated groundwater by the inlet rainwater) with different pH, different pCO_2, and different concentrations of cations and anions, changes the predominant uranyl species in solution as a function of distance and time in the streamtube. Based on the thermodynamic database in X1t, the predominant aqueous uranyl species in the contarninated groundwater are $(UO_2)_2(CO_3)(OH)_3^-$(47.3%), $UO_2(CO_3)_2^{2-}$(43.6%), and UO_2CO_3 (7.5%). With mixing, the predominant uranyl species in solution at the boundary become $(UO_2)_3(OH)_7^-$, $(UO_2)_2(CO_3)(OH)_3^-$, and UO_2OH^+ (Fig. 2.3b). The predominant surface species remain relatively constant throughout the simulation. The edge surface species in order of decreasing abundance are >(*e*)*AlOH*, >(*e*)*AlOH*$_2^+$, >(*e*)*AlOUO*$_2^+$, and >(*e*)*AlO*$^-$ (Fig. 2.3c). The basal plane surface species in order of decreasing abundance are >(*b*)*AlO*$^-$, >(*b*)*AlOUO*$_2^+$, >(*b*)*AlOH*, and >(*b*)*AlOH*$_2^+$.

A final point to make here is that as Table 2.2 indicates, the Cl^- (mg/kg) concentration in the initial contaminated groundwater was increased from our input estimate of 84 mg/kg to 810 mg/kg in order to charge balance our initial groundwater/smectite system. This new concentration of Cl^- (mg/kg) is well within the range of Cl^- concentrations reported at the Naturita site. Concentration versus distance profiles for Cl^-, the charge-balancing component, and Na^+, an unmodified tracer in the system, are identical, indicating that this initial change in Cl^-

concentration is carried throughout the simulation, and providing a check on the mass balance of the system.

2.5.3 Uncertainty Analysis: Latin Hypercube Sampling

Uranyl adsorption is expected to be predominantly a function of the equilibrium constants for $>(e)AlOUO_2^+$ and $>(e)AlO^-$ (Pabalan *et al.*, 1998). For this reason, we investigate the uncertainty in these two constants. The range of equilibrium constant values was chosen to be comparable to the range of surface protonation and deprotonation constants found by Hayes *et al.* (1991) who, using the DLM, fitted surface titration data for goethite, corundum, and rutile using total surface site densities of 1, 10, and 100 sites/nm^2. Fitted (de)protonation constants varied by over three log units to compensate for the variance in site density. The study by Hayes *et al.* (1991) remains the only investigation that thoroughly examined variable sensitivity within the DLM. Accordingly, for our sensitivity analysis, we varied the equilibrium constants for $>(e)AlOUO_2^+$ and $>(e)AlO^-$ approximately over three orders of magnitude.

To analyze the influences of adsorption constants on the numerical reactive-transport results, we used the Latin Hypercube Sampling (LHS) technique to generate normally distributed pairs of log K values. Unlike simple Monte Carlo approaches where samples are randomly generated, LHS employs a constrained sampling scheme (e.g., Iman and Shortencarier, 1984). On the basis of equal probability, the LHS technique generally divides the range of each variable (e.g., two log K's in our case) into n non-overlapping intervals. For a given probability density function (e.g., normal distribution), one random value from each interval is then selected. Subsequently, the n values obtained for one variable are paired with n values for the other variable, thus forming the n pairs of random values. Figure 2.4 presents 100 pairs of normally distributed log K's for $>(e)AlO^-$ and $>(e)AlOUO_2^+$, generated using the LHS software package developed by Wyss and Jorgensen (1998). Here the mean log K values for $>(e)AlO^-$ and $>(e)AlOUO_2^+$ are respectively chosen to be 9.73 and –2.7, and we used a $\Delta \log K = 0.75$ to represent one standard deviation from the mean log K. In the next section, we discuss the consequences of the log K variations (i.e., uncertainty) on our 1-D conceptual model.

2.5.4 Results of Uncertainty Analysis

The log $K>(e)AlO^-$ and log $K>(e)AlOUO_2^+$ variations for the 100 simulations yield different adsorbed uranium concentrations, as well as different distributions of aqueous species for the initial conditions of each transport simulation. The total uranium concentration in the system is 1200 ppm. Using the mean log K values for both surface species, the equilibrium concentration of uranium in solution is 3.14 ppm, well within the range observed at the Naturita site. For the 100 pairs of log K values used in the simulations, the initial uranium in solution varies from 2.5 x 10^{-4} ppm to 1100 ppm ($C_o = 180 \pm 290$ ppm). As Figs. 2.5a and b illustrate, while this initial aqueous uranium concentration is a strong function of log $K>(e)AlOUO_2^+$, it is less dependent upon the choice of log $K>(e)AlO^-$. The range of initial uranium concentrations in solution is significant, particularly considering that the MCL (maximum concentration level) is 0.03 ppm (USEPA, 2001). Again, however, this hypothetical smectite has 90 m^2/gm more edge surface area than estimated for clay minerals; therefore, the uranium concentrations in the system are

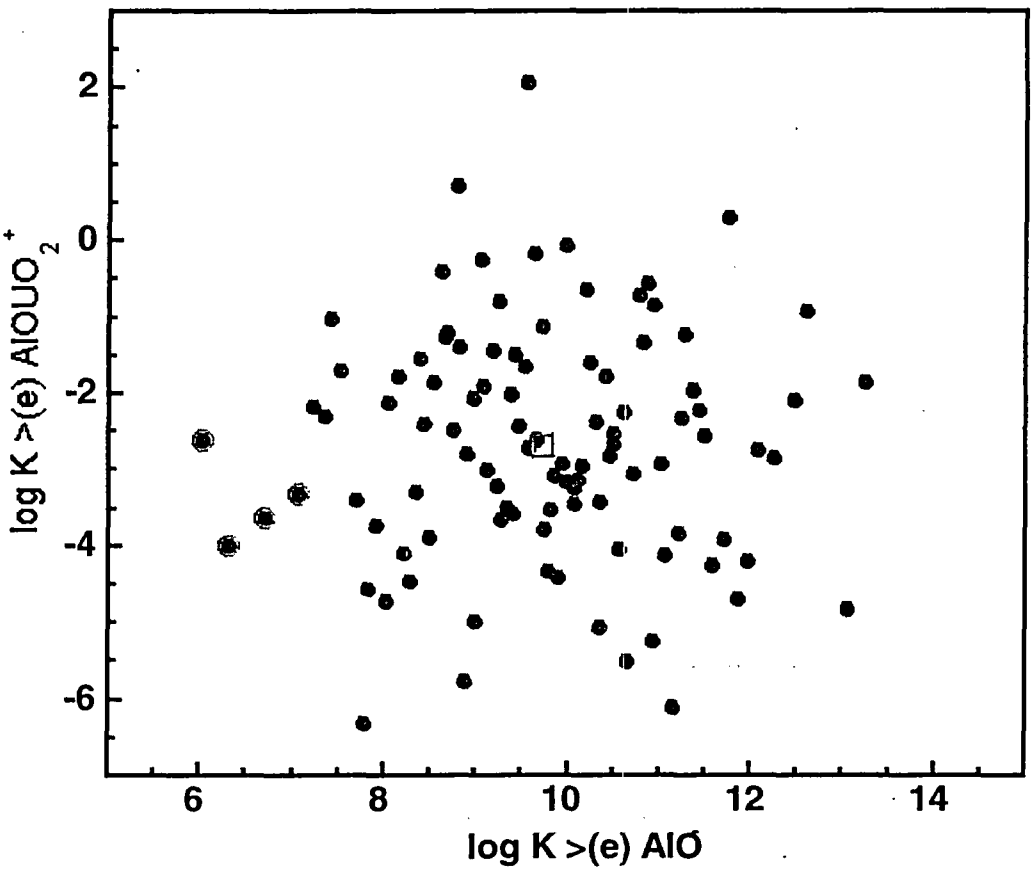

Figure 2.4 Log K variation for >(e) $AlOUO_2^+$ versus those of >(e) AlO^- for 100 pairs of values generated using Latin Hypercube Sampling technique. The value for the mean log K pair is shown with an open square and the open circles around four of the samples indicate the simulations that failed to run due to convergence problems.

exaggerated compared to those possible at a uranium mill tailings site like Naturita.

In order to analyze differences in concentration profile behavior, we have normalized the results of each simulation to the initial uranium concentration in aqueous solution (C_0) for that simulation. We find that the results can be generally divided into two main groups: Group A, in which the calculated concentration versus distance profiles exhibit a uniform concentration front (e.g., similar to those seen in Fig. 2.2) and Group B in which the profiles exhibit a sharp spike in uranium concentration at the inlet followed by an undulation in uranium concentration with distance. Representative profiles for these two different types of response are illustrated in Figs. 2.6a and b for various simulation times. We note that, while the calculated profiles of concentration versus distance represent the amount of uranium in solution, they fail to emphasize that the majority of the uranium present in the system often remains adsorbed onto the clay throughout the simulation. For example, for log K >(e)AlO^- = 11.71 and log K >(e)$AlOUO_2^+$ = -3.92, the initial equilibrium distribution of uranium is 0.11 mg/kg uranium in solution and over 1050 mg/kg uranium adsorbed. After two years of simulated time, the uranium in solution drops to below 0.01 mg/kg near the inlet while the uranium adsorbed remains approximately the same (1055 mg/kg) throughout the 1-D domain. On the other hand, in some

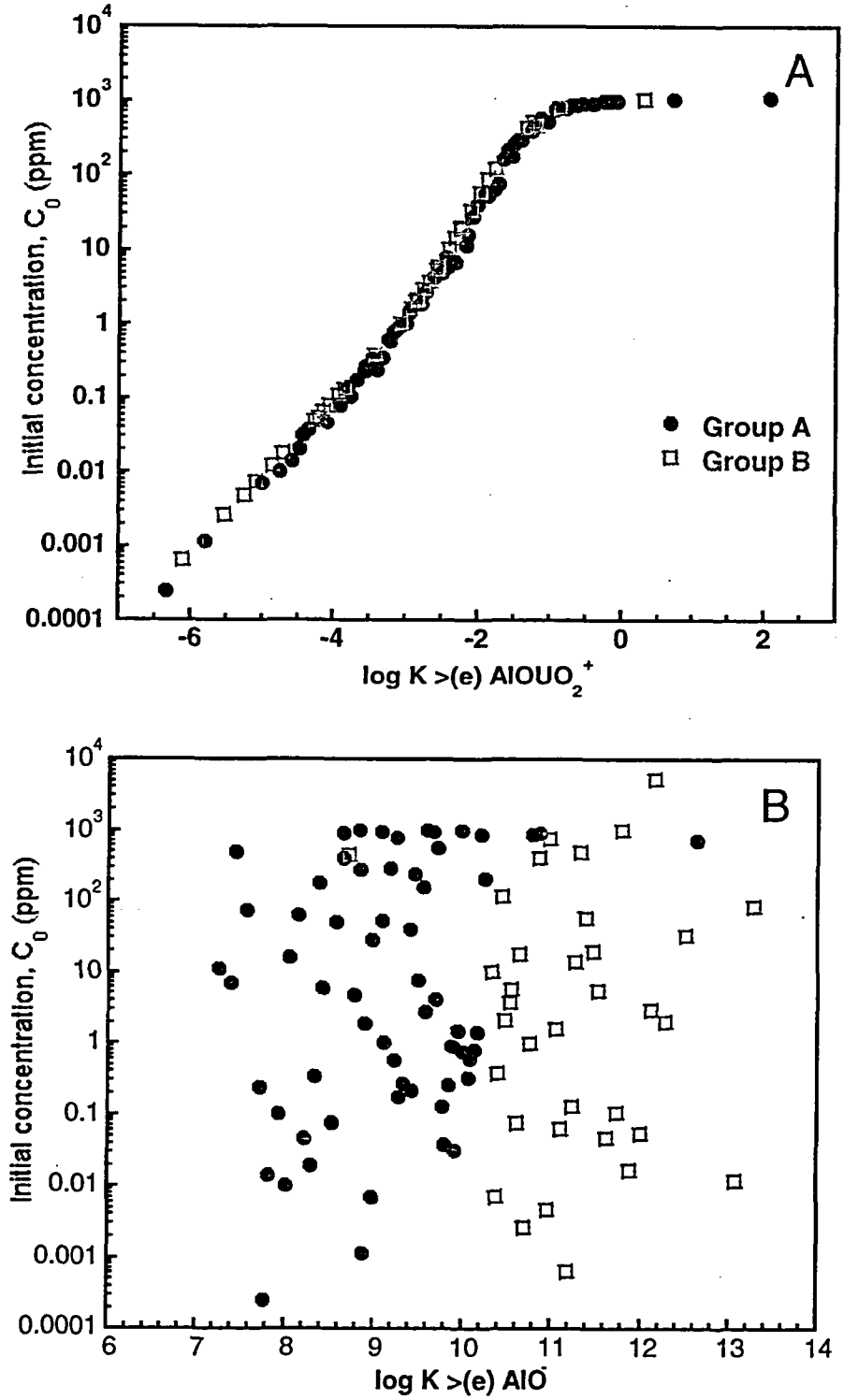

Figure 2.5 Initial concentrations for uranium in fluid versus (a) log K>(e) $AlOUO_2^+$ and (b) log K>(e) AlO^-. The concentrations are divided into two groups, A and B, because the 100 pairs of log K values sampled (see Fig. 2.3) lead to two distinctly different types of concentration profile behavior (see Fig. 2.7).

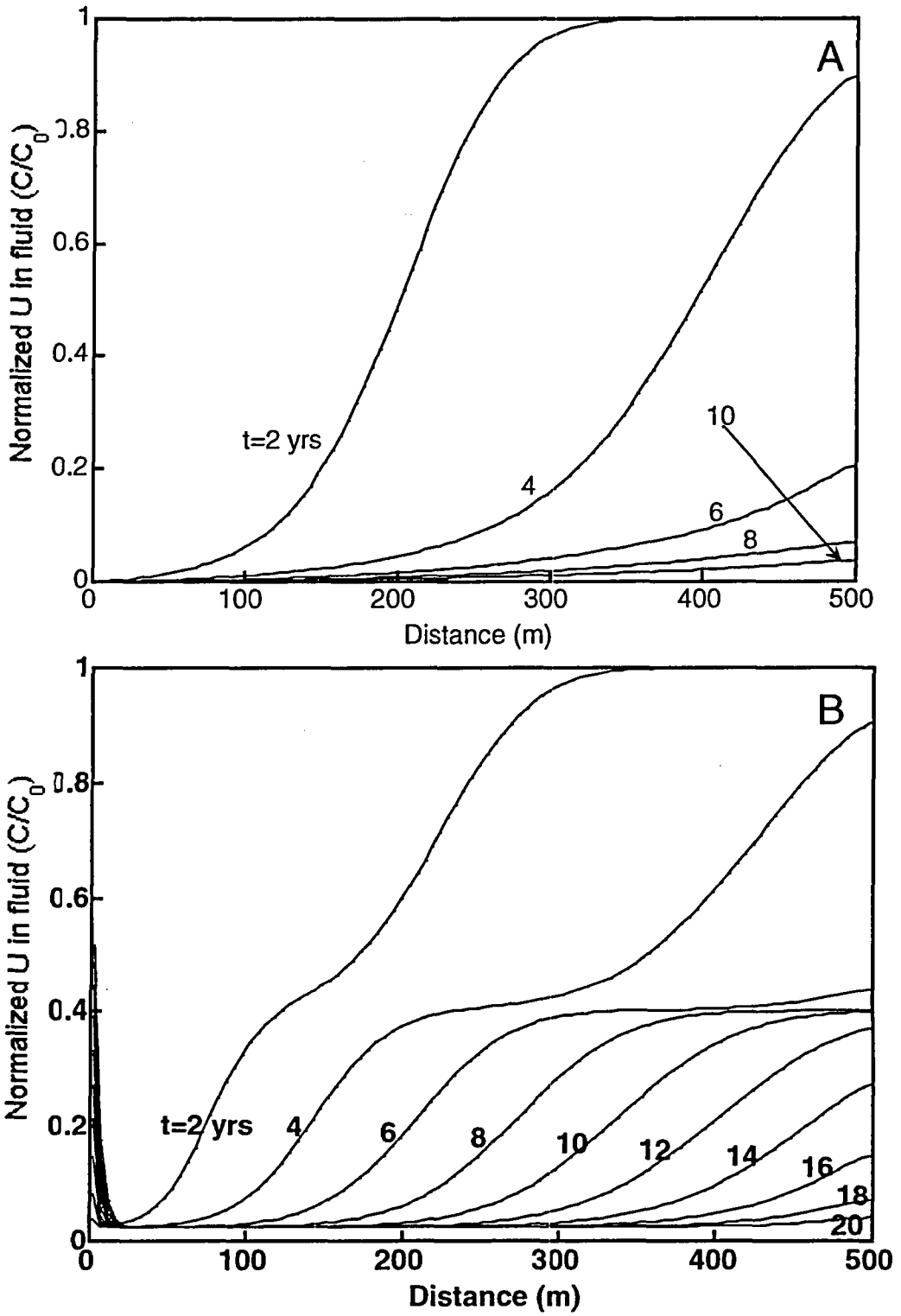

Figure 2.6 Temporal development of concentration profiles for aqueous uranium typical of (a) group A and (b) group B. Note that the log *K* values chosen for this Group A simulation result in a smaller fraction of uranium in solution than the baseline case illustrated in Fig. 2.2.

simulations, the uranium present is more equally distributed between the solution and the smectite surface; for example, for log $K>(e)AlO^-$ = 9.72 and log $K>(e)AlOUO_2^+$ = -1.14, the initial uranium concentrations are 560 mg/kg in solution and 490 mg/kg adsorbed.

Figure 2.7 illustrates the simulated concentration profiles, after two years of rainwater infiltration into the system, for 96 different pairs of log K values (as indicated on Fig. 2.4, four out of the 100 simulations failed to run to completion due to convergence problems). These concentrations profiles can again be clearly separated into two groups: Group A in which the $0.5C/C_0$ occurs approximately 200 m downstream from the inlet (Avg. $0.5C/C_o = 214 \pm 31$ m), and Group B in which $0.5C/C_0$ occurs closer to the inlet boundary (121 ± 49m). The baseline case discussed in detail above exhibits Group A behavior. Because of the choice of log K values in Group B, the two processes of uranium dilution by the influx of rainwater and the influx of uranium into solution from smectite dissolution, do not counteract each other as they did in the baseline case. Therefore, a sharp increase in aqueous uranium concentration is calculated at the inlet, followed by readsorption immediately downstream.

Interestingly enough, the same two-group responses can also be seen over all simulation times. For instance, Fig. 2.8 depicts the breakthough curves at the downstream boundary. While we can clearly distinguish the two groups, C/C_0 for most of Group A cases is less than 0.2 after about 6 years while there is generally a decreasing trend in the uranium concentration over the entire 20-year simulation for Group B. However, for a number of simulations, C/C_0 reduces to approximately 0.7 after about 6 years, following which it either remains unchanged or displays a slight increasing trend (see the five upper-most curves in Fig. 2.8). Because there are clearly two different concentration versus distance profile behaviors exhibited by Groups A and B, we

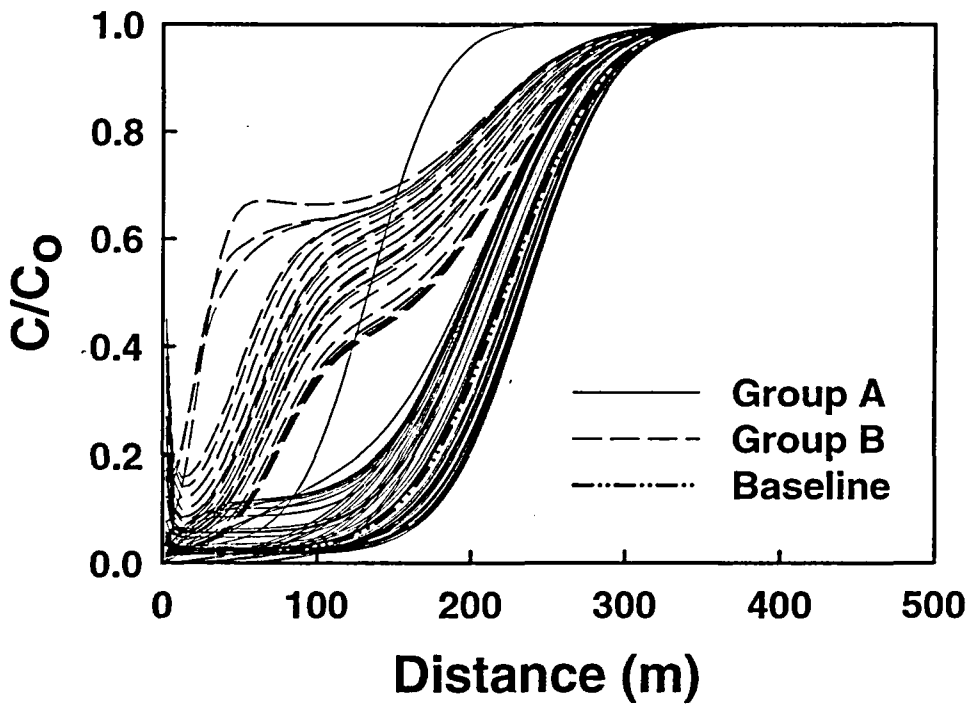

Figure 2.7 Normalized concentrations versus distance profiles of uranium in fluid versus distance, after 2 years, for 96 realizations. The profile for the baseline case (i.e., using mean log K values) is also indicated.

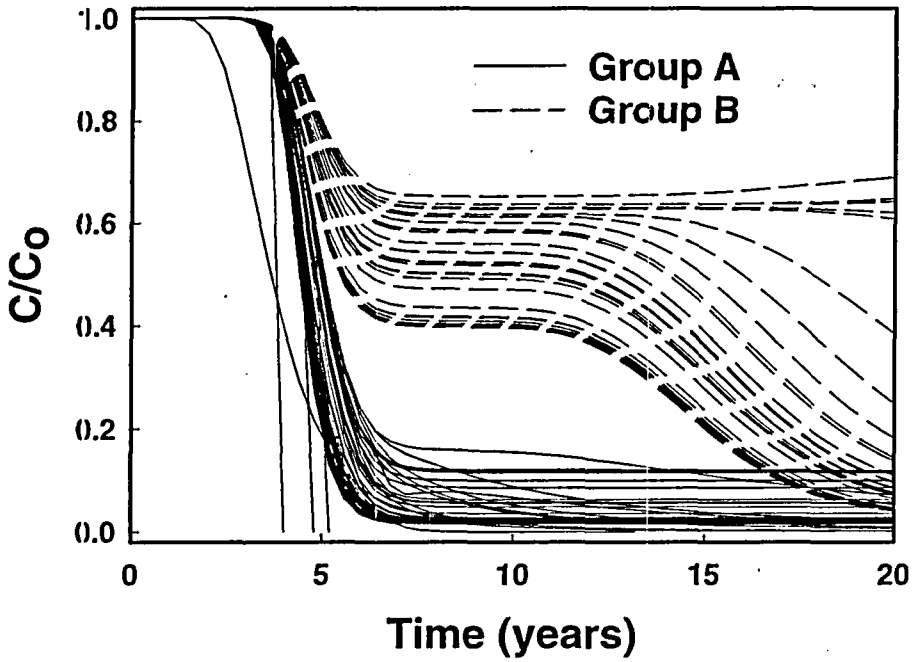

Figure 2.8 Breakthrough curves at the down-stream boundary, illustrating the variations of the normalized uranium concentration as a function of time, for the profiles in Fig. 2.7. The curves that abruptly drop after ~3-5 years indicate several simulations that did not run to completion (i.e., 20 years).

decided to check the effect of grid spacing on the numerical solution of a Group B simulation in the same way that we analyzed its effect on the concentration profiles calculated using the optimum (mean) log *K*'s (see Section 2.5.1, Fig. 2.2). Using grid spacings Δx of 5, 2.5 and 1.25 m we found that the concentration profiles for the Group B simulation were also insensitive to grid spacing for 5-year simulations.

We also decided to evaluate whether the distinction between Groups A and B is correlated to the covariance between log K>$(e)AlO^-$ and log K>$(e)AlOUO_2^+$. In our LHS selections of log K values, we chose the log K>$(e)AlO^-$ value independently of the value for log K>$(e)AlOUO_2^+$. However, these two log *K* values are covariant parameters. Typically, the acidity constants in a surface complexation model are determined by calibration to experimental surface titration data. Then, holding these surface acidity values constant, the adsorption log *K*s are determined by fitting adsorption data. Equations (2.3b) and (2.4) and the corresponding mean log *K* values for these reactions can be combined to give the following:

$$> AlO^- + UO_2^{2+} \leftrightarrow > AlOUO_2^+; \log K = -12.43 \qquad (2.5)$$

We calculated this log *K* for each of our 100 LHS pairs of log *K* values for the formation of $>(e)AlO^-$ and $>(e)AlOUO_2^+$. Then we divided our database of 100 simulations into two groups based on whether or not this combined log *K* value fell (1) within 1 log unit of -12.43 or (2) within 2 log units of -12.43. In neither case, did these groups show any correspondence to Groups A and B. Using the original mean log *K* values, the difference between -log K>$(e)AlO^-$ and the combined log *K* for reaction (2.5) is 2.7. As a second test of the effects of log *K* covariance, we divided our simulation database into two groups based on whether or not this difference is

greater or less than 2.7. Again, no correlation between these groups and Groups A and B was found.

Referring back to Fig. 2.5b, it is clear that Groups A and B separate according to the log K $>(e)AlO^-$: The majority of breakthrough profiles in Group A are from simulations in which the log $K>(e)AlO^-$ values range from 7 to 10, while those in Group B result from simulations in which the log $K>(e)AlO^-$ values range from 10.5 to 13.5. These two groups cannot be distinguished by the log $K>(e)AlOUO_2^+$. High and low initial concentrations of uranium are present in both Groups A and B; therefore, although our initial concentrations vary much more than those observed at Naturita (Kohler *et al.*, 2004; Curtis *et al.*, 2004), this range in concentrations does not account for the difference in Group A and B behavior. This observation is also supported by plots of the distances measured from the inlet to the center of the concentration profile (i.e., at 0.5 C/C_o) after two years of mixing versus the log K values shown in Fig. 2.9. Again, the two groups demonstrate a marked dependence on the log $K>(e)AlO^-$.

These results suggest that surface protonation may be critical in determining the shape and rate of migration of uranium concentration profiles. Increasing the log K for the formation of the surface species $>(e)AlO^-$, increases the calculated concentration of H^+ in solution [see equation (2.3b)]. From equation (2.2), higher pH values favor the increased dissolution of smectite and the corresponding release of uranium into solution. This explains the higher aqueous concentrations of uranium at the boundary for simulations in Group B.

The aqueous complexation of uranium is very sensitive to the pH values encountered in the simulations (pH 5.8 to 8.0). While we only include two uranyl surface complexes, these complexes might actually form from any of the aqueous uranyl species available. For example, many different reactions might contribute to the adsorption of uranyl to the smectite surface, including:

$$>(e)AlOH + UO_2^{2+} \leftrightarrow > (e)AlOUO_2^+ + H^+ \quad (2.6)$$

$$>(e)AlOH + UO_2(CO_3)_2^{2-} + H^+ \leftrightarrow > (e)AlOUO_2^+ + 2HCO_3^- \quad (2.7a)$$

$$2>(e)AlOH + (UO_2)_2(CO_3)(OH)_3^- + 2H^+ \leftrightarrow 2>(e)AlOUO_2^+ + HCO_3^- + 2H_2O \quad (2.7b)$$

$$3>(e)AlOH + (UO_2)_3(OH)_7^- \leftrightarrow 3>(e)AlOUO_2^+ + 7H_2O \quad (2.7c)$$

The extent of these reactions will also be affected by the concentration of H^+ available in solution. Therefore, the calculated distribution of aqueous as well as surface uranyl species is a function of the log K values chosen for $>(e)AlO^-$ and $>(e)AlOUO_2^+$.

The concentration profiles exhibited by Group A calculated with a complete reactive geochemical model are similar in shape to concentration profiles calculated using a constant distribution coefficient or K_d model. By selecting the inflection point of a Group A concentration profile after simulating two years of transport and reaction, a K_d value was estimated and was subsequently used to model uranium adsorption. The K_d, as it is calculated by Geochemist's Workbench and the X1t code (Bethke, 1996; 1997a), is defined as the number of moles of adsorbed species (UO_2^{2+}) per gram of solid (smectite) divided by the activity of the free ion (UO_2^{2+}) in solution. A comparison between the concentration profiles described by this K_d approach and the surface complexation model is provided in Fig. 2.10 after 2 and 4 years of simulated time. It is apparent that the profiles calculated using the two models differ in shape and location over time due to the difference in adsorption models. It should be pointed out that

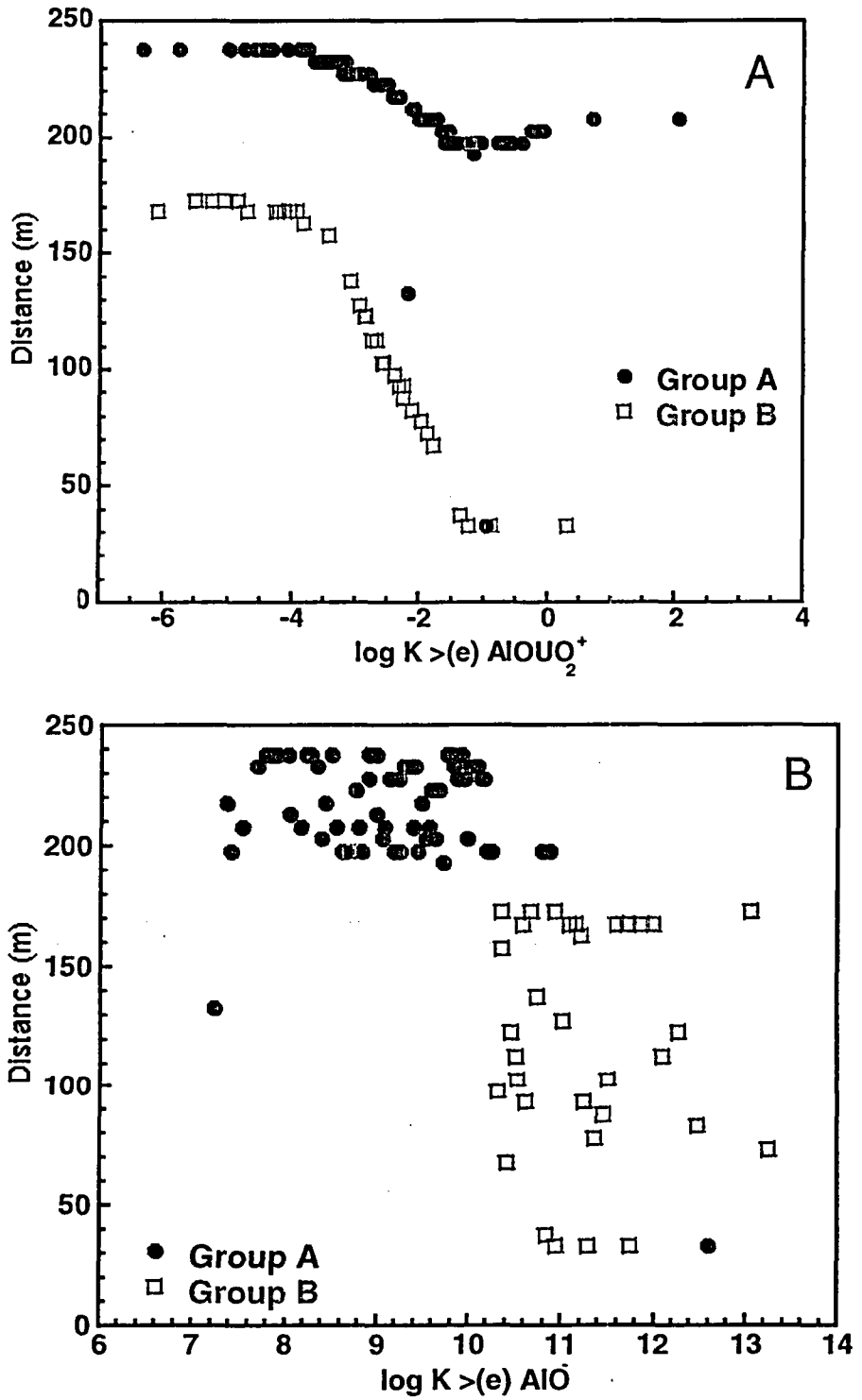

Figure 2.9 Breakthrough distance representing a C/C_0=0.5 of uranium in fluid versus (a) log K >$(e)AlOUO_2^+$ and (b) log K>$(e)AlO^-$ for a simulation time of two years. The various simulations are separated based on the two observed groups A and B.

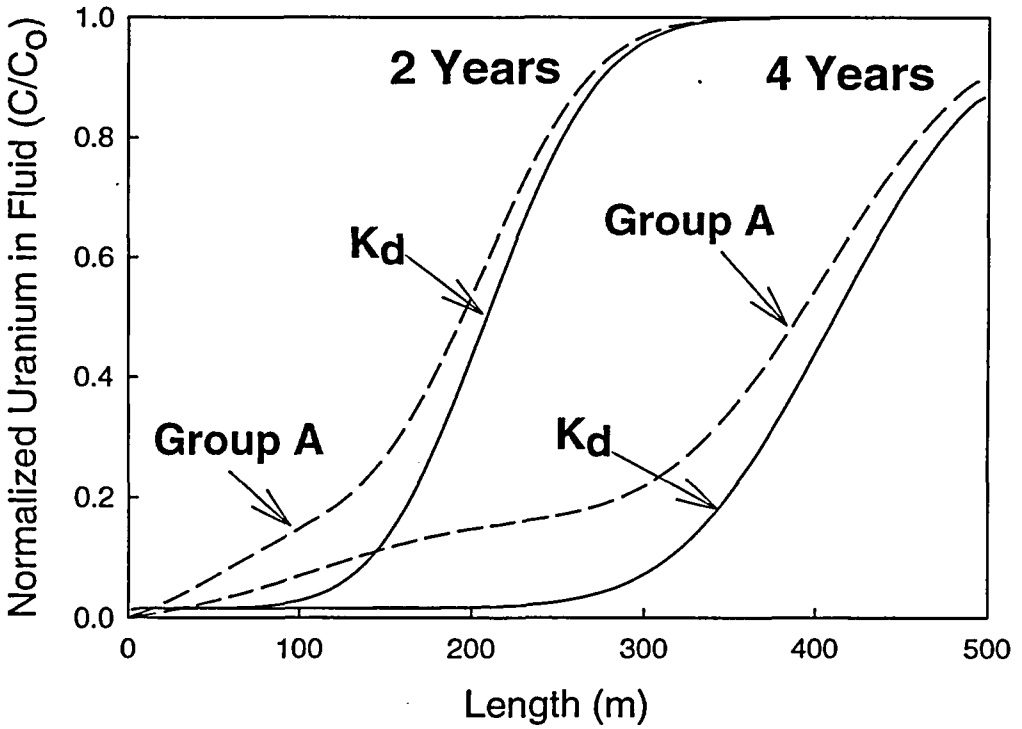

Figure 2.10 Comparison of normalized uranium in fluid with distance for a simulation from Group A and a comparable K_d model after 2 and 4 years of simulated time. Initial equilibrated aqueous uranium concentrations are 560 mg/kg for the Group A case and 1050 mg/kg for the K_d case although the total uranium contents are equivalent.

in the K_d approach implemented here, complete aqueous geochemical speciation is still included; therefore this approach still incorporates more reaction chemistry than is frequently considered in more simplistic reactive-transport models.

The log K >(e)AlO^- values appear to be the distinguishing variable between Groups A and B (see Figs. 2.9a and b). For Group A, the log K >(e)AlO^- ranges from 7 to 10 while for Group B, it ranges between 10.5 and 13. The log K >(e)$AlOH_2^+$ remains constant at –8.33. Therefore, the pH of the pristine point of zero charge (pH_{ppzc}), or the pH at which protonated and deprotonated sites achieve charge balance for the Al edge sites, varies from 7.66 to 9.16 for Group A and 9.42 to 10.66 for Group B. For Group A, the smectite surface is more nearly neutral, while for Group B, the smectite surface is positively charged over the entire pH range encountered in the simulations. This distinction between the smectite surface charge for Groups A and B suggests that uranyl adsorption will occur more readily in Group A. This observation is consistent with the simulation results depicted in Figs. 2.7 and 2.8.

In conclusion, the variation in values for adsorption constants for >(e)AlO^- and >(e)$AlOUO_2^+$ examined in this study affects both the overall stability of smectite and the surface properties of this mineral. As a consequence, calculations of uranyl migration are strongly affected by these perturbations and will lead to significant variations in the calculated concentration profiles.

2.6 Illustrative Two-Dimensional Simulations

To determine the effects of the variation of adsorption constant values on the temporal variations in uranium plume geometry, we also initiated a series of preliminary simulations based on a 2-D conceptual model. The 2-D aerial region consisted of a 500 m long by 200 m wide domain to represent the near-field environment of the Naturita site. For this system the longitudinal and transverse dispersivity values were set to Δ_L = 5 m and $\Delta_T = \alpha_L/10$ = 0.5 m which is found to be reasonable under measured field conditions (e.g., see Gelhar, 1986; Neuman, 1990; Domenico and Schwartz, 1990). The groundwater and the water discharged into the domain (i.e., the inlet boundary condition) were assumed to be initially free of uranium and have a composition similar to that of uncontaminated groundwater at the Naturita site (see Table 2.2). While groundwater discharge rate (i.e., the Darcy flux) at the inlet boundary was assumed to be 20 m/yr, leachate (see Table 2.2 for composition) was introduced through an injection well at a rate of 20 m^3/day. The well was located 50 m downstream from the inlet boundary and 100 m from the lower boundary of the domain. In addition, to explore the influence of subsurface heterogeneity, the aquifer porosity, ϕ, was described using a normal distribution with a mean and standard deviation of 0.25 and 5% respectively. We note that within the context of the X2t model, the underlying intrinsic permeability, k, varies according to, $k=9.87\text{x}10^{(-18+15\phi)}$ m^2. For the 2-D simulations described below, we use uniform grid spacing with $\Delta x=\Delta y$=10 m, where Δy represents the grid spacing in the transverse direction.

Figure 2.11 depicts the uranium plume geometries for two different pairs of log K values selected to represent the general behavior of the two groups, A and B, derived from the 1-D simulations. In a 20-year period, the uranium plume described by Group A adsorption constants migrates further downstream and spreads more widely in the transverse direction than that of the uranium plume calculated using adsorption constants from Group B. These results are not in obvious agreement with the conclusions from the 1-D simulations. However, the concentration profiles in the 1-D simulations effectively represent uranyl desorption from smectite, while the uranium plumes depicted in the 2-D simulations reflect the influence of uranyl adsorption. In addition, the fluid compositions in the 1-D simulations differ in f_{CO2} and pH, and differ more greatly in electrolyte concentrations than the fluid compositions used in the 2-D simulations. Combined, these differences will influence the concentration of adsorbed uranyl.

Although the shapes of the contaminant plumes illustrated in Fig. 2.11 are not dramatically different from each other nor significantly different from the shapes of contaminant plumes described by K_d models, it is clear from the 1-D simulations that although a single snapshot of a contaminant migration simulation can be adequately mimicked by a K_d model, the time and distance evolution of a plume will be described very differently using a surface complexation model.

2.7 Conclusions

Our probabilistic investigation demonstrates that the uncertainty in two thermodynamic values, for describing adsorption in complex natural systems, using 1- and 2-D reaction-transport two models can dramatically change the shape of contaminant concentration profiles in 1-D and contaminant plumes in 2-D. For the 100 pairs of log K values selected for the simulations, the initial uranium concentration in solution varies over seven orders of magnitude, from approximately 0.0001 to 1000 ppm. In the 1-D simulations, two different groups of concentration

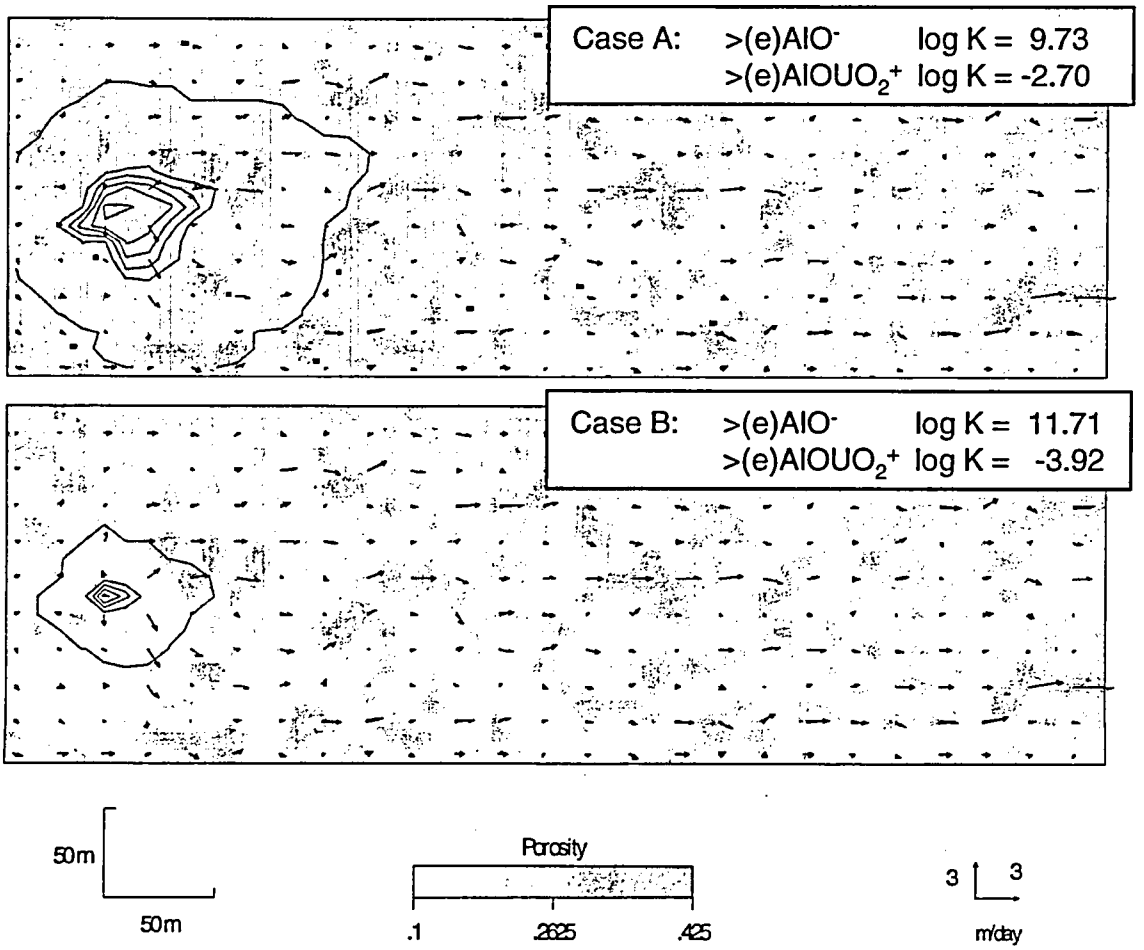

Figure 2-11. Map view of the results of twenty years of reactive transport of uranium obtained from two representative situations (Case A and Case B realizations) based on the variation in the thermodynamic values for the critical sorption parameters. The outermost contour for each plot represents a background level of $1x10^{-6}$ ppm level of uranium in the groundwater, with a contour interval of 0.5 ppm up to 2.5 ppm at the innermost contour. Variation in porosity, generated by a normal distribution about a mean 0.25 porosity value with a 5% standard deviation, is represented by the gray shading. Groundwater velocity arrows are presented at every other nodal point of the simulation grid.

profiles, A and B can readily be distinguished. In Group A, the concentration profiles exhibit a classical sigmoidal shape. In Group B, the concentration profiles display greater changes in aqueous uranium concentration (C/C_o) over smaller distances and times than in Group A. These two groups of concentration profiles differ because of the values chosen for log K $>(e)AlO^-$ (i.e., 7 to 10 for Group A and 10.5 to 13 for Group B). Variations in the value of log K $>(e)AlO^-$ effectively change the point of zero charge for the smectite and the influence of electrostatics in uranyl adsorption. In addition, the shape of the Group B concentration profiles are influenced by smectite dissolution at the inlet and variations in ionic strength due to the mixing of dilute rainwater and uranium mill-tailings leachate.

In the 2-D simulations, the spread of the uranyl plume in both the longitudinal and transverse directions is influenced by variations in the adsorption constants. These results suggest that

further investigation into the effects of adsorption constant uncertainty on plume shape and size is warranted. A more detailed examination of the fraction of uranium adsorbed from both the 1-D and 2-D simulations will provide a link between the 1-D and 2-D results.

2.8 Acknowledgments

The authors would like to acknowledge the insightful discussions with Craig Bethke, Gary Curtis, James Davis, Edward O'Donnell, and Hank Westrich that helped during the course of the research. Edward O'Donnell, Ralph Cady, John Randall, Henry Westrich, Jon Helton and Chen Zhu provided valuable reviews of the original manuscript. This work was supported by the Nuclear Regulatory Commission, Office of Nuclear Regulatory Research. We are very grateful for the advice and support provided by our NRC program manager Edward O'Donnell during the funding period. Sandia National Laboratories is a multi-program laboratory operated by the Sandia Corporation, a Lockheed Martin Company, for the United States Department of Energy under Contract DE-AC04-94AL85000.

3. ADSORPTION PROCESSES: AT WHAT SPATIAL SCALE DO WE NEED TO UNDERSTAND THEM?

3.1 Abstract

The use of coupled reactive-transport models to depict contaminant migration in the field is seriously limited by our lack of knowledge regarding adsorption at the mineral-water interface. Surface complexation models (SCMs) can be readily incorporated into reactive-transport codes. However, internally consistent parameter sets for these models are rare and limited to small subsets of the reactions that may occur in the field. Different SCMs describe the electric double-layer of the mineral-water interface to different levels of detail. These models have not been validated in the field, and the detail required to adequately describe field geochemical processes remains unresolved. In addition, the adsorption reactions that accompany an SCM have not typically been verified by detailed, spectroscopic studies of the mineral-water interface. Molecular modeling can be used to investigate the stoichiometries and relative adsorption energies of viable surface complexes, and to set bounds on the uncertainties associated with different SCMs.

3.2 Introduction

Coupled reactive-transport models are used to explore many environmental problems including leachate migration from uranium mill tailings sites, and both municipal and hazardous waste landfills. The hydrological and geochemical parts of a reactive-transport model are typically developed separately, and in many cases suffer from the combination of a very complex hydrological model with a simplistic geochemical model. This dichotomy becomes particularly evident when examining the approaches used to describe reactions at the mineral-water interface.

Characterizing reactions that occur at the mineral-water interface in a way that can be used to describe macroscopic, field-scale geochemical processes is one of the most difficult problems facing geochemists today. This problem encompasses the interaction of both inorganic and organic aqueous species with mineral surfaces, and, with our increasing awareness of integrated geochemical and biological processes, now extends to investigations of reactions at bacteria-water interfaces and between bacteria and mineral surfaces. This chapter focuses on the problem of characterizing reactions at the mineral-water interface and how this problem propagates into reactive-transport simulations using the equilibrium adsorption of metal cations to oxide minerals for illustration.

A reactive-transport model is typically accompanied by thermodynamic databases of formation constants for the aqueous species in solution and solubility constants for solid phases. Different thermodynamic databases for aqueous speciation exist, and they differ both in the species included for each aqueous component as well as in the formation constants for these species. The solubility constants included in a thermodynamic database are often only for the precipitation and dissolution of end-member solid phases that are simplistic representations of the solid solutions and nanocrystalline minerals found in the field. Nonetheless, the overall thermodynamic approaches to describe aqueous speciation and solubility are generally

accepted. This is not true for adsorption processes.

Contaminant adsorption is dependent on numerous variables that are difficult to quantify including the surface area and surface site density of the adsorbing minerals, the properties of the interface between the mineral surface and bulk solution, and both the structure and composition of the adsorbing species. The simplest model for describing contaminant adsorption is the empirical distribution coefficient or K_d model that relates the equilibrium concentration of a species A adsorbed on a given mineral to the concentration of A in solution, $A_{(ads)} = K_d A_{(aq)}$. This model is frequently used in simple reactive-transport calculations because it is easily incorporated into the advection-dispersion equations (Koretsky, 2000). However, a K_d is based on a single batch equilibration experiment at specific conditions (e.g., pH, ionic strength, etc.) and is only applicable to the measured system. Macroscopic adsorption experiments on metal oxide powders in electrolyte solutions demonstrate that the percent metal adsorbed typically increases dramatically from 10 to 90% over a pH range of 1 to 2 units. Therefore extending the use of a K_d value even over a narrow pH range may lead to very poor assessments of contaminant migration.

Figure 3.1 is a schematic of a leachate plume that extends from a municipal landfill, through an unsaturated soil into an underlying aquifer. The compositions provided in Figure 3.1 for the landfill leachate, the groundwater, and the soil include fewer components than at a field site; nonetheless, this geochemical system is sufficiently complex to illustrate several points. First, major element chemistry of the landfill leachate differs from that of the groundwater. The salt concentration (KCl and NaCl) or ionic strength of the landfill leachate is greater than that of the groundwater, and the landfill leachate is more acidic than the groundwater. Second, the landfill leachate is a source of Pb^{2+} and Cd^{2+} contamination. As the leachate migrates into the aquifer, Pb^{2+} and Cd^{2+} are removed from solution by adsorption to soil minerals such as Fe-, Al-, and Mn-oxides and hydroxides. As landfill leachate continues to enter the subsurface environment, the composition of both the groundwater and the mineral surfaces will change as a function of time and distance due to fluid mixing and reaction. In order to successfully predict the migration of metals in this changing environment, the adsorption model incorporated into a reactive-transport code must be able to account for metal adsorption from solutions that span the pH values and ionic strengths represented by the leachate and natural groundwater. In addition, the model must account for metal adsorption onto solid surfaces that range in metal surface coverage because the solid surfaces may become progressively more saturated with time. Thermodynamically-based, surface complexation models (SCMs) have been developed to describe adsorption processes over ranges of solution and surface composition. These models describe the electric double layer of the oxide-water interface using site binding formulations and electrostatic models. Several of these models, including the constant capacitance model (CCM), the diffuse-double-layer model (DDLM), and the triple-layer model (TLM), treat the surfaces of metal oxides on a single-site basis; i.e., all of the sites on a mineral surface exhibit averaged properties. The surface sites protonate and deprotonate, contributing to the development of surface charge.

The different SCMs describe the mineral-water interface to different levels of detail (Westall, 1986; Brown *et al.*, 1999). Mineral surfaces are charged, and a potential gradient exists between the mineral surface and the bulk aqueous solution. Each single-site model requires two equilibrium constants to account for surface protonation and deprotonation. Contaminant ions bind differently to the mineral surface in each model. In the CCM and DDLM, ions bind directly to the surface. In the TLM (Fig. 3.2), ions can adsorb at two different potential "planes" in the

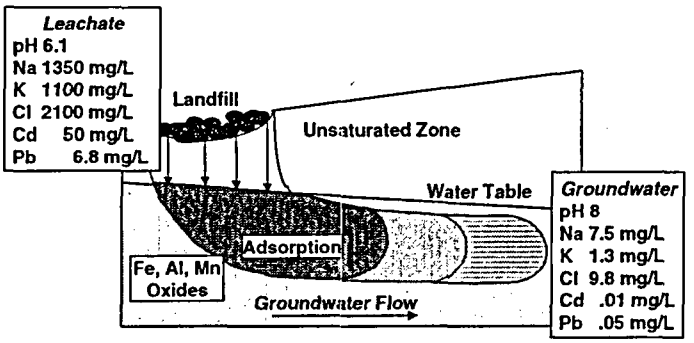

Figure 3.1 Simplified model of municipal landfill leachate migrating into an underlying aquifer. Cd^{2+} and Pb^{2+} from the leachate, reducing contamination downstream. Leachate compositions are reported in Criscenti *et al.* (1996).

electric double layer. The adsorption constants established using the CCM are valid at only one ionic strength. The DDLM accounts for some ionic strength effects through its description of the diffuse layer. The TLM specifically accounts for the adsorption of electrolyte ions; therefore the TLM can account for surface reactions over a wider range of ionic strengths.

Multi-site surface complexation models like the revised MUSIC model (Hiemstra *et al.*, 1996) take into consideration the different types of surface sites that can exist on a metal oxide surface based on coordination environment. As an example, Figure 3.3 illustrates two surfaces of ZnO protonated according to the revised MUSIC model for a pH 7 at 25°C (Criscenti *et al.*, 2003). The surface sites are defined to be the oxygen atoms at the ZnO surface. Some of these oxygen atoms are bound to the bulk ZnO crystal structure through one bond, while others are bonded to the underlying Zn atoms of the crystal structure through two or more bonds. Each of these site types has a different acidity constant, a different propensity to protonate. For ZnO, at a pH of 7 and 25°C, the monodentate oxygen atoms are doubly-protontated, the bridging or bidentate oxygen atoms remain unprotonated, and only some of the tridendate oxygen atoms are singly-protonated. This level of detail is not included in the single-site models described above in which these three site-

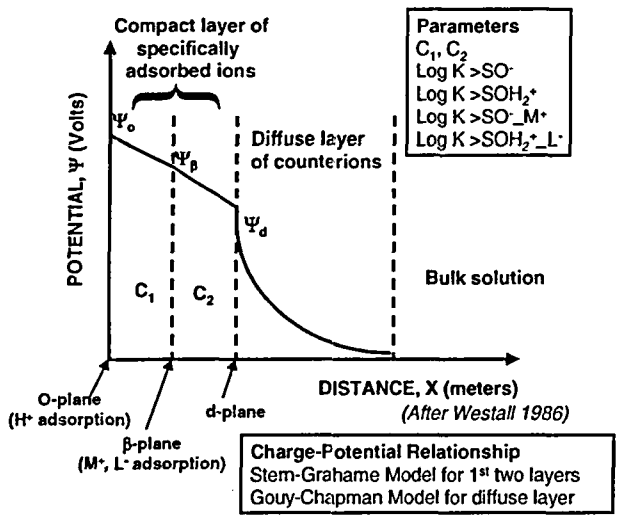

Figure 3.2 Triple-Layer Model. Potential gradient from a mineral plane out into bulk aqueous solution. Protonation and deprotonation occur on the 0-plane, electrolyte cation (M^+) and anion (L^-) adsorption occurs on the β-plane. For a complete discussion of parameters and potential equations see Westall (1986).

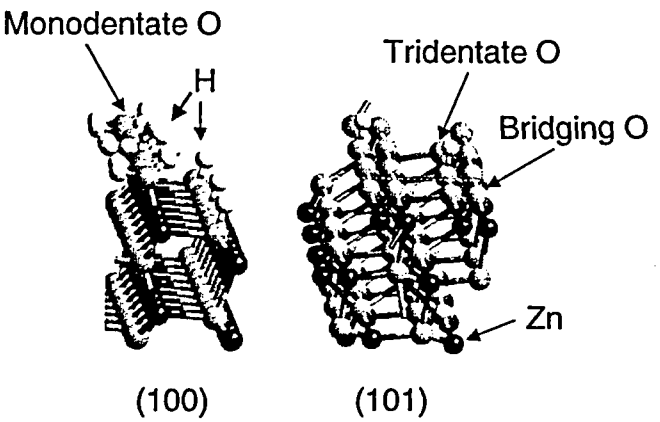

Figure 3.3 ZnO (100) and (101) surface atoms protonated according to the revised MUSIC model (Hiemstra *et al.* 1996).

types would be represented by one "average" site-type.

Equilibrium adsorption reactions and constants for the single-site and multi-site SCMs have been established primarily from experimental data for single mineral, single contaminant systems, with the idea that once these surface reactions and constants have been established within the model framework, a component additivity approach, in which the components and relative abundances of the pure phases in a natural system can be used to calculate adsorption processes in a complex environmental system. Another approach being considered is the generalized composite method (GCM, Davis *et al.*, 1998), in which SCM reactions and equilibrium constants are established from experimental data on natural soils. Average SCM parameters are then derived for a mixture of solid phases. This method requires fewer parameters, however, apparent equilibrium constants derived using this approach only apply to the system studied. Using a non-electrostatic SCM, Davis *et al.* (1998) showed that the derived stability constants could be used over a range of pH where K_d would range over three orders of magnitude (Koretsky, 2000). Therefore, this approach appears to be more successful than the K_d approach for describing adsorption processes in the field; but is less mechanistic than the CCM, DLM, TLM, or MUSIC models.

3.3 Examples of Reactive-Transport Modeling with SCMs

For over a decade, simple one- (1-) and two-dimensional (2-D) transport models have been coupled to more complex geochemical models to demonstrate the hazards of using simple K_ds to "predict" the fate of metal contaminants in the subsurface environment. For example, using a non-electrostatic SCM with adsorption constants for several ions (i.e., H^+, Ca^{2+} SO_4^{2-}, and Cd^{2+}) onto hydrous ferric oxide (Krupka *et al.*, 1988), Criscenti (1996) illustrated that the proton adsorption capacity of hydrous ferric oxide may enhance the acid buffering capacity of a soil. In the calculations, acidic landfill leachate migrates into a porous aquifer of groundwater and hydrous ferric oxide (similar to saturated zone, Fig. 3.1). Proton adsorption maintains the contaminated groundwater at pH 7 for an extended time, allowing for the adsorption of large concentrations of Cd^{2+}. Eventually, the hydrous ferric oxide surface sites are fully loaded with protons and Cd^{2+}. Continued influx of acidic landfill leachate lowers the groundwater pH from 7

to 6 and adsorbed Cd^{2+} is released back into solution.

These calculations illustrate at least two complexities that would be neglected in traditional K_d-based models. A simple K_d model for Cd^{2+} adsorption does not account for the interdependence of the solution pH and the protonation of the solid surface, nor for the pH dependence of Cd^{2+} adsorption. Because the adsorption of a contaminant metal occurs in a complex environmental system, it cannot readily be decoupled from other geochemical reactions including aqueous speciation, competitive adsorption, and precipitation-dissolution. Equilibrium geochemical models solve all of these reactions simultaneously, and calculations that couple complex chemistry with a transport model suggest that field geochemistry will not be adequately described by a simple K_d.

In a second example (Criscenti *et al.*, 2002) that is broadly based on the hydrogeology and mineralogy of the Naturita mill tailings site, a two-site DDLM is used to model uranyl adsorption to smectite. One-dimensional reactive-transport simulations are used to investigate how the uncertainty in adsorption constant values will affect the calculated removal of adsorbed uranium from contaminated soil due to the influx of rainwater. Two smectite site-types are defined as aluminum basal and edge sites. Keeping the other surface complexation model parameters constant (e.g., surface site density, capacitance), the effect of uncertainty in the adsorption constants for two edge species, $>AlO^-$ and $>AlOUO_2^+$, on calculated uranyl migration are examined. The uncertainty in each of these adsorption constants is described by a normal distribution of values defined by an average log K and standard deviation. Pairs of log K values for the formation of $>AlO^-$ and $>AlOUO_2^+$ were selected using Latin Hypercube Sampling (LHS). One hundred simulations were performed with these different log K pairs.

The simulation results separate into two distinct groups of uranium migration curves (Fig. 3.4). In Group A, the migration curves exhibit a classical sigmoidal shape whereas in Group B, the curves display higher uranium concentrations in solution over greater distances and times. These groups are distinguished from each other by two distinct ranges of log K $>AlO^-$ values (Group A: 7-10; Group B: 10.5-13.5) suggesting that this equilibrium constant influences calculated uranium concentrations more than log K $>AlOUO_2^+$.

Both of these examples indicate that the dominant reactions influencing calculated adsorption processes in reactive-transport simulations may be reactions other than that specifically describing the stoichiometry of contaminant metal adsorption. In these studies, the protonation and deprotonation reactions on surface sites were critical to determining the simulated contaminant migration patterns.

3.4 Scaling Issues

The reactive-transport simulations described above clearly demonstrate the need for a comprehensive metal adsorption model that can be incorporated into a reactive-transport code so that the coupling between aqueous speciation, solubility and adsorption processes can be investigated in multicomponent geochemical-hydrological systems. To date, SCMs provide the best descriptions of adsorption that can be used in these codes. However, in part due to the paucity of consistent parameters for use with these models, SCMs have only infrequently been applied in reactive-transport simulations. Limited systematic databases of parameters for SCMs that are now available include Dzombak and Morel (1990); Katz and Boyle-Wight (2001); and

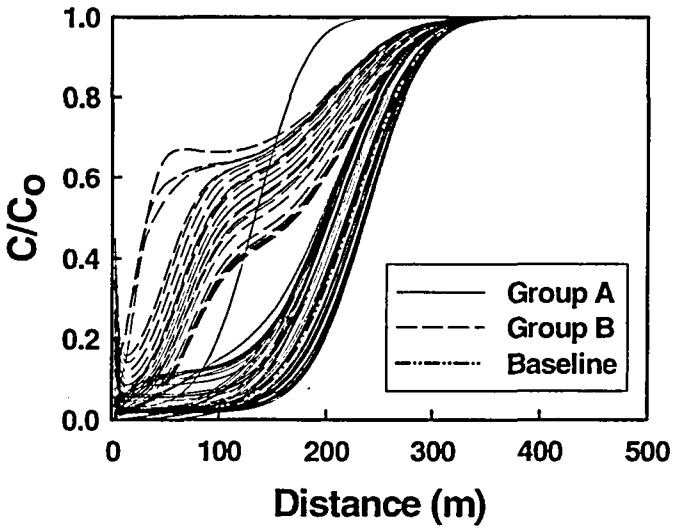

Figure 3.4 Normalized concentration profiles of uranium in fluid versus distance after two years for 100 LHS realizations. The simulated results fall into two groups, A and B. The profile for the baseline case (i.e., using mean log *K* values) is also indicated. (Criscenti *et al.*, 2002).

Sverjensky and Sahai (1996), Sahai and Sverjensky (1997a, b), and Criscenti and Sverjensky (1999, 2002).

Another reason for the limited use of SCMs is that it is still unclear which parameters are important to include in these databases. We have not clearly determined if an adequate description of contaminant adsorption requires an SCM model that uses a (1) detailed description of different site-types on each mineral surface (e.g., MUSIC, Hiemstra *et al.*, 1996), (2) an average description of surface sites and the electric double layer for each mineral present, (e.g., TLM, Davis *et al.*, 1978; Davis and Leckie, 1978) or (3) an average description of the surface sites and solid-water interface for a bulk soil (e.g., GCM, Davis *et al.*, 1998). It is likely that each of these models will be found valuable for different applications, perhaps at different spatial scales.

Within each SCM framework, we need to describe the mineral-water interface and appropriate adsorption reactions. For both single-site and multi-site models, the stoichiometries of metal adsorption reactions are determined by fitting macroscopic adsorption data. This data is collected over a range of pH values from systems of a simple electrolyte solution, a solid oxide, and a trace metal (e.g., M^{2+}). The more comprehensive datasets include measurements over a range of ionic strengths and metal concentrations. Fitting this data within the context of an SCM involves comparing calculated adsorption edge and isotherm curves for different possible surface species including $>SOM^{+}$, $>SOMOH$, $>SOHMCl^{+}$, (where $>SOH$ represents a neutral surface site and M^{2+} is a divalent metal) to the experimental data. In only a few studies (e.g., Criscenti and Sverjensky, 2002) are the adsorption reactions found by fitting one dataset validated on another.

More recently, different spectroscopic techniques, including X-ray absorption spectroscopy (XAS), have been used in combination with macroscopic adsorption data to establish the nature of adsorbed species to be included in SCMs. From XAS, the average distance between a

contaminant ion and the metal atoms of the crystal structure is determined. From these results, we can surmise if the adsorbing ion binds to one or more surface sites (e.g., mono- vs. bidentate, corner vs. edge-sharing) and whether the metal surface complex is inner-sphere or outer sphere. Most spectroscopic studies have focussed on the geometry of metal adsorption to a mineral surface. Only a few spectroscopic studies have examined the adsorption of inorganic anions with divalent metal cations or the presence of ternary complexes (Ostergren *et al.* 2000a, b; Weesner and Bleam ,1998; Randall *et al.*, 1999; Collins *et al.*, 1999a; Boyle-Wight *et al.*, 2002a, b; Bargar *et al.*, 1998).

3.5 How Can Molecular Modeling Help?

Ab initio and molecular mechanics modeling can be used to provide significant information regarding the (1) nature of surface sites, (2) the stoichiometry of adsorbing species both in terms of the number of bonds an adsorbing species will make with a mineral surface and metal-ligand pairing at the surface, (3) the structure of water at the mineral-water interface and the corresponding structure in the presence of an adsorbing species, and (4) the relative adsorption energies of different possible surface species. *Ab initio* and molecular modeling simulations can also be valuable tools to examine how different factors like (1) short- and long-range solvation of the ion both in solution and at the mineral surface, (2) the periodic structure of the mineral surface, and (3) the structure and dielectric constant of interfacial water, influence the adsorption process as a whole. Illustrations of several of these are provided below.

3.5.1. Surface Sites-H_2O on Boehmite

The very nature of a "surface site" is debated in the literature. The SCMs assume that each oxygen atom on a mineral surface is a surface site that can be protonated. Simply due to packing considerations, it is unlikely that all of these oxygen atoms will be available for metal adsorption. XAS studies suggest that many metals form bidentate complexes with oxide surfaces (e.g., Bargar *et al.*, 1998). In the context of an SCM, this might suggest that a divalent metal binds to two surface sites or might require a new definition of a surface site. Several XAS studies of metal adsorption onto oxide surfaces over a range of surface coverages suggest that the metal surface complex that forms varies as a function of metal loading – that the metal becomes coordinated to fewer surface atoms with increasing surface coverage (e.g., Roberts *et al.*, 2003; Spadini *et al.*, 2003). Again the definition of a "surface site" becomes ambiguous.

Figure 3.5 is a snapshot from a classical molecular dynamics (MD) simulation of the (100) surface of boehmite [AlOOH] with less than one monolayer of adsorbed water molecules. An isolated adsorbed water molecule (circled in Fig. 3.5) sits between two Al atoms of the crystal structure and interacts electrostatically with four hydroxide groups on the boehmite surface. As the water molecules interact among themselves along the surface, they no longer sit between two Al atoms of the boehmite structure. Instead, they align between two surface hydroxyl groups (box in Fig. 3.5) to form hydrogen bonded linear networks. Similar differences in the nature of a "surface site" corresponding to XAS results for metal adsorption might also be observed through molecular modeling as a function of metal loading on a mineral surface.

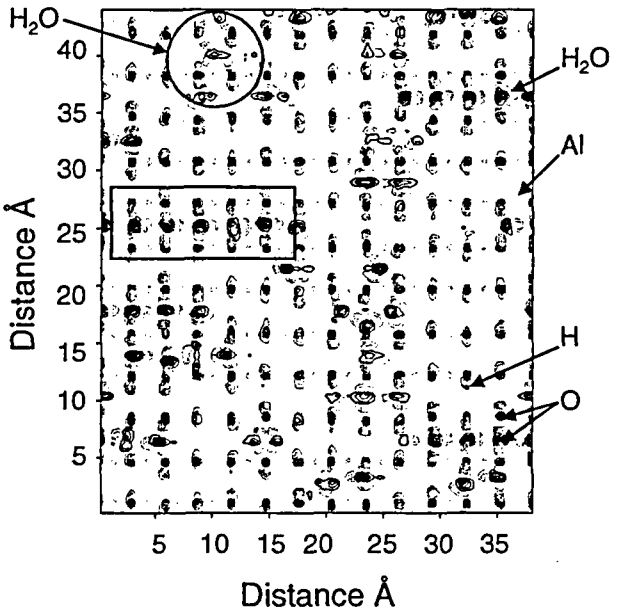

Figure 3.5 Boehmite (100) surface with 70 adsorbed water molecules.

3.5.2 Pb^{2+} Adsorption onto Goethite from NaCl Solutions

Figure 3.6 illustrates another snapshot from a classical molecular dynamics simulation performed to examine the adsorption of lead on a neutral gibbsite surface from an aqueous NaCl solution. This figure demonstrates that large-scale MD simulations can be used to investigate both the binding configuration of metals to mineral surfaces (i.e., inner-sphere vs. outer sphere, bidentate vs. monodentate) and the association of the binding metal with aqueous ligands. In this example, a slab model of the hydroxylated basal surface (26Å x 20Å x 18Å) of gibbsite with a 30Å water layer is used to represent the system. The results suggest that from this solution (0.2M NaCl, 0.1M $PbCl_2$), Pb^{2+} combination with a Cl^- anion (Criscenti and Cygan, 2004).

3.5.3 Ab initio Quantum Mechanics Calculations

While large-scale classical MD simulations provide a reasonable picture of the mineral-water interface and the interactions that occur there, these calculations do not allow for the formation or breaking of bonds. Molecular cluster calculations are used to investigate the protonation of different surface sites and compare relative surface site acidities (e.g., Kubicki and Apitz, 1998). This type of information is necessary for multi-site SCMs. Calculated vibrational frequencies for aluminosilicate, aluminum oxide and aluminum hydroxide clusters compare well with experimental vibrational spectra for these surfaces suggesting that these simple clusters can be used successfully to represent the reactivity of these mineral surfaces (e.g., Kubicki *et al.*, 1996; Kubicki and Apitz, 1998).

Quantum mechanics calculations on small clusters are also used in combination with X-ray absorption fine-structure (EXAFS) data to determine the mechanism of metal binding on oxide surfaces. For example, Collins *et al.* (1999a) found several geometries for Hg^{2+} adsorption to goethite that were consistent with EXAFS data, but only one that gave calculated Hg-Fe

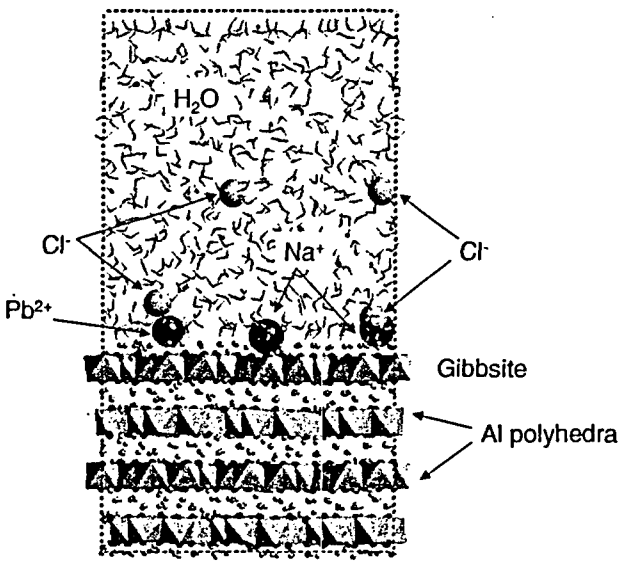

Figure 3.6 Snapshot from 150 ps molecular dynamics simulation to examine lead adsorption the basal plane (001) of gibbsite from a NaCl solution.

distances consistent with those observed. Randall *et al.* (1999) combined quantum calculations and EXAFS data to constrain the geometry of cadmium surface complexes on goethite. Quantum mechanics calculations can also allow us to investigate how different variables individually contribute to the optimum geometry, stoichiometry, and energy of adsorption. For example, in all SCMs, the Gibbs free energy of adsorption is described as a function of the dielectric constant of water at the solid-water interface. Using an *ab initio* quantum mechanical approach, the effects of the dielectric constant of water on the energetics of adsorption can be examined independently of other parameters. Calculations performed using a polarizable continuum model (PCM, Tomasi,1994) in combination with an integral equation formulation (IEF, Cances *et al.*, 1997) were used to investigate how the dielectric constant of water influences the energetics of cobalt chloride complexation. The results, illustrated in Figure 3.7, suggest that ion-pairing will occur more readily in low-dielectric-constant water like that at a mineral surface than in bulk solution (Criscenti and Kubicki, 2001).

3.6 Conclusions

Although both quantum and molecular mechanics calculations focus on the submicroscopic details of the adsorption process, if used in a consistent manner to examine adsorption processes, they may provide us with a new, more quantitative way to bound the uncertainties associated with "averaging" surface site characteristics and/or selecting only one or two surface reactions to describe the adsorption of a contaminant over a range of environmental conditions. In other words, these detailed studies, in addition to providing us with a very detailed mechanistic understanding of the adsorption process may also provide us with a more definitive perspective on how detailed an SCM is necessary for different applications and for incorporation into reactive-transport models.

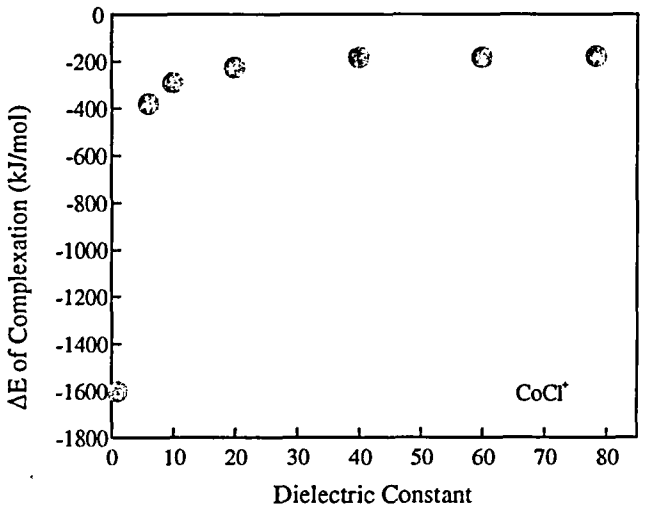

Figure 3.7 ΔE of complexation for the reaction $Co^{2+} + Cl^- \leftrightarrow CoCl^+$ in aqueous solutions at different dielectric constants.

3.7 Acknowledgments

This chapter was published as L. J. Criscenti "Adsorption processes: At what spatial scale do we need to understand them?" In: Proceedings of the 11th International Symposium on Water-Rock Interaction, WRI-11, 27th June – 2 July 2004, Saratoga Springs, NY. Eds. R. B. Wanty and R. R. Seal, A. A. Balkema Publishers, New York, p. 909-916. Examples used in this paper are taken from research sponsored by the Sandia National Laboratories Laboratory Directed Research and Development program, the ASC program, the Nuclear Regulatory Commission, and the Department of Energy, Basic Energy Sciences program. Sandia is a multiprogram laboratory operated by Sandia Corporation, a Lockheed Martin company, for the U.S. Department of Energy under contract DE-AC04-94AL85000. Reviews by Patrick V. Brady, Randall T. Cygan, and James D. Kubicki are greatly appreciated.

4. THE TRIPLE LAYER MODEL AND SURFACE SPECIATION

4.1 Introduction

Various chemical surface complexation models have been developed to describe potentiometric titration and metal adsorption data at the oxide-solution interface. Surface complexation models provide descriptions of metal adsorption using an equilibrium approach that defines surface species, chemical reactions, mass balances, and charge balances. These models provide insight into the stoichiometry and reactivity of adsorbed species. Application of these models to reference oxide minerals has been extensive but their use in describing ion adsorption by clay minerals and mixed sediments has been limited. As previously noted in Section 1., surface complexation models share at least four common assumptions: (1) mineral surfaces can be described as flat planes of surface hydroxyl sites and equations can be written to describe reactions at these specific sites; (2) reactions at mineral surfaces are at local equilibrium and can be described using mass law equations; (3) variable charge at the mineral surface is a direct result of chemical reactions at the surface; (4) the effect of surface charge on measured equilibrium constants can be calculated and the intrinsic equilibrium constants can then be extracted from experimental measurements (Dzombak and Morel, 1990; Koretsky, 2000).

There are two fundamentally different approaches to using surface complexation models to evaluate field site data. The first is to use the generalized composite model (Davis *et al.* 1998; Kohler *et al.* 2004). The second is to use a component additivity model in which the modal distribution of different adsorbent solids is estimated and each of these solids is assigned at least one type of surface site and one equilibrium constant for the partitioning of a contaminant between the solid and the aqueous phase. The generalized composite model has been thoroughly addressed in the following NUREG documents (Davis and Curtis, 2005; Curtis, 2005). This approach is not predictive, but may be useful in determining the short-term evolution of a contaminant plume. The component additivity approach should theoretically be predictive in nature and generally applicable to all field sites. However, it requires an extensive database of parameters which has yet to be developed in a consistent manner. When this approach has been used to model contaminant migration at a field site, adsorption by the soil or sediment has usually been represented by adsorption to the one solid phase that appears to be predominant adsorbent.

The Triple Layer Model (TLM) is one surface complexation model that may, in the long term, prove useful to calculate adsorption to mixed sediments from different leachates and groundwater compositions. Recent progress in TLM development and a database of TLM parameters for this model are discussed in Sections 4.2 and 4.3. In addition, because the stoichiometry of the surface species is important to establishing an appropriate database of adsorption constants, Section 4.4 reviews recent spectroscopic studies to determine how divalent metals bind to mineral surfaces. These studies provide information on the types of surface species that need to be considered in macroscopic models of adsorption.

4.2 Triple Layer Model

The triple layer model (Davis *et al.*, 1978; Davis and Leckie, 1978) represents the oxide-water interface by three planes of charge: (1) the oxide surface or 0-plane where the generic surface

sites >*SOH* protonate or deprotonate; (2) the β-plane, a small distance from the surface where electrolyte ions are supposed to adsorb; and (3) the d-plane which represents the start of the diffuse layer where a diffuse swarm of counterions balance the local charge density at the surface. A key advantage to the TLM over the constant capacitance model (Schindler et al, 1976; Stumm et al., 1980) and the diffuse layer model (Dzombak and Morel, 1990) is that by accounting for the adsorption of the electrolyte ions, the model can be used to calculate equilibrium adsorption over a wider range of ionic strengths and solution compositions.

In the TLM, the adsorption of a proton to a neutral surface site is described by the reaction

$$> SOH + H^+_{aq} \leftrightarrow > SOH^+_2 \tag{4.1}$$

where ">" indicates that the complex is bound to the mineral surface and "aq" indicates that the species is in solution. This reaction has the following equilibration constant:

$$K_1 = \frac{a_{>SOH^+_2}}{a_{>SOH} a_{H^+_{aq}}} 10^{F\Psi_o / 2.303RT} \tag{4.2}$$

where a_i represents the activity of the ith species, F is Faraday's constant, Ψ_o is the electric potential at the 0-plane, R is the ideal gas constant and T is temperature in degrees Kelvin. The adsorption of a proton to a negatively charged site is described by an analogous reaction and equilibrium constant:

$$> SO^- + H^+_{aq} \leftrightarrow > SOH; K_2 = \frac{a_{>SOH}}{a_{>SO^-} a_{H^+_{aq}}} 10^{F\Psi_o / 2.303RT} \tag{4.3}$$

The total concentration of surface sites, N_T, (moles kg^{-1}) is finite and is calculated from the site density N_s (sites nm^{-2}) according to:

$$N_T = N_s x A x C_s x \frac{1}{N_A} x \frac{1}{\rho} x 10^{18} = \left(m_{>SOH} + m_{>SOH^+_2} + m_{>SO^-} + ...\right) \tag{4.4}$$

where A is the specific surface area ($m^2\ g^{-1}$) of the mineral, C_s is the amount ($g\ L^{-1}$) of solid mineral dispersed in the solution, ρ is the solution density ($kg\ L^{-1}$), N_A is Avogadro's number, the factor 10^{18} converts nm^2 to m^2, and $m_{>i}$ represents the molal concentration of the ith surface site (moles kg^{-1}) (Sahai and Sverjensky 1998). The concentrations of surface complexes can be used to calculate surface charge on the 0- and β-planes. Charge balance requires that the sum of the charges on the three planes (0, β, and d) is zero:

$$\sigma_0 + \sigma_\beta + \sigma_d = 0 \tag{4.5}$$

The charge-potential relationships in the TLM are

$$\sigma_0 = C_1\left(\Psi_0 - \Psi_\beta\right) \tag{4.6}$$

and

$$\sigma_d = C_2(\Psi_d - \Psi_\beta) \tag{4.7}$$

where C_1 and C_2 are the capacitances between the 0- and β-planes and between the β-plane and d-plane respectively. For a 1:1 electrolyte, the potential and charge at the d-plane are related by Gouy-Chapman theory:

$$\sigma_d = (8\varepsilon_o\varepsilon_w RT\bar{I}\rho)^{1/2}\sinh\frac{F\Psi_d}{2RT} \quad (4.8)$$

where ε_o is the permittivity of free space, ε_w is the dielectric constant of the aqueous medium, and $\bar{I}$ is the true ionic strength (molal) of the system.

In the TLM, the reactions for adsorption of a 1:1 electrolyte (C^+A^-) in the β-plane are:

$$> SOH + C^+ \leftrightarrow\!> SO^- - C^+ + H^+ \quad (4.9)$$

$$> SOH + H^+ + A^- \leftrightarrow\!> SOH_2^+ - A^- \quad (4.10)$$

where C^+ is the cation and A^- is the anion of the electrolyte and the dashes indicate that adsorption occurs in the β-plane. Divalent metal ions can adsorb either in the 0-plane or in the β-plane by many different surface complexation reactions including:

$$> SOH + M^{2+} \leftrightarrow\!> SOM^+ + H^+ \quad (4.11)$$

$$2 > SOH + M^{2+} \leftrightarrow (> SO)_2M + 2H^+ \quad (4.12)$$

$$> SOH + M^{2+} \leftrightarrow\!> SO^- - M^{2+} + H^+ \quad (4.13)$$

$$> SOH + M^{2+} + H_2O \leftrightarrow\!> SO^- - MOH^+ + 2H^+ \quad (4.14)$$

$$> SOH + M^{2+} + A^- \leftrightarrow\!> SOHM^{2+} - A^- \quad (4.15)$$

More than one version of the TLM has been used in the past (e.g., Davis *et al.*, 1978; Hayes and Leckie, 1987). When different standard and reference states are assigned in the TLM, different "best fit" surface complexes are obtained when applying the TLM to the same experimental adsorption data. For example, Hayes and Leckie (1987) expressed both the chemical potentials for aqueous and surface species by the expression:

$$\mu_i = \mu_i^o + 2.303RT\log m_i + zF\phi_i \quad (4.16)$$

defining the standard state for both solution and surface species as 1 mol L^{-1} at zero surface charge and no ionic interaction. The reference state for all species was chosen to be infinite dilution relative to the aqueous phase and zero surface charge. The assumption that Eq. (4.16) applies to all aqueous ions is equivalent to abandoning the use of any form of aqueous ion activity coefficients. The outcome is particularly serious when fitting adsorption data at several ionic strengths. Using this formulation, Hayes and Leckie (1987) found that the surface species $>SOCd^+$ and $>SOPb^+$ best fit their adsorption data for Cd^{2+} and Pb^{2+} onto goethite from solutions ranging in ionic strength from 0.001M to 1.0 M $NaNO_3$. However, when the activity coefficients for aqueous ions were given by a version of an extended Debye-Huckel equation for 1:1 electrolytes (Helgeson *et al.*, 1981), these same data were best fit with surface complexes involving the electrolyte anion $>SOHCd^+ - NO_3^-$ and $>SOHPb^+ - NO_3^-$ (Criscenti and Sverjensky, 1999). Ironically, Hayes (1987) found that his pressure-jump kinetic data were best described by this type of complex.

4.3 Obtaining Model Parameter Values

4.3.1 Standard States for the Activities of Surface Species

A variety of standard states for the activities of surface species have been explicitly defined or

implied by the way equilibrium adsorption constants within a surface complexation model framework have been established (Sverjensky, 2003). The choice of standard state affects the equilibrium constant values resulting from fitting adsorption data. The standard states that have been used for surface species include the hypothetical 1.0 Molar standard state, the hypothetical 1.0 molal standard state, and the hypothetical 1.0 mole per kilogram of solid standard state. Kulik (2000, 2002a, b) examined the standard states used for the Gibbs free energies of individual surface and aqueous species. He focused on the drawbacks to the hypothetical 1.0 Molar standard state for surface species, such as the built-in dependence on the site density of the solid (Kulik, 2002a). In fact, the molarities of both surface sites and species depend on site densities, surface areas, and solid concentrations (Sverjensky, 2003). These dependencies result in fitted equilibrium constants which cannot be directly compared without correcting for differences in the quantity or properties of the solids used in the experiments.

Sverjensky (2003) proposed new standard states, leading to equilibrium constants independent of the surface area, site density and the amount of the solid sorbent. These new standard states are dependent only on surface site occupancy and can be used with any surface complexation model. Different standard states are defined for the activities of the sorbent sites and the sorbate species. The theoretical relationships that apply for all adsorption reactions are developed below using Eq. (4.1) as an example reaction.

For the sorbent sites, the standard state refers to unit activity of the sites on a completely unsaturated surface (i.e., all sorbent sites are >*SOH*) at any temperature and pressure.

$$\overline{\mu}_{>SOH} = \mu^{\#}_{>SOH} + RT \ln \lambda_{>SOH} X_{>SOH} \tag{4.17}$$

where $\overline{\mu}_{>SOH}$ is the electrochemical potential of >*SOH*, $\mu^{\#}_{>SOH}$ is the standard chemical potential for the sorbent sites, $\lambda_{>SOH}$ is the rational activity coefficient for >*SOH*, $X_{>SOH}$ is the mole fraction of >*SOH* (the number of moles of >*SOH* per mole of surface sites), and $\lambda_{>SOH} \rightarrow 1$ as $X_{>SOH} \rightarrow 1$. The >*SOH* sites are depicted to follow Raoult's Law at high mole fractions. Therefore, the standard state molarity for sorbent sites is not unity. Instead, the standard state molarity depends on the site density, surface area and amount of the actual sorbent solid:

$$M^{\#}_{>SOH} = \left(\frac{N_s}{N_A}\right) A_s C_s \tag{4.18}$$

where $M^{\#}_{>SOH}$ represents the standard state molarity of sorbent sites >*SOH*, N_s is surface site density on the s^{th} solid sorbent (sites m^{-2}), A_s is the BET surface area on the s^{th} solid sorbent ($m^2\ g^{-1}$), C_s is the amount of the s^{th} sorbent solid ($g\ L^{-1}$) and N_A is Avogadro's number (6.023×10^{23} sites mol^{-1}).

For the sorbate, the standard state refers to unit activity of surface species on a completely saturated surface (i.e., all sorbent sites are occupied by sorbate) with zero potential at any temperature and pressure referenced to infinite dilution. The electrochemical potential for $>SOH_2^+$ is:

$$\overline{\mu}_{>SOH_2^+} = \mu^{\ddagger}_{>SOH_2^+} + RT \ln \lambda_{>SOH_2^+} X_{>SOH_2^+} + F\Psi_{>SOH_2^+} \tag{4.19}$$

where $\mu^{\ddagger}_{>SOH_2^+}$ is the standard chemical potential for the sorbate species, $>SOH_2^+$, and $\lambda_{SOH_2^+} \rightarrow$

1 as $\Psi_{>SOH_2^+} \rightarrow 0$ and $X_{>SOH_2^+} \rightarrow 1$. Henry's Law is followed at low mole fractions. In the standard state, the sorbate species will have an abundance determined by a ***hypothetical*** site density, surface area, and amount of solid sorbent. Sverjensky (2003) selected the following values standard state values for all solids: $N^{\ddagger} = 10 \times 10^{18}$ sites m^{-2}, $A^{\ddagger} = 10\ m^2\ g^{-1}$, and $C^{\ddagger} = C_s$. Then

$$M^{\ddagger}_{>SOH_2^+} = \left(\frac{N^{\ddagger}}{N_A}\right) A^{\ddagger} C^{\ddagger} \tag{4.20}$$

Using these new standard states for the sorbent sites and sorbate species, the equilibrium constant for the surface protonation reaction, Eq. (4.1), is given by:

$$K_1^{\theta} = \left(\frac{X_{>SOH_2^+}}{X_{>SOH} a_{H^+}}\right) 10^{\frac{F\Psi_o}{2.303RT}} = \left(\frac{M_{>SOH_2^+}}{M_{>SOH} a_{H^+}}\right)\left(\frac{N_s A_s}{N^{\ddagger} A^{\ddagger}}\right) 10^{\frac{F\Psi_o}{2.303RT}} \tag{4.21}$$

These new equilibrium constants are independent of the properties of the solid or the amount of solid. Without this dependency, equilibrium constants derived from adsorption data on different samples of the same solid, and from adsorption data on different types of solids, can be directly compared.

4.3.2 Surface Site Density

The surface site density, N_s, is an important parameter in surface complexation models related to the total number of reactive functional groups. Surface site density values can be obtained using a wide variety of experimental methods, calculated from crystal dimensions, or optimized to fit experimental adsorption data (Davis and Kent, 1990). Experimental methods include potentiometric titration, tritium exchange, maximum ion adsorption, and infrared spectroscopy. Reviews of measured site densities are provided by James and Parks (1982), Davis and Kent (1990), and Koretsky *et al.* (1998). While goodness-of-fit was found to be insensitive to changes in value of surface site density from 1-100 sites nm^{-2} (Hayes *et al.*, 1991), the actual values of the surface complexation constants changed. To allow the development of self-consistent parameter databases for surface complexation models, Davis and Kent (1990) recommended a surface site density value of 2.31 sites nm^{-2} for natural materials. This value closely approximates surface site densities for iron and manganese oxides and the edges of clay minerals. An alternative reference site density of 12.05 sites nm^{-2} was proposed by Kulik (2002a) for all mineral-water surfaces because it corresponds roughly to the density of water molecules in a surface monolayer and represents a maximal density of monodentate surface complexes. The standard state proposed by Kulik (2002a) for a surface species is when 1 mole of it occupies all sites of reference total density on all the surface of 1 mole of the sorbent suspended in 1 kg of water-solvent at P = 1 bar and defined T, in the absence of external fields and at zero surface potential. In contrast, Sverjensky (2003) chose the standard state properties of a surface species to be $N^{\ddagger} = 10 \times 10^{18}$ sites m^{-2}, $A^{\ddagger} = 10\ m^2\ g^{-1}$, and $C^{\ddagger} = C_s$

Koretsky *et al.* (1998) focused on applying crystal chemical considerations to calculate surface site densities. They studied the predominant cleavage or growth faces for a suite of minerals including goethite, hematite, corundum, kaolinite, albite, anorthite, and quartz. Using calculated bond strengths and charges, the "ideal" slices through the crystal structures were defined to be the charge-neutral or nearly charge-neutral slices produced with a minimum total strength of bonds severed. Setting the number of broken bonds at the surface equal to the number of reactive surface sites, or considering partial charges of coordinatively unsaturated atoms at the

surface, gave the best agreement with available experimentally-determined site densities from tritium exchange experiments. In addition, the types of surface hydroxyl groups predicted using this approach were in qualitative agreement with those observed from surface infrared spectroscopy (Koretsky *et al.*, 1998; Koretsky, 2000).

4.3.3 Capacitances

Sverjensky (2005) suggested that triple layer model fits to surface charge data are not dependent on the value for C_2. However, the value for C_2 is important for the prediction of zeta potentials. The small value of 0.2 F m^{-2} implies a rather large distance between the β- and the d-planes of the model. Sverjensky (2005) proposes that the separation of these two planes is influenced by the size of the electrolyte cation on the β-plane and assumes $C_1 = C_2$. Using this assumption, good agreement between predicted and experimental zeta potentials was found for rutile in LiCl and CsCl solutions (Kallay *et al.*, 1994) and for hematite in $NaNO_3$ solutions (Schudel *et al.*, 1997).

Sverjensky (2001) showed that the capacitance values C_1, obtained for a wide variety of oxides and electrolyte types through the use of a consistent formulation of the triple layer model (Sahai and Sverjensky, 1997a), fell into two groups. For rutile, anatase, and magnetite, values of C_1 increased with decreasing crystallographic radius of the electrolyte cation from Cs^+ to Li^+. For quartz, amorphous silica, goethite, hematite, and alumina, values of C_1 increased with decreasing hydrated electrolyte cation radius from Li^+ to Cs^+. The distance between the *o*- and ß-planes was influenced by both the size and state of hydration of the adsorbing electrolyte ions at the ß-plane, and the presence of water molecules between the planes. For minerals with high dielectric constants such as rutile, anatase, and magnetite, the work required for the removal of waters of solvation from cations near the mineral surfaces was negligible (James and Healy, 1972). Therefore, it could be inferred that the electrolyte cations adsorbed to these minerals as dehydrated, inner-sphere complexes. On the other hand, for minerals of lower dielectric constant such as hematite, goethite, alumina, quartz, and amorphous silica, C_1 increased in the order of decreasing hydrated radius. The work required to remove waters of solvation near low dielectric constant surfaces was larger than for high dielectric constant surfaces (James and Healy, 1972). Therefore it could be inferred that the electrolyte cations formed hydrated, outer-sphere complexes on these mineral surfaces. It should be noted that, regardless of the mineral involved, the electrolyte cations all bouid to the ß-plane of the triple-layer model forming inner-sphere or outer-sphere complexes depending on the dielectric properties of the mineral.

Sverjensky (2001) described both series by a model of the rutile-water interface whose parameters were consistent with X-ray standing-wave experimental results (Fenter *et al.*, 2000). The model predicted distances of 3.3 Å for adsorbed Rb^+ and 2.9 Å for adsorbed Sr^{2+}. These predictions compared well to the reported experimentally-determined distances of 3.4 Å and 2.8 Å, respectively. The model also suggested that trace amounts of metals (e.g., Sr^{2+}, Ca^{2+}) other than the electrolyte cations, should form inner-sphere complexes if adsorbed to the β-plane of rutile and similar solids, and form outer-sphere complexes if adsorbed to the β-plane of quartz, goethite, and similar solids. These predictions were consistent with the results of X-ray standing wave and EXAFS studies (Fenter *et al.*, 2000; O'Day *et al.*, 2000; Sahai *et al.*, 2000; Axe *et al.*, 2000).

4.3.4 Protonation-Dissociation Constants

Values for protonation-dissociation constants can also be predicted using solvation and crystal chemical theory (Sverjensky and Sahai, 1996). Using the standard states defined above (Sverjensky, 2003), the values of $\log K_1^\theta$ and $\log K_2^\theta$ can be calculated from the $\log K_{ZPC}^\theta$ and $\log K_n^\theta$ which are defined next. At the zero point of charge (pH_{ZPC}), the surface of a metal oxide has a net zero charge and the surface equilibrium can be expressed by:

$$> SO^- + 2H^+ => SOH_2^+ \tag{4.22}$$

and

$$pH_{ZPC} = 0.5 \log K_{ZPC}^\theta = 0.5(\log K_1^\theta + \log K_2^\theta) \tag{4.23}$$

The overall equation for equilibrium surface protonation is:

$$> SO^- + > SOH_2^+ = 2 > SOH \tag{4.24}$$

and equilibrium constant expression is:

$$\log K_n^\theta = \log \frac{a_{>SOH}^2}{a_{>SO^-} a_{>SOH_2^+}} = \log K_2^\theta - \log K_1^\theta \tag{4.25}$$

Sverjensky and Sahai (1996) proposed that the standard Gibbs free energy of the vth surface protonation reaction ($\Delta G_{r,v}^0$) can be broken into three terms according to:

$$\Delta G_{r,v}^0 = \Delta G_{s,v}^0 + \Delta G_{pi,v}^0 + \Delta G_{ii,v}^0 \tag{4.26}$$

where $\Delta G_{s,v}^0$ represents a Born solvation contribution, $\Delta G_{pi,v}^0$ represents an electrostatic interaction term, and $\Delta G_{ii,v}^0$ represents a term intrinsic to the aqueous proton. The Born solvation term is treated by building on earlier studies of metal adsorption (James and Healy, 1972). The proton interaction term is built by summing an attractive interaction between the proton and the surface oxygen with a repulsive interaction between the proton and the underlying metal of the solid sorbent (Yoon *et al.*, 1979).

Predictive equations for the equilibrium surface protonation constants derived using the approach of Sverjensky and Sahai (1996) are:

$$\log K_{ZPC}^\theta = \frac{-\Delta\Omega_{r,ZPC}}{2.303RT}\left(\frac{1}{\varepsilon_s}\right) - B_{ZPC}\left(\frac{s}{r_{H^+}}\right) + \log K_{ii,ZPC}^* \tag{4.27}$$

and

$$\log K_n^\theta = -B_n\left(\frac{s}{r_{H^+}}\right) + \log K_{ii,n}^* \tag{4.28}$$

where ε_s and $\left(\frac{s}{r_{H^+}}\right)$ represent the dielectric constant and the Pauling bond strength per angstrom respectively, for the s^{th} solid. The term involving the dielectric constant of the solid arises from the solvation term in Eq. (4.26) and the terms involving the Pauling bond strength arise from the electrostatic interaction term. The $\Delta\Omega_{r,ZPC}$, B_{ZPC}, B_n, $\log K_{ii,ZPC}^*$, and $\log K_{ii,n}^*$ terms are coefficients obtained by calibrating the equations with experimentally-derived

equilibrium constants. The symbol $\Delta\Omega_{r,ZPC}$ in Eq. (4.27) represents a Born solvation coefficient for the reaction:

$$\Delta\Omega_{r,ZPC} = \Omega_{>SOH_2^+} - \Omega_{>SO^-} = \Omega^{abs.}_{>SOH_2^+} - \Omega^{abs.}_{>SO^-} \tag{4.29}$$

where the symbols represent the conventional ($\Omega_{>SOH_2^+}$, $\Omega_{>SO^-}$) and absolute Born coefficients, ($\Omega^{abs.}_{>SOH_2^+}$, $\Omega^{abs.}_{>SO^-}$). The relationship between the conventional and absolute Born coefficients for the j^{th} surface species is given by:

$$\Omega^{abs.}_j = \Omega_j + \Omega^{abs.}_{>SOH} \tag{4.30}$$

based on the convention that $\Omega^{abs}_{>SOH} = 0.0$. The absolute solvation coefficient of the j^{th} surface species is calculated using:

$$\Omega^{abs.}_j = \frac{\eta Z_j^2}{4R_{e,j}} \tag{4.31}$$

where $R_{e,j}$ represents the effective electrostatic radius for the surface species, Z_j represents the charge on the j^{th} species and η=166.027 kcal Å mole^{-1} (Sverjensky, 1993). The effective electrostatic radius of surface species is defined as:

$$R_{e,j} = r_{x,j} + \gamma_Z \tag{4.32}$$

where $r_{x,j}$ represents a crystallographic radius and γ_Z represents a constant for cations or anions or a given charge. Sverjensky and Sahai (1996) showed that values for the coefficients $\Delta\Omega_{r,ZPC}$, B_{ZPC}, B_n, $\log K^*_{ii,ZPC}$, and $\log K^*_{ii,n}$ in Eqs. (4.27) and (4.28) can be found within the frameworks of the constant capacitance, diffuse layer, or triple layer model by regressing experimentally-determined values for $\log K^{\theta}_{ZPC}$ and $\log K^{\theta}_n$. These equations can then be used to determine surface protonation-dissociation constants for other metal oxides given the dielectric constants and the Pauling bond strength per angstrom for the metal-oxygen bonds within these solid phases.

4.3.5 Metal Surface Complexation Constants

The equilibrium constants for electrolyte cation and anion adsorption for the triple layer model can also be predicted using the internally-consistent parameter sets developed by Sverjensky and Sahai (1996), Koretsky *et al.* (1998), Sahai and Sverjensky (1997a) and expanded upon by more recent papers (Criscenti and Sverjensky, 1999, 2000; Sverjensky, 2005). The standard Gibbs free energy for adsorption of the vth electrolyte cation or anion is broken down into three terms representing a Born solvation contribution, an electrostatic interaction between the adsorbate and the surface, and an energy intrinsic to the aqueous adsorbate. This expression is analogous to that provided for surface protonation in Eq. (4.26). The equilibrium constants for the electrolyte cation and anion can be predicted from expressions similar to that for the $\log K^{\theta}_{ZPC}$ (Eq. 4.27):

$$\log K^{\theta}_{M^+} = \frac{-\Delta\Omega_{r,M^+}}{2.303RT}\left(\frac{1}{\varepsilon_s}\right) - B_{M^+}\left(\frac{s}{r_{M^+}}\right) + \log K^*_{ii,M^+} \tag{4.33}$$

$$\log K^{\theta}_{L^-} = \frac{-\Delta\Omega_{r,L^-}}{2.303RT}\left(\frac{1}{\varepsilon_s}\right) - B_{L^-}\left(\frac{s}{r_{L^-}}\right) + \log K^{*}_{ii,L^-} \quad (4.34)$$

where s represents the Pauling bond strength (Sverjensky and Sahai, 1996), and r_{M^+} and r_{L^-} represent the distances of the adsorbing ions being repulsed by the underlying cation of the solid and the surface oxygen, respectively (Sverjensky, 2005). Values of r_{M^+} are estimated by prediction from crystal structure analysis and a theoretical analysis of capacitances (Sverjensky, 2001), while values for r_{L^-} are approximated by adding a characteristic distance for each surface to an effective crystallographic radius for L^-. These values are used in regression calculations to obtain the repulsion coefficients B_{M^+} and B_{L^-} and the ion-specific $\log K^{*}_{ii,M^+}$ and $\log K^{*}_{ii,L^-}$. Figure 4.1 illustrates the results of several linear regressions using $\log K^{\theta}_{M^+}$ and $\log K^{\theta}_{L^-}$ values determined by fitting experimental surface charge data using the triple-layer model. Figure 4.1c shows the inverse correlation between $\Delta\Omega_{r,M^+}$ and the effective electrostatic radius of the ion, $R_{e,i}$. Figure 4.1d illustrates that $\log K^{*}_{ii,M^+}$ can be correlated to the aqueous phase equilibrium metal hydrolysis constant, log $K_{M(OH)}$. Analogous correlations can be made for the monovalent anions (Sverjensky, 2005).

Criscenti and Sverjensky (1999, 2002) continued to build the internally-consistent set of triple layer model equilibrium constants developed by Sverjensky and Sahai (1996) and Sahai and Sverjensky (1997a, b), by re-examining sets of adsorption edge and isotherm data for divalent metal cation adsorption onto oxide surfaces. They found that transition and heavy metal adsorption was best described by metal adsorption on the 0-plane of the triple-layer model, a result similar to that of Hayes and Leckie (1987). However, in contrast to previous investigations, they found that the adsorption of these metals on solids such as goethite, γ-Al_2O_3, corundum, and anatase, having dielectric constants between 10 and 22, was best described by surface complexes of the metal with the electrolyte anion. Metal (M^{2+}) adsorption from $NaNO_3$ solutions is described by:

$$> SOH + M^{2+} + NO_3^- \Rightarrow SOHM^{2+} - NO_3^- \quad (4.35)$$

from $NaClO_4$ solutions by:

$$> SOH + M^{2+} + ClO_4^- \Rightarrow SOHMClO_4^+ \quad (4.36)$$

and from NaCl solutions by:

$$> SOH + M^{2+} + Cl^- \Rightarrow SOHMCl^+ \quad (4.37)$$

Adsorption of these same metals onto solids like quartz and silica, with low dielectric constants between 4 and 5, may be accompanied by the electrolyte anion in $NaClO_4$ solutions, but in $NaNO_3$ and NaCl solutions, metal adsorption occurred as $>SOM^+$ or $>SOMOH$. The large Born solvation free energies on low dielectric constant solids opposed the co-adsorption of the electrolyte anion. Using the triple-layer model with metal-anion surface complexes, isotherms of metal adsorption over a range of surface coverages could be described with a single-site model, presenting an alternative to the concept that changes in isotherm slope reflect the filling of different types of surface sites (Criscenti and Sverjensky, 2002).

4.4 Establishing Surface Species

4.4.1 Ionic Strength Effects

One approach to determine metal surface species is to fit bulk adsorption data over a range of ionic strengths and surface coverages using a surface complexation model as described above (Criscenti and Sverjensky, 1999, 2002). The use of ionic strength dependence of adsorption to distinguish between inner- and outer-sphere surface complexes has been advocated for metal ions before (Hayes and Leckie, 1987). Ions showing little ionic strength dependence in their adsorption behavior such as lead, cadmium (Hayes and Leckie, 1987), and arsenate (Hsia *et al.*, 1994; Goldberg and Johnston, 2001) were considered specifically adsorbed as strong inner-sphere surface complexes. Ions showing ionic strength dependence in their adsorption behavior such as barium (Hayes, 1987) and arsenite (Goldberg and Johnston, 2001) were considered to be weakly bound as outer-sphere surface complexes. McBride (1997) refined this concept, indicating that ions that show decreasing adsorption with increasing ionic strength are adsorbed outer-sphere while ions that show little ionic strength dependence or show increasing adsorption with increasing ionic strength are adsorbed inner-sphere.

Criscenti and Sverjensky (1999) showed that transition and heavy metals that were thought to not exhibit ionic strength dependence in adsorption behavior, in fact do exhibit a small dependence that is a function of the solution electrolyte. In $NaNO_3$ solutions, these ions exhibited no ionic strength dependence in their adsorption behavior, in NaCl solutions, they consistently exhibited decreasing adsorption with increasing ionic strength, and in $NaClO_4$ solutions, they exhibited increasing adsorption with increasing ionic strength. Despite these differences, divalent transition and heavy metal adsorption can be described using the TLM as inner-sphere complexes. However, this generalization may not hold up as more experiments are conducted in electrolyte solutions other than $NaNO_3$.

As more spectroscopic research is conducted to examine the adsorption of metals at solid-water interfaces, the use of bulk adsorption trends ***alone*** to determine the stoichiometry of surface species and associated equilibrium constants has become more questionable. For example, although Sr^{2+} is an alkaline earth metal and exhibits a strong ionic strength dependence when adsorbed to rutile, X-ray standing-wave experimental data suggest that Sr^{2+} adsorbs as an inner-sphere complex to rutile at a distance of 2.9 Å (Fenter *et al.*, 2000). The bulk data can be described by competitive adsorption between the electrolyte cation, Na^+ and Sr^{2+}; i.e., the higher the ionic strength, the more Na^+ adsorbs to the surface displacing Sr^{2+} (Zhang *et al.*, 2004). Because of the many variables involved in multicomponent systems, the surface species included in a thermodynamic SCM database must be constrained by atomistic studies.

4.4.2 X-Ray Absorption Spectroscopy

X-ray absorption spectroscopy (XAS) is one approach that is being used extensively to study adsorption at the solid-water interface. One advantage to XAS spectroscopy is that adsorption experiments can be carried out in aqueous systems (Fendorf *et al.*, 1994). X-ray absorption spectroscopy has been used to examine the sorption of both cations and anions to oxide and silicate minerals found in soils, with an emphasis on ions that are potential contaminants in the environment.

Cationic contaminants include numerous heavy metals and transition metals, and several alkaline earth metals and alkalis. The adsorption reactions of Pb^{2+}, Cd^{2+}, Co^{2+}, Hg^{2+}, Cu^{2+}, Zn^{2+}, Ni^{2+}, UO_2^{2+}, Sr^{2+}, Cs^{+}, and NpO_2^{+} onto different oxide, hydroxide, and aluminosilicate minerals have all been investigated using XAS. The following paragraphs provide a brief synopsis of the XAS studies that have been done on these systems. The nature of the surface complexes formed has been found to be a function of crystal structure, sorbing cation, ligands present in solution, and surface coverage.

X-ray absorption spectroscopy has provided evidence for inner-sphere, bidentate surface complexes of Pb^{2+} on γ-Al_2O_3 (Chisholme-Brause *et al.*, 1990; Bargar *et al.* 1996, 1997a; Strawn *et al.*, 1998), goethite (Roe *et al.*, 1991; Bargar *et al.*, 1997b), hematite (Bargar *et al.*, 1997b), and amorphous iron oxide (Trivedi *et al.*, 2003). Using grazing-incidence XAFS on single crystals of (α-Al_2O_3, Bargar *et al.* (1996) reported that inner-sphere Pb^{2+} complexes formed preferentially on the (0001) surface while outer-sphere Pb^{2+} complexes formed on the (11 $\bar{0}$2) surface. On montmorillonite, the type of Pb^{2+} surface complex that formed was a function of ionic strength (Strawn and Sparks, 1999). At low ionic strengths, Pb^{2+} adsorption to montmorillonite was pH-independent and XAS suggested that an outer-sphere complex formed. At higher ionic strength, Pb^{2+} adsorption became pH-dependent and XAS suggested that inner-sphere complexes formed. Dyer *et al.* (2003) were able to describe Pb^{2+} adsorption on amorphous iron oxide with the triple layer model using the bidentate mononuclear and monodentate mononuclear surface species observed in the XAS study of Trivedi *et al.* (2003).
Randall *et al.* (1999) studied the structure and composition of Cd^{2+} sorption complexes on several iron oxyhydroxide minerals: goethite, lepidocrocite, akagenite, and schwertmannite using EXAFS. In all cases, adsorbed Cd^{2+} formed inner-sphere complexes over a wide range of pH and Cd^{2+} concentration. However, the bonding mechanism differed between minerals and depended on the availability of different types of adsorption sites at the mineral surface. For example, Cd^{2+} sorbed to goethite by the formation of bidentate surface complexes at corner-sharing sites while Cd^{2+} sorbed to lepidocrocite by the formation of surface complexes at bi- and/or tridentate edge-sharing sites. Manceau *et al.* (2000) also found Cd^{2+} to form bidentate surface complexes at corner-sharing sites on goethite, but mononuclear, fully hydrated surface complexes on lepidocrocite. Venema *et al.* (1996) successfully described Cd^{2+} adsorption on goethite with the CD-MUSIC model using the surface species observed in the EXAFS study of Spadini *et al.* (1994).

Cobalt adsorption onto corundum (Towle *et al.*, 1999) and kaolinite (O'Day *et al.* 1994) has been studied using XAS. For Co^{2+} adsorption onto kaolinite, O'Day *et al.* (1994) found that at low surface coverages, Co^{2+} sorbed as an inner-sphere, bidentate complex. Using grazing-incidence XAFS on single crystals of corundum, Towle *et al.* (1999) found that Co^{2+} adsorbed in an inner-sphere fashion forming a tridentate complex on the (0001) surface and a tetradentate complex on the (11bar02) surface.

X-ray absorption spectroscopy has been used to investigate Zn^{2+} adsorption onto ferrihydrite, goethite, a mixture of α-Al_2O_3 and γ-Al_2O_3, and hydrous manganese oxide. Trivedi *et al.* (2001a, b) concluded that Zn^{2+} adsorbed to both hydrous ferric oxide and hydrous manganese oxide as an outer-sphere complex, but formed an inner-sphere complex on goethite. In contrast, Waychunas *et al.* (2002) found that Zn^{2+} formed inner-sphere, tetrahedrally coordinated bidentate surface complexes on ferrihydrite at low surface coverages. Trainor *et al.* (2000) found that on alumina, at low surface coverages, Zn^{2+} also formed inner-sphere, bidentate,

tetrahedrally coordinated surface complexes.

Collins *et al.* (1999a) found that Hg^{2+} sorbed to goethite as an inner-sphere, bidentate complex. Cheah *et al.* (1998) found that Cu^{2+} sorbed to amorphous silica and γ-Al_2O_3 as monomeric, monodentate, inner-sphere surface complexes. However, bidentate complexes may also form on γ-Al_2O_3. Using polarized EXAFS, Dähn *et al.* (2003) determined that Ni^{2+} sorbed to montmorillonite edge sites as an inner-sphere mononuclear surface complex. Inner-sphere surface complexes were observed with XAS for Cr^{3+} adsorption on manganese (Manceau and Charlet, 1992) and iron oxides (Charlet and Manceau, 1992).

Strontium adsorption onto soil minerals is an important retardation mechanism for $^{90}Sr^{2+}$. Chen *et al.* (1998) investigated the adsorption of Sr^{2+} onto kaolinite, illite, hectorite, and montmorillonite over a range of ionic strengths and from two different electrolyte solutions, $NaNO_3$ and $CaCl_2$. In all cases, the EXAFS spectra suggested Sr^{2+} adsorbed to clay minerals as an outer-sphere, mononuclear complex. Sahai *et al.* (2000) also found that for amorphous silica, goethite, and kaolinite substrates, Sr^{2+} adsorbed as a hydrated surface complex. On the other hand, Collins *et al.* (1998) concluded from EXAFS spectra that Sr^{2+} adsorbed as an inner-sphere complex on goethite.

Bostick *et al.* (2002) studied Cs^+ adsorption onto vermiculite and montmorillonite with EXAFS and found that Cs^+ formed both inner- and outer-sphere complexes with both aluminosilicates. The inner-sphere complexes bound to the siloxane groups in the clay structure. Waite *et al.* (1994) were successful in describing uranyl adsorption to ferrihydrite with the diffuse layer model using the inner-sphere, mononuclear, bidentate surface complex observed with EXAFS. Combes *et al.* (1992) found that NpO_2^+ adsorbed onto goethite as a mononuclear surface complex.

X-ray absorption fine structure studies on metal and metalloid anions include arsenate, and chromate (Fendorf *et al.*, 1997) on goethite, arsenate (Waychunas *et al.*, 1993) on goethite and hydrous iron oxide, and arsenate on gibbsite (Ladeira *et al.*, 2001). Mixtures of inner- and outer-sphere surface complexes were observed for arsenite on γ-Al_2O_3 (Arai *et al.*, 2001). Manning and Goldberg (1996) postulated a mixture of bidentate and monodentate surface complexes in modeling arsenate adsorption on goethite, consistent with the results of Waychunas *et al.* (1993). Using EXAFS, Manning *et al.* (1998) observed a bidentate, binuclear bridging complex for arsenite adsorbed on goethite. This complex was incorporated into the constant capacitance model and an excellent fit of arsenite adsorption data was obtained. Grossl *et al.* (1997) used the EXAFS results of Fendorf *et al.* (1997) to describe arsenate and chromate adsorption on goethite using the constant capacitance model.

4.4.3 X-ray Reflectivity

X-ray reflectivity measurements can provide important about mineral-water interfaces in situ by accurately determining the position of an adsorbed monolayer relative to the substrate surface. By measuring x-ray reflectivity of calcite with and without lead, it was established that the lead ions were located in the surface atomic layer (Sturchio *et al.*, 1997). X-ray reflectivity measurements found rubidium to be specifically adsorbed to the rutile surface at the tetradentate site (Zhang *et al.*, 2004). These authors were able to include this information in the CD-MUSIC model to obtain an accurate description of rubidium adsorption.

4.4.4 *Ab initio* and Molecular Modeling

Ab initio and molecular modeling can be used to investigate the stoichiometries and relative adsorption energies of viable surface complexes, and to set bounds on the uncertainties associated with different surface complexation models (Criscenti, 2004). *Ab initio* and molecular mechanics modeling provides significant information regarding: (1) the stoichiometry of adsorbing species both in terms of the number of bonds an adsorbing species will make with a mineral surface and metal-ligand pairing at the surface; (2) the structure of water at the mineral-water interface and the corresponding structure in the presence of an adsorbing species; (3) the relative adsorption energies of different possible surface species. *Ab initio* and molecular modeling simulations can also be valuable tools to examine how different factors like: (1) short- and long-range solvation of the ion both in solution and at the mineral surface; (2) the periodic structure of the mineral surface; (3) the structure and dielectric constant of interfacial water, influence the adsorption process as a whole (Criscenti, 2004).

Quantum mechanics calculations on small clusters of atoms can be used in combination with X-ray absorption fine-structure (EXAFS) data to determine the mechanism of metal binding on oxide surfaces. For example, Collins *et al.* (1999a) found several geometries for Hg^{2+} adsorption to goethite that were consistent with EXAFS data, but only one that gave calculated Hg-Fe distances consistent with those observed. In this geometry, Hg^{2+} adsorption occurred via two oxygen atoms bound to edge-sharing Fe sites on the (110) surface. This same group of researchers (Randall *et al.*, 1999; Collins *et al.*, 1998, 1999b) combined quantum calculations and EXAFS data to constrain the geometry of Cd^{2+} and Sr^{2+} surface complexes on goethite and found that these metals bound to the same type of site as mercury. Peacock and Sherman (2004a) used *ab initio* calculations in support of their EXAFS data to determine the stoichiometry of adsorbed Cu^{2+} species on several iron oxides. These surface complex stoichiometries were then used to fit experimental Cu^{2+} adsorption data within a diffuse layer or triple layer model framework. The same type of investigation was conducted for vanadium adsorption to goethite (Peacock and Sherman, 2004b). In this case, the fits to sorption edge data using the surface complexes determined from *ab initio* cluster calculations and EXAFS data were more nebulous.

Classical molecular mechanics approaches have also been used to investigate the adsorption of metal ions to different mineral surfaces from aqueous solution. For example, using a molecular dynamics approach with interatomic force fields, Cygan *et al.* (1998) examined Cs^{+} adsorption onto fully-hydroxylated kaolinite surfaces from chloride solutions. Using a different force field approach, Steele *et al.* (2000) investigated the adsorption of Cu^{2+}, Zn^{2+}, and Cd^{2+} to the (001) muscovite surface. The calculations showed that these metals do not form strong bonds with the smooth basal plane of muscovite. However, upon the introduction of edge-like defects, both Cu^{2+} and Zn^{2+} cations bound strongly to the defect sites with bond lengths and coordination numbers in agreement with experiment.

A large research effort has been underway to develop a comprehensive picture of the interface between aqueous solutions and the (110) surface of rutile (α-TiO_2). This effort has combined molecular-scale and macroscopic approaches including experimental measurements, quantum calculations, molecular simulations, and Gouy-Chapman-Stern models (Zhang *et al.*, 2004). *Ab initio* calculations and molecular dynamics simulations, validated through direct comparison with X-ray standing-wave measurements, were used to predict ion distributions not measured experimentally. Surface oxygen proton affinities computed using the CD-MUSIC model have been improved by the incorporation of *ab initio* bond lengths and partial charges. All cations

considered (Na^+, Rb^+, Ca^{2+}, Sr^{2+}, Zn^{2+}, Y^{3+}, Nd^{3+}) were found to adsorb as "inner sphere" species directly to surface oxygen atoms, while the specific binding geometries and reaction stoichiometries were dependent on ionic radius. This investigation, illustrated the success of using different types of modeling to investigate adsorption reactions.

4.5 Summary

In summary, substantial progress has been made to establish an internally-consistent thermodynamic database for the triple-layer model. In particular, efforts to define standard states for the solid-water interface, now allow us to interpret existing bulk adsorption datasets collected using different solid to liquid ratios using a normalized approach. X-ray standing-wave measurements, X-ray absorption spectroscopy, molecular modeling, and *ab initio* modeling all contribute to greater understanding of surface complexation, and in particular, to the nature of contaminant surface species that need to be incorporated into larger-scale thermodynamic models. Combined approaches in combination with efforts to correlate data from different solid-water systems could lead to major breakthroughs in adsorption modeling in the next decade.

4.6 Acknowledgments

This chapter represents a subset of material written by L.J. Criscenti and S. Goldberg for the draft white paper on reactive processes written by the Interagency Memorandum of Understanding Working Group 3: Subsurface Reactive Transport Modeling as well as a draft chapter on adsorption modeling written by Sabine Goldberg and Louise Criscenti for an International Union of Pure and Applied Chemistry (IUPAC) volume. This collaboration between Sandia National Laboratories and the USDA-ARS, George E. Brown Jr. Salinity Laboratory evolved through the Interagency MOU interaction (see Section 1.). Further information on the working group and the MOU can be found on the internet at www.iscmem.org.

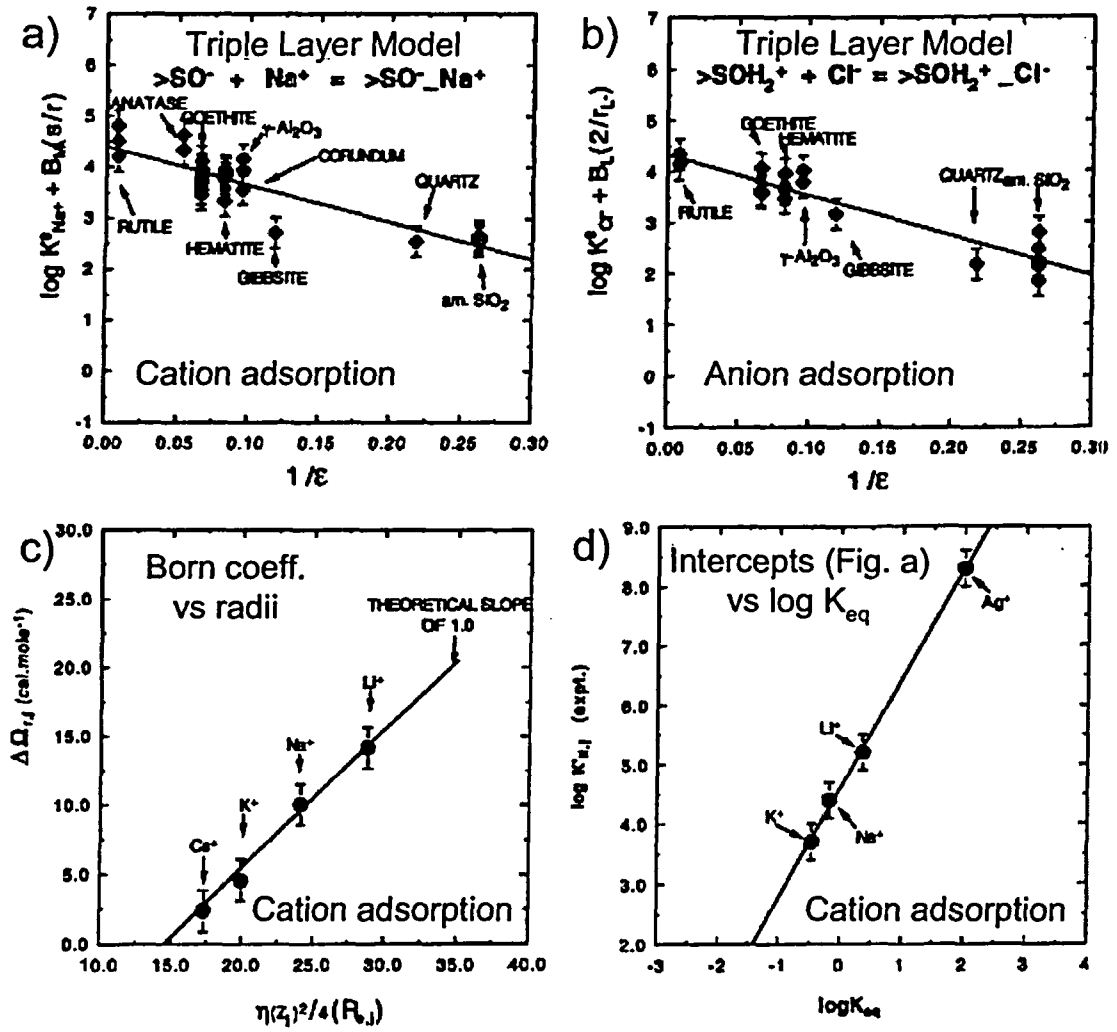

Figure 4.1 Correlations between adsorption constants and mineral properties. (a) Values of $\log K^{\theta}_{M^+}$ as a function of the dielectric constant $\left(\frac{1}{\varepsilon_s}\right)$ and values of the bond strength per Å $\left(\frac{s}{r_{M^+}}\right)$; (b) values of $\log K^{\theta}_{L^-}$ as a function of the dielectric constant $\left(\frac{1}{\varepsilon_s}\right)$ and the repulsive term in Å $\left(\frac{2}{r_{L^-}}\right)$; (c) values of $\Delta\Omega_{r,M^+}$ as a function of the effective electrostatic radius $\left(\frac{1}{R_{e,j}}\right)$ and values of $r_{x,j}$; (d) linear free energy correlations for values of $\log K^{*}_{i,M^+}$ with the aqueous phase equilibrium association constants $\log K_{M(OH)^0}$. Adapted from Sverjensky (2005) with permission from Elsevier.

5. CONCLUSIONS

Adsorption onto soil and mineral surfaces is responsible for the attenuation and retardation of metal species in groundwaters and the subsurface environment. Although much research has been completed in the past several decades on the mechanisms of adsorption, the development of conceptual models that can be used to successfully predict radionuclide adsorption is still far from being complete. The first part of this study illustrated the impact of using poorly constrained adsorption parameters in a reactive-transport code may have on predicted contaminant concentrations downstream from a waste site. It was determined that the choice of the log *K* thermodynamic parameter for hydrolysis of the clay edge site was critical in controlling the extent of the uranium migration for an idealized groundwater system. The second part described how atomic-scale investigations can be used to improve the thermodynamic-based adsorption models (SCMs) available with reactive-transport codes. Different techniques, including X-ray absorption spectroscopy, quantum and molecular mechanics modeling can be used to provide significant information regarding the properties of the mineral-water interface including surface site types and density; and, the stoichiometry of adsorbed species. The final part of the report reviewed progress in developing a comprehensive and internally-consistent database of adsorption parameters for a specific SCM (i.e., the triple-layer model). This is one of the critical goals for the NRC and its performance assessment efforts—a general adsorption model and database that can be incorporated into the reactive-transport models that are used to assess potential risk at contaminated field sites.

There are several major geochemical issues with using the SCMs available today to understand adsorption processes in the field. The first issue is that we do not know if the SCMs and adsorption parameters that have been collected to date on very simple experimental systems can truly represent adsorption processes in the field. With the development of HRTEM and various synchrotron-based analytical techniques (including XAS, X-ray reflectivity, and surface microtomography) we are now learning that the main adsorbents in complex soil systems may not be the ones that we originally identified. Clearly no amount of data collected to establish adsorption parameters for goethite, as an example, will be useful if goethite is not the dominant adsorbent in the soil in question. In addition, SCMs have been developed primarily using simple experimental systems involving one solid, one electrolyte, and one trace metal species. Recent research shows that competitive adsorption of Pb^{2+} and Cd^{2+} on iron oxide (Katz and Chen, 2003) can be predicted using the adsorption parameters developed from single-metal experiments. Limited effort has been done to evaluate the use of these SCM databases with multi-mineral systems or multicomponent natural waters.

Another important issue with accurately calculating adsorption processes in the field is that adsorption occurs at complicated solid-water interfaces on the scale of Ångstroms to nanometers. We should remember that SCMs have been adapted to apply to complex aqueous-solid systems from simple theories intended to describe ion distributions from an electrode into bulk solution. Adaptations have included: (1) different descriptions of the electric potential gradient from a mineral surface to the bulk solution, (2) different positions for ion adsorption along this gradient, (3) different numbers and types of surface sites, and (4) different stoichiometries and structures for the adsorbed metal species. Investigations of mineral-water interfaces through spectroscopic and/or modeling techniques should focus on establishing which of these, or other as yet unidentified variables, are the *principle* ones influencing ion adsorption. The advantage of computational chemistry methods is not the ability to reproduce reality but to investigate the effects of different interfacial variables on contaminant adsorption with the hope

of establishing a new set of rules that can be applied with some level of generalization to different metals, adsorbents, and solution compositions.

6. REFERENCES

Allison, J.D., D.S. Brown, K.J. Novo-Gradac (1991) MINTEQA2/PRODEFA2, A Geochemical Assessment Model for Environmental Systems: Version 3.0 User's Manual. Report EPA/600/3-92/021, U.S. E.P.A., Athens, GA.

Anderson, G.M. (1976) Error propagation by the Monte Carlo method in geochemical calculations. *Geochim. Cosmochim. Acta* **40**:1533-1538.

Arai, Y., E.J. Elzinga, and D.L. Sparks (2001) X-ray absorption spectroscopic investigation of arsenite and arsenate at the aluminum oxide-water interface. *J. Coll. Inter. Sci.* **235**:80-88.

Axe, L., T. Tyson, P. Trivedi, and T. Morrison (2000) Local structure analysis of strontium sorption to hydrous manganese oxide. *J. Coll. Inter. Sci.* **224**:408-416.

Bain, J.G., K.U. Mayer, D.W. Blowes, E.O. Frind, J.W.H. Molson, R. Kahnt, and U. Jenk (2001) Modelling the closure-related geochemical evolution of groundwater at a former uranium mine. *J. Contam. Hydrol.* **52**:109-135.

Bargar, J.R., S.N. Towle, G.E. Brown, Jr., and G.A. Parks (1996) Outer-sphere Pb(II) adsorbed at specific surface sites on single crystal α-alumina. *Geochim. Cosmochim. Acta* **60**:3541-3547.

Bargar, J.R., G.E. Brown, Jr., and G.A. Parks (1997a) Surface complexation of Pb(II) at oxide-water interfaces. 1. XAFS and bond-valence determination of mononuclear and polynuclear Pb(II) sorption products on aluminum oxides. *Geochim. Cosmochim. Acta* **61**:2617-2637.

Bargar, J.R., G.E. Brown, Jr., and G.A. Parks (1997b) Surface complexation of Pb(II) at oxide-water interfaces. 2. XAFS and bond-valence determination of mononuclear Pb(II) sorption products and surface functional groups on iron oxides. *Geochim. Cosmochim. Acta* **61**:2639-2652.

Bargar, J.R., G.E. Brown, Jr., and G.A. Parks (1998) Surface complexation of Pb(II) at oxide-water interfaces: III. XAFS determination of Pb(II) and Pb(II)-chloro adsorption complexes on goethite and alumina. *Geochim. Cosmochim. Acta* **62**:193-207.

Berner, E.K. and R. A. Berner (1996) *Global Environment: Water, Air and Geochemical Cycles.* Prentice Hall, New Jersey, 376 pp.

Bethke, C.M. (1996) *Geochemical Reaction Modeling: Concepts and Applications.* Oxford University Press, New York, 397 pp.

Bethke, C.M. (1997a) *Xt Model of Transport in Reacting Geochemical Systems, Notes to Accompany the Xt Modeling Workbook.* Hydrogeology Program, University of Illinois, Urbana-Champaign.

Bethke, C.M. (1997b) Modelling transport in reacting geochemical systems. *Comptes Rendus de l'Académie des Sciences: Sciences de la Terre et des Planètes* **324**:513-528.

Bethke, C.M. (1998) *The Geochemist's Workbench: A User's Guide to Rxn, Act2, Tact, React and Gtplot. Release 3.0.* Craig M. Bethke, University of Illinois.

Bethke, C.M. and Brady, P.V. (2000) How the K_d approach undermines groundwater cleanup. *Ground Water*, **38**:35-443.

Bostick, B.C., M.A. Vairavamurthy, K.G. Karthikeyan, and J. Chorover (2002) Cesium adsorption on clay minerals: An EXAFS spectroscopic investigation. *Environ. Sci. Technol.* **36**:2670-2676.

Boyle-Wight, E.J., L.E. Katz, and K.F. Hayes (2002a) Macroscopic studies of the effects of selenate and selenite on cobalt sorption to γ-Al_2O_3. *Environ. Sci. Technol.* **36**:1212-1218.

Boyle-Wight, E.J., L.E. Katz, and K.F. Hayes (2002b) Spectroscopic studies of the effects of selenate and selenite on cobalt sorption to γ-Al_2O_3. *Environ. Sci. Technol.* **36**:1219-1225.

Brady, P.V., R.T. Cygan, and K.L. Nagy (1996) Molecular controls on kaolinite surface charge. *J. Coll. Inter. Sci.* **183**:356-354.

Brady, P.V., R.T. Cygan, and K.L. Nagy (1998) Surface charge and metal sorption to kaolinite. In: Jenne, E.A. (Ed.), *Adsorption of Metals by Geomedia: Variables, Mechanisms, and Model Applications.* Academic Press, New York, pp. 371-382.

Brown, G.E., Jr., V.E. Henrich, W.H. Casey, D.L. Clark, C.M. Eggleston, A.R. Felmy, D.W. Goodman, M. Grätzel, G. Maciel, M.I. McCarthy, K.H. Nealson, D.A. Sverjensky, M.F. Toney, and J.M. Zachara (1999) Metal oxide surfaces and their interactions with aqueous solutions and microbial organisms. *Chem. Rev.* **99**:77-174.

Cancès, E., B. Mennucci, and J. Tomasi (1997) A new integral equation formalism for the polarizable continuum model: Theroetical background and applications to isotropic and anisotropic dielectrics. *J. Chem. Phys.* **107**:3032-3041.

Charlet, L. and A.A. Manceau (1992) X-ray absorption spectroscopic study of the sorption of Cr(III) at the oxide-water interface. II. Adsorption coprecipitation, and surface precipitation of hydrous ferric oxide. *J. Coll. Inter. Sci.* **148**:443-458.

Cheah, S.F., G.E. Brown, Jr., and G.A. Parks (1998) XAFS spectroscopy study of Cu(II) sorption on amorphous SiO_2 and γ-Al_2O_3: Effect of substrate and time on sorption complexes. *J. Coll. Inter. Sci.* **208**:110-128.

Chen, C.-C., C. Papelis, and K.F. Hayes (1998) Extended X-ray absorption fine structure (EXAFS) analysis of aqueous Sr^{II} ion sorption at clay-water interfaces. In: E.A. Jenne (Ed.), *Adsorption of Metals by Geomedia: Variables, Mechanisms, and Model Applications.* Academic Press, New York, pp. 333-348.

Chisholme-Brause, C.J., K.F. Hayes, A.L. Roe, G.E. Brown, Jr., G.A. Parks, and J.O. Leckie (1990) Spectroscopic investigation of Pb(II) complexes at the γ-Al_2O_3/water interface. *Geochim. Cosmochim. Acta* 54:1897-1909.

Chisholm-Brause, C.J., J.M. Berg, R. A. Matzner, and D.E. Morris (2001) Uranium(VI) sorption complexes on montmorillonite as a function of solution chemistry. *J. Coll. Inter. Sci.* **233**:38-49.

Collins, C.R., D.M. Sherman, and K.V. Ragnarsdóttir (1998) The adsorption mechanism of Sr^{2+} on the surface of goethite. *Radiochim. Acta* **81**:201-206.

Collins, C.R., D.M. Sherman, and K.V. Ragnarsdóttir (1999a) Surface complexation of Hg^{2+} on goethite: Mechanism from EXAFS spectroscopy and density functional calculations. *J. Coll. Inter. Sci.* **219**:345-350.

Collins C.R., K.V. Ragnarsdottir, and D.M. Sherman (1999b) Effect of inorganic and organic ligands on the mechanism of cadmium sorption to goethite. *Geochim. Cosmochim. Acta* **63**:2989-3002.

Combes, J.M., C.J. Chisholme-Brause, G.E. Brown, G.A. Parks, S.D. Conradson, P.G. Eller, I.R. Triay, D.E. Hobart, and A. Meijer (1992) EXAFS spectroscopic study of neptunium(V) sorption at the α-FEOOH/water interface. *Environ. Sci. Technol.* **26**:376-382.

Criscenti, L.J. (1996) *Investigations of coupled geochemical and transport modeling for the Hazardous Waste Identification Rule.* Athens, GA: US Environmental Protection Agency. EPA/600/SR-96/141.

Criscenti, L.J. (2004) Adsorption processes: At what spatial scale do we need to understand them? Proceedings of the 11th International Symposium on Water-Rock Interaction, WRI-11, 27th June – 2 July 2004, Saratoga Springs, NY. Eds. R.B. Wanty and R.R. Seal, A.A. Balkema Publishers, NY, p. 909-916.

Criscenti, L.J. and R.T. Cygan (2004) Molecular dynamics simulations of the gibbsite-water interface with sodium chloride and lead. Abstracts of Papers of the American Chemical Society; Mar 28, 2004; v. 227, pt. 1, p. U1215-U1215.

Criscenti, L.J. and J.D. Kubicki (2001) Influence of dielectric constant on metal surface complexation. *Abstracts of Papers of the Am. Chem. Soc.* **221**: U528

Criscenti, L.J. and D.A. Sverjensky (1999) The role of electrolyte anions (ClO_4^-, NO_3^-, Cl^-) in divalent metal (M^{2+}) adsorption on oxide and hydroxide surfaces in salt solutions. *Am. J. Sci.* **299**:828-899.

Criscenti, L.J. and D.A. Sverjensky (2002) A single-site model for divalent transition and heavy metal adsorption over a range of metal concentrations. *J. Coll. Inter. Sci.* **253**:329-352.

Criscenti, L.J., G.F. Laniak, and R.L. Erikson (1996) Propagation of Uncertainty through Geochemical Code Calculations. *Geochim. Cosmochim. Acta* **60**, 3551-3568.

Criscenti, L.J., M. Eliassi, R.T. Cygan, and C.F. Jové-Colón (2002) *Effects of adsorption constant uncertainty on contaminant plume migration: One- and two-dimensional numerical studies.* Washington, DC: US Nuclear Regulatory Commission. NUREG/CR-6780

Criscenti, L.J., R.T. Cygan and J.A. Voigt (2003) Molecular Modeling of the Adsorption of Anionic and Molecular Species to Zincite Surfaces, 225th American Chemical Society National Meeting, New Orleans, COMP 160.

Curtis, G.P. (2005) *Documentation and Applications of the Reactive Geochemical Transport Model RATEQ.* Washington, DC: US Nuclear Regulatory Commission. NUREG/CR-6871.

Curtis, G.P., P. Fox, M. Kohler, and J.A. Davis (2004) Comparison of in situ uranium K_d values with a laboratory determined surface complexation model. *Appl. Geochem.* **19**:1643-1653.

Cygan, R.T., K.L. Nagy, and P.V. Brady (1998) Molecular models of cesium sorption on kaolinite. In: Jenne, E.A. (Ed.), *Adsorption of Metals by Geomedia: Variables, Mechanisms, and Model Applications*, Academic Press, New York, pp. 383-399.

Dähn, R., A.M. Scheidegger, A. Manceau, M.L. Schlegel, B. Baeyens, M.H. Bradbury, and D. Chateigner (2003) Structural evidence for the sorption of Ni(II) atoms on the edges of montmorillonite clay minerals: A polarized X-ray absorption fine structure study. *Geochim. Cosmochim. Acta* **67**:1-15.

Davis, J.A. (2001) *Surface Complexation Modeling of Uranium(VI) Adsorption on Natural Assemblages.* NUREG/CR-6708, U. S. Nuclear Regulatory Commission, Rockville, MD.

Davis, J.A. and G.P. Curtis (2003) *Application of Surface Complexation Modeling to Describe Uranium(VI) Adsorption and Retardation at the Uranium Mill Tailings Site at Naturita, Colorado.* NUREG/CR-6820. U.S. Nuclear Regulatory Commission, Rockville, MD.

Davis, J.A. and G.P. Curtis (2005) Consideration of Geochemical Issues in Groundwater Restoration at Uranium In-Situ Leach Mining Facilities. NUREG/CR-6870, U.S. Nuclear Regulatory Commission, Washington, DC.

Davis, J.A. and D.B. Kent (1990) Surface complexation modeling in aqueous *geochemistry. In: Hochella, Jr., M.F., White, A.R. (Eds.), Mineral-Water Interface Geochemistry. Reviews* in *Mineralogy*, **23**, Mineralogical Society of America, Washington, D. C., pp. 177-260.

Davis, J.A. and J.O. Leckie (1978) Surface ionization and complexation at the oxide/water interface. II. Surface properties of amorphous iron oxyhydroxide and adsorption of metal ions. *J. Coll. Inter. Sci.* **67**:90-107.

Davis, J.A., R.O. James, and J.O. Leckie (1978) Surface ionization and complexation at the oxide/water interface I. Computation of electrical double layer properties in simple electrolytes. *J. Coll. Inter. Sci.* **63**:480-499.

Davis, J.A., J.A. Coston, D.B. Kent, and C.C. Fuller (1998) Application of the surface complexation concept to complex mineral assemblages. *Environ. Sci. Technol.* **32**:2820-2828.

Davis, J.A., D.E. Meece, M. Kohler, and G.P. Curtis (2004) Approaches to surface complextaion modeling of uranium(VI) adsorption on aquifer sediments. *Geochim. Cosmchim. Acta* **68**:3621-3641.

Domenico, P.A. and F.W. Schwartz (1990) *Physical and Chemical Hydrogeology*, John Wiley and Sons, New York.

Dyer, J.A., P. Trivedi, N.C. Scrivner, and D.L. Sparks (2003) Lead sorption onto ferrihydrite. 2. Surface complexation modeling. *Environ. Sci. Technol.* **37**:915-922.

Dzombak, D.A. and F.M.M. Morel (1990) *Surface Complexation Modeling: Hydrous Ferric Oxide.* John Wiley and Sons, New York.

Erikson, R.L., C.J. Hostetler, and M.L. Kemnar (1990) *Mobilization and Transport of Uranium at*

Uranium Mill Tailings Disposal Sites. NUREG/CR-5169 PNL-7154, Nuclear Regulatory Commission (NRC), Washington, D.C.

Fendorf, S.E., D.L. Sparks, G.M. Lamble, and M.J. Kelley (1994) Applications of X-ray absorption fine-structure spectroscopy to soils. *Soil Sci. Soc. Am. J.* **58**:1583-1695.

Fendorf, S.E., M.J. Eick, P. Grossl, and D.L. Sparks (1997) Arsenate and chromate retention mechanisms on goethite: I. Surface structure. *Environ. Sci. Technol.* **31**:315-320.

Fenter, P., L. Cheng, S. Rihs, M.L. Machesky, M.J. Bedzyk, and N.C. Sturchio (2000) Electrical double-layer structure at the rutile-water interface as observed in situ with small-period X-ray standing waves. *J. Coll. Inter. Sci.* **225**:154-165.

Frind, E.O. and D. Germain (1986) Simulation of contaminant plumes with large dispersive contrast: Evaluation of alternating direction Galerkin models. *Wat. Resources Res.* **22**:1857-1873.

Gelhar, L.W. (1986) Stochastic subsurface hydrology from theory to applications. *Wat. Resources Res.* **22**:135S-145S.

Goldberg, S. and C.T. Johnston (2001) Mechanisms of arsenic adsorption on amorphous oxides evaluated using macroscopic measurements, vibrational spectroscopy, and surface complexation modeling. *J. Coll. Inter. Sci.* **234**:204-216.

Grossl, P., M.J. Eick, D.L. Sparks, S. Goldberg, and C.C. Ainsworth (1997) Arsenate and chromate retention mechanisms on goethite: II. Kinetic evaluation using a pressure-jump relaxation technique. *Environ. Sci. Technol.* **31**:321-326.

Hamed, M.M., P.B. Bedient, and J.P. Conte (1996) Numerical stochastic analysis of groundwater contaminant transport and plume containment. *J. Contam. Hydrol.* **24**:1-24.

Hayes, K.F. (1987) *Equilibrium, spectroscopic, and kinetic studies of the ion adsorption at the oxide/aqueous interface.* PhD. Thesis, Stanford University, Stanford.

Hayes, K.F. and J.O. Leckie (1987) Modeling ionic strength effects on cation adsorption at hydrous oxide/solution interfaces. *J. Coll. Inter. Sci.* **115**:564-572.

Hayes, K.F., G. Redden, W. Ela, and J.O. Leckie (1991) Surface complexation models: An evaluation of model parameter estimation using FITEQL and oxide mineral titration data. *J. Coll. Inter. Sci.* **142**:448-469.

Helgeson, H.C., D.H. Kirkham, and G.C. Flowers (1981) Theoretical prediction of the thermodynamic behavior of aqueous electrolytes at high pressures and temperatures: IV. Calculation of activity coefficients, osmotic coefficients, and apparent molal and standard and relative partial molal properties to 600°C and 5 KB. *Am. J. Sci.* **281**:1249-1516.

Hennig, C., T. Reich, R. Dähn, and A.M. Scheidegger (2002) Structure of uranium sorption complexes at montmorillonite edge sites. *Radiochim. Acta* **90**:653-657.

Hiemstra, T., P. Venema, and W.H. van Riemsdijk (1996) Intrinsic proton affinity of reactive surface groups of metal (hydr)oxides: The bond valence principle. *J. Coll. Inter. Sci.* **184**: 680-692.

Hsia, T.H., S.L. Lo, C.F. Lin, and D.Y. Lee (1994) Characterization of arsenate adsorption on hydrous iron oxide using chemical and physical methods. *Colloids Surf. A: Physicochem. Eng. Aspects* **85**:1-7.

Hyun, S.P., Y.H. Cho, P.S. Hahn, and S.J. Kim (2001) Sorption mechanism of U(VI) on a reference montmorillonite: Binding to the internal and external surfaces. *J. Radioanal. Nucl. Chem.* **250**:55-62.

Iman, R.L. and M.J. Shortencarier (1984) *A Fortran 77 Program and User's Guide for the Generation of Latin Hypercube and Random Samples for Use with Computer Models.* NUREG/CR-3624, Technical Report SAND83-2365, Sandia National Laboratories, Albuquerque, NM.

Jacobs Engineering Group Inc. (1994) *UMTRA Project Water Sampling and Analysis Plan: Naturita, Colorado.* DOE/AL/62350-121F, Department of Energy (DOE) – Grand Junction Office (GJO): Grand Junction, CO.

James, R.O. and T.W. Healy (1972) Adsorption of hydrolyzable metal ions at the oxide-water interface. III. A thermodynamic model of adsorption. *J. Coll. Inter. Sci.* **40**:65-81.

James R.O. and G.A. Parks (1982) Characterization of aqueous colloids by their electrical double-layer and intrinsic surface chemical properties. *Surf. Colloid Sci.* **12**:119-216.

Jové Cólón, C.F., P.V. Brady, M.D. Siegel, R. Lindgren (2001) Historical Case Analysis of Uranium Plume Attenuation. *Soil Sed. Contam.* **10**:71-115.

Jové Cólón, C.F., C. Sanpawanitchakit, H. Xu, R.T. Cygan, J.A. Davis, D.M. Meece (2005) *A Combined Analytical Study to Characterize Uranium Soil Contamination: The Case of the Naturita UMTRA Site and the Role of Grain Coatings.* (in prep, NUREG document).

Katz, L.E. and C.C. Chen (2003) Surface complexation modeling of multicomponent metal ion adsorption on oxide and clay minerals. *Abstracts of Papers of the American Chemical Society*, Sept. 2003; v. 226, p. U510-U510.

Katz, L.E. and E.J. Boyle-Wight (2001) Application of spectroscopic methods to sorption model parameter estimation. *Soil Sci. Soc. Amer. Spec. Pub.* **56**:213-255.

Kohler, M., G.P. Curtis, D.E. Meece, and J.A. Davis (2004) Methods for estimating adsorbed uranium(VI) and distribution coefficients of contaminated sediments. *Environ. Sci. Technol.* **38**:240-247.

Koretsky, C. (2000) The significance of surface complexation reactions in hydrologic systems: A geochemist's perspective. *J. Hydrol.* **230**:127-171.

Koretsky, C.M., D.A. Sverjensky, and N. Sahai (1998) Surface site types on oxide and silicate minerals based on crystal chemistry: Implications for site densities, multi-site adsorption, surface infrared spectroscopy, and dissolution kinetics. *Am. J. Sci.* **298**:349-438.

Krupka, K.M., R.L. Erikson, S.V. Mattigod, J.A. Schramke, and C.E. Cowan (1988) *Thermochemical data used by the FASTCHEM package.* California. Electric Power Research Institute (EPRI): EA-5872.

Kubicki, J.D. and S.E. Apitz (1998) Molecular cluster models of aluminum oxide and aluminum hydroxide surfaces. *Am. Miner.* **83**:1054-1066.

Kubicki, J.D., G.A. Blake, and S.E. Apitz (1996) Ab initio calculations on aluminosilicate Q^3 species: Implications for atomic structures of mineral surfaces and dissolution mechanisms of feldspars. *Am. Miner.* **81**:789-799.

Kulik, D.A. (2002a) Sorption modelling by Gibbs energy minimisation: Towards a uniform thermodynamic database for surface complexes of radionuclides. *Radiochim. Acta* **90**:815-832.

Kulik, D.A. (2002b) A Gibbs energy minimization approach to model sorption equilibria at the mineral-water interface: Thermodynamic relations for multi-site surface-complexation. *Am. J. Sci.* **302**:227-279.

Kulik, D.A., S.U. Aja, V.A. Sinitsyn, and S.A. Wood (2000) Acid-base surface chemistry and sorption of some lanthanides on K^+-saturated Marblehead illite: II. A multisite-surface complexation modeling. *Geochim. Cosmochim. Acta* **64**:195-213.

Ladeira, A.C.Q., V.S.T. Ciminelli, H.A. Duarte, M.C.M. Alves, and A.Y. Ramos (2001) Mechanism of anion retention from EXAFS and density functional calculations: Arsenic(V) adsorbed on gibbsite. *Geochim. Cosmochim. Acta* **65**:1211-1217.

Landa, E.R. and J.R. Gray (1995) U.S. Geological Survey – Research on the environmental fate of uranium mining and millings wastes. *Environ. Geol.* **26**:19-31.

Manceau, A. and L. Charlet (1992) X-ray absorption spectroscopic study of the sorption of Cr(III) at the oxide-water interface. I. Molecular mechanism of Cr(III) oxidation on Mn oxides. *J. Coll. Inter. Sci.* **148**:425-442.

Manceau, A., K.L. Nagy, L. Spadini, and K.V. Ragnarsdottir (2000) Influence of anionic layer structure of Fe-oxyhydroxides on the structure of Cd surface complexes. *J. Coll. Inter. Sci.* **228**:306-316.

Manning, B.A. and S. Goldberg (1996) Modeling competitive adsorption of arsenate with phosphate and molybdate on oxide minerals. *Soil Sci. Soc. Am. J.* **60**:121-131.

Manning, B.A., S.E. Fendorf, and S. Goldberg (1998) Surface structures and stability of arsenic(III) on goethite. Spectroscopic evidence for inner-sphere complexes. *Environ. Sci. Technol.* **32**:2383-2388.

McBride, M.B. (1997) A critique of diffuse double layer models applied to colloid and surface chemistry. *Clays Clay Miner.* **45**:598-608.

McKinley, J.P., J.M. Zachara, S.C. Smith, and G.D. Turner (1995) The influence of uranyl hydrolysis and multiple site-binding reactions on adsorption of U(VI) to montmorillonite. *Clay*

Clay Min. **43**:586-598.

Morrison, S.J. and L.S. Cahn (1991) Mineralogical residence of alpha-emitting contamination and implications for mobilization from uranium mill tailings. *J. Contam. Hyd.* **8**:1-21.

Neuman, S.P. (1990) Universal scaling of hydraulic conductivities and dispersivities in geologic media. *Wat. Resources Res.* **26**:1749-1758.

Nitzsche, O., G. Meinrath, and B. Merkel (2000) Database uncertainty as a limiting factor in reactive transport prognosis. *J. Contam. Hydrol.* **44**:223-237.

Nordstrom, D.K. and J.W. Ball (1989) Mineral saturation states in natural waters and their sensitivity to thermodynamic and analytical errors. *Sci. Geol. Bull.* **42**:269-280.

O'Day, P.A., G.A. Parks, and G.E. Brown, Jr. (1994) Molecular structure and binding sites of cobalt(II) surface complexes on kaolinite from X-ray absorption spectroscopy. *Clays Clay Miner.* **42**:337-355.

O'Day, P.A., M. Newville, P.S. Neuhoff , N. Sahai, and S.A. Carroll. (2000) X-ray absorption spectroscopy of strontium(II) coordination I. Static and thermal disorder in crystalline, hydrated, and precipitated solids and in aqueous solution. *J. Coll. Inter. Sci.* **222**:184-197.

Ostergren, J.D., T.P. Trainor, J.R. Bargar, G.E. Brown, Jr., and G.A. Parks (2000a) Inorganic ligand effects on Pb(II) sorption to goethite (α-FeOOH) I. Carbonate. *J. Coll. Inter. Sci.* **225**:466-482.

Ostergren, J.D., G.E. Brown, Jr., G.A. Parks, and P. Persson (2000b) Inorganic ligand effects on Pb(II) sorption to goethite (α-FeOOH) – II. Sulfate. *J. Coll. Inter. Sci.* **225**:483-493.

Pabalan, R.T., D.R. Turner, F.P. Bertetti, and J.D. Prikryl (1998) Uranium^{VI} sorption onto selected mineral surfaces: Key geochemical parameters. In: Jenne, E.A. (Ed.), *Adsorption of Metals by Geomedia: Variables, Mechanisms, and Model Applications.* Academic Press, New York, pp. 99-130.

Papelis, C., K.F. Hayes, and J.O. Leckie (1988) *HYDRAQL: A Program for the Computation of Chemical Equilibrium Compositions of Aqueous Batch Systems including Surface-Complexation Modeling of Ion Adsorption at the Oxide/Solution Interface.* Technical Report No. 306, Stanford University, Stanford, CA.

Peacock, C.L. and D.M. Sherman (2004a) Copper(II) sorption onto goethite, hematite, and lepidocrocite: A surface complexation model based on ab initio molecular geometries and EXAFS spectroscopy. *Geochim. Cosmochim. Acta* **68**:2623-2637.

Peacock, C.L. and D.M. Sherman (2004b) Vanadium(V) adsorption onto goethite (α-FeOOH) at pH 1.5 to 12: A surface complexation model based on ab initio molecular geometries and EXAFS spectroscopy. *Geochim. Cosmochim. Acta* **68**:1723-1734.

Randall, S.R., D.M. Sherman, K.V. Ragnarsdottir, and C.R. Collins (1999) The mechanism of cadmium surface complexation on iron oxyhydroxide minerals. *Geochim. Cosmochim. Acta* **63**:2971-2987.

Roberts, D.R., R.G. Ford, and D.L. Sparks (2003) Kinetics and mechanisms of Zn complexation on metal oxides using EXAFS spectroscopy. *J. Coll. Inter. Sci.* **263**:364-376.

Roe, A. L., K. F. Hayes, C. Chisholm-Brause, G.E. Brown, Jr., G.A. Parks, K.O. Hodgson, and J.O. Leckie (1991) In situ X-ray absorption study of lead ion surface complexes at the goethite-water interface. *Langmuir* **7**:367-373.

Sahai, N. and D.A. Sverjensky (1997a) Evaluation of internally consistent parameters for the triple-layer model by the systematic analysis of oxide surface titration data. *Geochim. Cosmochim. Acta* **61**:2801-2826.

Sahai, N. and D.A. Sverjensky (1997b) Solvation and electrostatic model for specific electrolyte adsorption. *Geochim. Cosmochim. Acta* **61**:2827-2848.

Sahai, N. and D.A. Sverjensky (1998) GEOSURF: A computer program for modeling adsorption on mineral surfaces from aqueous solution. *Comp. Geosci.* **24**:853-873.

Sahai, N., S.A. Carroll, S. Roberts, and P.A. O'Day (2000) X-ray absorption spectroscopy of strontium(II) coordination. II. Sorption and precipitation at kaolinite, amorphous silica, and goethite surfaces. *J. Coll. Inter. Sci.* **222**:198-212.

Schecher, W.D. and C.J. Driscoll (1987) An evaluation of uncertainty associated with aluminum equilibrium constants. *Wat. Resources Res.* **23**:525-534.

Schecher, W.D. and C.J. Driscoll (1988) An evaluation of the equilibrium calculations within acidification models: the effect of uncertainty in measured chemical components. *Wat. Resources Res.* **24**:533-540.

Schindler, P.W., B. Fürst, R. Dick, and P.U. Wolf (1976) Ligand Properties of Surface Silanol Groups I. Surface Complex Formation with Fe^{3+}, Cu^{2+}, Cd^{2+}, and Pb^{2+}. *J. Coll. Inter. Sci.* **55**: 469-475.

Schlegel, M.L., L. Charlet, L., and A. Manceau (1999) Sorption of metal ions on clay minerals II. Mechanism of Co sorption on hectorite at high and low ionic strength and impact on the sorbent stability. *J. Coll. Inter. Sci.* **220**:392-405.

Schudel, M., S.H. Behrens, H. Holthoff, R. Kretzschmar, and M. Borkovec (1997) Absolute aggregation rate constants of hematite particles in aqueous suspensions: A comparison of two different surface morphologies. *J. Coll. Inter. Sci.* **196**:241-253.

Spadini, L., A. Manceau, P.W. Schindler, and L. Charlet (1994) Structure and Stability of Cd^{2+} Surface Complexes on Ferric Oxides 1. Results from EXAFS Spectroscopy. *J. Coll. Inter. Sci.* **168**:73-86.

Spadini, L., P.W. Schindler, L. Charlet, A. Manceau, and K.V. Ragnarsdottir (2003) Hydrous ferric oxide: evaluation of Cd-HFO surface complexation models combining Cd_k EXAFS data, potentiometric titration results, and surface site structures identified from mineralogical knowledge. *J. Coll. Inter. Sci.* **266**:1-18.

Steele, H.M., K. Wright, M.A. Nygren, and I.H. Hillier (2000) Interactions of the (001) surface muscovite with Cu(II), Zn(II), and Cd(II): A computer simulation study. *Geochim. Cosmochim.*

Acta **64**:257-262.

Stipp, S.L. (1990) Speciation in the Fe(II)-Fe(III)-SO_4-H_2O system at 25°C and low pH: Sensitivity of an equilibrium model to uncertainties. *Environ. Sci. Technol.* **24**:699-706.

Strawn, D.G. and D.L. Sparks (1999) The use of XAFS to distinguish between inner- and outer-sphere lead adsorption complexes on montmorillonite. *J. Coll. Inter. Sci.* **216**:257-269.

Strawn, D.G., A.M. Scheidegger, and D.L. Sparks (1998) Kinetics and mechanisms of Pb(II) sorption and desorption at the aluminum oxide water interface. *Environ. Sci. Technol.* **32**:2596-2601.

Stumm, W. Kummert, R., and L. Sigg (1980) A ligand exchange model for the adsorption of inorganic and organic ligands at hydrous oxide interfaces. *Croatica Chem. Acta* **53**:291-312.

Sturchio, N.C., R.P. Chiarello, L.W. Cheng, P.F. Lyman, M.J. Bedzyk, Y.L. Qian, H.D. You, D. Yee, P. Geissbuhler, L.B. Sorensen, Y. Liang, and D.R. Baer (1997) Lead adsorption at the calcite-water interface: Synchrotron X-ray standing wave and X-ray reflectivity studies. *Geochim. Cosmochim. Acta* **61**:251-263.

Sverjensky, D.A. (1993) Physical surface-complexation models for sorption at the mineral-water interface. *Nature* **364**: 776-780.

Sverjensky, D.A. (2001) Interpretation and prediction of triple-layer model capacitances and the structure of the oxide-electrolyte-water interface. *Geochim. Cosmochim. Acta* **65**:3643-3655.

Sverjensky, D.A. (2003) Standard states for the activities of mineral surface sites and species. *Geochim. Cosmochim. Acta* **67**:17-28.

Sverjensky, D.A. (2005) Prediction of surface charge on oxides in salt solutions: Revisions for 1:1 (M^+L^-) electrolytes. *Geochim. Cosmochim. Acta* **69**:225-257.

Sverjensky, D.A. and N. Sahai (1996) Theoretical prediction of single-site surface-protonation equilibrium constants for oxides and silicates in water. *Geochim. Cosmochim. Acta* **60**:3773-3797.

Sylwester, E.R., E.A. Hudson, and P.G. Allen (2000) The structure of uranium (VI) sorption on silica, alumina, and montmorillonite. *Geochim. Cosmochim. Acta* **64**:2431-2438.

Tebes-Stevens, C.L. and A.J. Valocchi (2000) Calculation of reaction parameter sensitivity coefficients in multicomponent subsurface transport models. *Adv. Wat. Res.* **23**:591-611.

Tebes-Stevens, C.L., F. Espinoza, and A.J. Valocchi (2001) Evaluating the sensitivity of a subsurface multicomponent reactive transport model with respect to transport and reaction parameters. *J. Contam. Hydrol.* **52**:3-27.

Thompson, H.A., G.A. Parks, and G.E. Brown, Jr. (1998) Structure and composition of Uranium^{VI} sorption complexes at the kaolinite-water interface. In: Jenne, E.A. (Ed.), *Adsorption of Metals by Geomedia: Variables, Mechanisms, and Model Applications.* Academic Press, New York, pp.

349-370.

Tomasi, J. (1994) Application of continuum solvation models based on a quantum mechanical Hamiltonian. *Amer. Chem. Soc. Symp. Ser.* **568**:10-23.

Towle, S.N., J.R. Bargar, G.E. Brown, Jr. and G.A. Parks (1999) Sorption of Cu(II) on metal oxide surfaces. II. Identification of $Co(II)_{(aq)}$ adsorption sites on the (0001) and (1 $\bar{1}$02) surfaces of α-Al_2O_3 by grazing incidence XAFS spectroscopy. *J. Coll. Inter. Sci.* **217**:312-321.

Trainor, T.P., G.E. Brown, Jr., and G.A. Parks (2000) Adsorption and precipitation of aqueous Zn(II) on alumina powders. *J. Coll. Inter. Sci.* **231**:359-372.

Trivedi, P., L. Axe, and T.A. Tyson (2001a) XAS studies of Ni and Zn sorbed to hydrous manganese oxide. *Environ. Sci. Technol.* **35**:4515-4521.

Trivedi, P., L. Axe, and T.A. Tyson (2001b) An analysis of zinc sorption to amorphous versus crystalline iron oxides using XAS. *J. Coll. Inter. Sci.* **244**:230-238.

Trivedi, P., J.A. Dyer, and D.L. Sparks (2003) Lead sorption onto ferrihydrite. 1. A macroscopic and spectroscopic assessment. *Environ. Sci. Technol.* **37**:908-914

Turner, D.R. and S.A. Sassman (1996) Approaches to sorption modeling for high-level waste performance assessment. *J. Contam. Hydrol.* **21**:311-332.

USEPA (2001) *National Primary Drinking Water Standards.* EPA-816-F-01-003, United States Environmental Protection Agency, Office of Water (4606), Washington, D.C.

Venema, P., T. Hiemstra, and W.H. van Riemsdijk (1996) Multisite adsorption of cadmium on goethite. *J. Coll. Inter. Sci.* **183**:515-527.

Waite, T.D., J.A. Davis, T.E. Payne, G.A. Waychunas, and N. Xu (1994) Uranium (VI) adsorption to ferrihydrite: Application of a surface complexation model. *Geochim. Cosmochim. Acta* **58**:5465-5478.

Waychunas, G. A., B. A. Rea, C.C. Fuller, and J.A. Davis (1993) Surface chemistry of ferrihydrite: Part 1. EXAFS studies of the geometry of coprecipitated and adsorbed arsenate. *Geochim. Cosmochim. Acta* **57**:2251-2269.

Waychunas, G.A., C.C. Fuller, and J.A. Davis (2002) Surface complexation and precipitate geometry for aqueous Zn(II) sorption on ferrihydrite. I. X-ray absorption extended fine structure spectroscopy analysis. *Geochim. Cosmochim. Acta* **66**:1119-1137.

Weesner, F.J. and W.F. Bleam (1998) Binding characteristics of Pb^{2+} on anion-modified and pristine hydrous oxide surfaces studied by electrophoretic mobility and X-ray absorption spectroscopy. *J. Coll. Inter. Sci.* **205**:380-389.

Westall, J.C. (1980) Chemical equilibrium including adsorption on charged surfaces. In: M.C. Kavanaugh and J.O. Leckie (Eds.), *Particles in Water. Advances in Chemistry Series,* vol. **189**, American Chemical Society, Washington, p. 35-43.

Westall, J.C. (1986) Reactions at the oxide-solution interface – chemical and electrostatic models. *Amer. Chem. Soc. Sym. Ser.* **323**:54-78.

Westall, J.C., J.L. Zachary, and F.M.M. Morel (1976) *MINEQL: A Computer Program for the Calculation of Chemical Equilibrium Compositions of Aqueous Systems.* Technical Note No. 18, Ralph M. Parsons Laboratory, Department of Civil Engineering, Massachusetts Institute of Technology, Cambridge, MA.

Wolery, T.J. (1992) EQ3NR, *A Computer Program for Geochemical Aqueous Speciation-Solubility Calculations: Theoretical Manual, User's Guide, and Related Documentation (Version 7.0).* Report No. UCRL-MA-110662 PT III.

Wyss, G.D and K.H. Jorgensen (1998) *A User's Guide to LHS: Sandia's Latin Hypercube Sampling Software.* Technical Report SAND98-0210, UC-505, Sandia National Laboratories, Albuquerque, NM.

Yoon, R.H., T. Salman, and G. Donnay (1979) Predicting points of zero charge of oxides and hydroxides. *J. Coll. Inter. Sci.* **70**:483-493.

Zachara, J.M. and J.P. McKinley (1993) Influence of hydrolysis on the sorption of metal cations by smectites: Importance of edge coordination reactions. *Aquat. Sci.* **55**:250-261.

Zhang, P.C., P.V. Brady, S.E. Arthur, W.Q. Zhou, D. Sawyer, and D.A. Hesterberg (2001) Adsorption of barium(II) on montmorillonite: an EXAFS study. *Coll. Surf. A- Physicochem. Engin. Aspects* **190:**239-249.

Zhang Z., P. Fenter, L. Cheng, N.C. Sturchio, M.J. Bedzyk, M. Predota, A. Bandura, J.D. Kubicki, S.N. Lvov, P.T. Cummings, A.A. Chioalvo, M.K. Ridley, P. Bénézeth, L. Anovitz, D.A. Palmer, M.L. Machesky, and D.J. Wesolowski (2004) Ion adsorption at the rutile-water interface: Linking molecular and macroscopic properties. *Langmuir* **20**:4954-4969.

Zhu, C. and D.S. Burden (2001) Mineralogical compositions of aquifer matrix as necessary initial conditions in reactive contaminant transport models. *J. Contam. Hydrol.* **51**:145-161.

Zhu, C., F.Q. Hu, and D.S. Burden (2001) Multi-component reactive transport modeling of natural attenuation of an acid groundwater plume at a uranium mill tailings site. *J. Contam. Hydrol.* **52**:85-108.

Zhu, C., Anderson, G.M., and D.S. Burden (2002) Natural Attenuation Reactions at a Uranium Mill Tailings Site, Western U.S.A. *Groundwater* **40**:5-13.

NRC FORM 335 (9-2004) NRCMD 3.7

U.S. NUCLEAR REGULATORY COMMISSION

BIBLIOGRAPHIC DATA SHEET

(See instructions on the reverse)

1. REPORT NUMBER (Assigned by NRC, Add Vol., Supp., Rev., and Addendum Numbers, If any.)

NUREG/CR-6893

2. TITLE AND SUBTITLE

Modeling Adsorption Processes: Issues in Uncertainty, Scaling, and Prediction

3. DATE REPORT PUBLISHED

MONTH	YEAR
February	2006

4. FIN OR GRANT NUMBER

Y6464

5. AUTHOR(S)

L. J. Criscenti (1), M. Eliassi (1), R.T. Cygan (1), C. F. Jové Cólón (1), S. Goldberg (2)

6. TYPE OF REPORT

Technical Report

7. PERIOD COVERED *(Inclusive Dates)*

June 2002 - December 2005

8. PERFORMING ORGANIZATION - NAME AND ADDRESS *(If NRC, provide Division, Office or Region, U.S. Nuclear Regulatory Commission, and mailing address; if contractor, provide name and mailing address.)*

(1)Sandia National Laboratories
Albuquerque, NM 87185 - 0735

(2) USDA - ARS George B. Brown Jr. Salinity Laboratory
Riverside, CA 92507

9. SPONSORING ORGANIZATION - NAME AND ADDRESS *(If NRC, type "Same as above"; if contractor, provide NRC Division, Office or Region, U.S. Nuclear Regulatory Commission, and mailing address)*

Division of Systems Analysis and Regulatory Effectiveness
Office of Nuclear Regulatory Research
U.S. Nuclear Regulatory Commission
Washington, DC 20555-0001

10 SUPPLEMENTARY NOTES

E. O'Donnell, NRC Project Manager

11. ABSTRACT *(200 words or less)*

Adsorption to mineral surfaces is largely responsible for the retardation of contaminant metals in the subsurface environment. This report covers three different aspects of modeling adsorption with an emphasis on the use of surface complexation models (SCMs). The first study demonstrates how adsorption constant uncertainty propagates through a one-dimensional reactive-transport code and can strongly influence uranyl concentrations as a function of distance and time from a contaminant source. Adsorption occurs at the solid-water interface which can be investigated at different scales: electronic, atomistic, and thermodynamic. The second study describes how the small-scale investigations provide insight into the development of accurate bulk thermodynamic models that are used in conjunction with hydrological flow and transport models used to describe contaminant migration. The third study reviews recent progress in the development of an internally-consistent database of parameters for a specific SCM, the triple-layer model.

12. KEY WORDS/DESCRIPTORS *(List words or phrases that will assist researchers in locating the report.)*

adsorption, uranyl ion, Naturita, surface complexation model, triple layer model

13. AVAILABILITY STATEMENT

unlimited

14. SECURITY CLASSIFICATION

(This Page)
unclassified

(This Report)
unclassified

15. NUMBER OF PAGES

16. PRICE

Federal Recycling Program